ROLE OF DYNEIN AND KINESIN IN VIRAL PROLIFERATION

&

DYNEIN INHIBITORS

by © Tati Padou, Martinet-Sayi'Mone

A thesis submitted to the School of Graduate Studies in partial fulfillment of the requirements for the degree of

Master of Science in Pharmacy

School of Pharmacy

Memorial University of Newfoundland

November 2021

St. John's, Newfoundland and Labrador, Canada

Abstract

Dynein and kinesin are motor proteins involved in the retrograde and anterograde, respectively, transport of cargoes, including viral genomes following infection. Current literature reveals that both proteins play critical roles in ensuring successful viral proliferation. The literature also shows that the motor proteins are involved in the immunological response of host cells. Small-molecule inhibitors of kinesin and dynein inform of the function of the proteins during viral proliferation and immunological response.

The investigation of the binding profile of small-molecule inhibitors of dynein, namely, ciliobrevin and analogues as well as dynapyrazole A and B, and the protonated forms of the lead compounds at the AAA1 binding site of dynein revealed the identity of the residues interacting with the inhibitors. This research project also analyzed the effect of isomerization of ciliobrevin on its binding profile, the impact of protonation of lead compounds on the binding affinity of the inhibitors, and the intramolecular interactions in dynein. The results suggest a potential residue in the AAA1 subunit of cytoplasmic dynein 1 that could be involved in the ‘glutamate switch’ mechanism, which according to the literature, has not been observed in dynein 1.

Acknowledgments

I acknowledge the support of my supervisor, Dr. Laleh Alisaraie. Thank you for your time and contribution to this work. I have learnt valuable lessons while being under your supervision.

I sincerely thank my family for their emotional support and for always encouraging me to move forward despite the numerous difficulties I faced during the completion of this degree. Thank you very much, mom, dad, ya Nathy, Collina, Malith, Nandi, and the best grandmother ever, Jackie.

A personal thank you note to my lab co-worker and friend Karina for your encouraging words and your company during this journey. I admire your strength and resilience, and I am happy I had the opportunity to meet you. All the best in your projects!

I thank Rachel for her contribution to the Chemdraw figures. I sincerely appreciate your help. I would also like to thank previous members of Dr. Alisaraie's laboratory.

I acknowledge financial support from the School of Graduate Studies (SGS) at Memorial University of Newfoundland and the Natural Sciences and Engineering Research Council (NSERC).

Finally, I would like to personally thank you, Yehoshua Ha Mashiach, for your support and your guidance through this accomplishment. Thank you for the lessons you taught me and for not allowing me to retract. Thank you for always watching over my mind and for preventing me from a burn-out through your invaluable support.

I dedicate this thesis to my mom, father, sisters, brother, and friends.

Table of Contents

List of Tables

List of Figures

List of Abbreviations

AAA+: ATPases Associated with various cellular Activities

MT: Microtubules

HPV: Human Papillomavirus

KHC: Kinesin Heavy Chain

APC: Antigen-Presenting Cell

MTOC: Microtubule-Organizing Centre (MTOC)

IS: Immunological Synapse

SV40: Simian Virus 40

RAV: Rabies Lyssavirus

HBV: Hepatitis B Virus

PCV: Porcine Circovirus

HCV: Hepatitis C Virus

WSSV: White Spot Syndrome Virus

PRV: Pseudorabies Virus

MLV: Murine Leukemia Virus

IAV: Influenza A Virus

LCMV: Lymphocytic Choriomeningitis Virus

LASV: Lassa mammarenavirus

MACV: Machupo Virus

JUNV: Junín Virus

List of Appendices

Introduction and Overview

Dynein and kinesin are motor proteins that perform their motor functions via microtubules (MTs), which are proteins in a hollow shape composed of alternating α and β heterodimer G-proteins, acting as an arranged system of tracks that allow delivery of cargoes, such as mRNA, nucleus, mitochondria, and vesicles. Dynein belongs to the ATPases Associated with various cellular Activities (AAA+) superfamily, meaning they employ energy generated from hydrolysis of ATP to accomplish their functions. The motor protein ensures the retrograde transport from the cell periphery to the perinuclear region, whereas kinesin directs the anterograde transport, from the perinuclear area to the cell periphery. Dynein and kinesin participate in cellular functions such as cell division, immunological response, and embryogenesis. Defects in the motor proteins can cause pathologies such as cancer, neurodegenerative diseases (NDDs), which include Parkinson's disease (PD), Alzheimer's disease (AD), and Huntington's disease (HD).

During viral infection, viruses exploit the delivery function of kinesin and dynein to ensure viral proliferation. Chapter 1, an article in preparation for publication, reviews the role of the motor proteins in the export and import of viral genome following viral infection and their role in the immunological response of the host cells. Chapter 2, a published article co-authored with Dr. Alisaraie, focuses on small-molecule inhibitors of dynein, ciliobrevin and analogues, and dynapyrazole A and B, revealing their binding profile using computational chemistry and structural biology methods, as the binding site of the inhibitors had not been analyzed in the literature.

This research work contributes to the fields of biochemistry, medicinal chemistry, and pharmacy, as the knowledge provided through the scientific review in Chapter 1 summarizes the ambivalent role of dynein and kinesin in both viral proliferation and immunological response. The scientific investigation in Chapter 2 guides on avenues to improve the selectivity of the inhibitors on dynein isoforms, uncovers the identity of residues interacting with the inhibitors, directs future research on improving the potency and reducing the toxicity of the small-molecule inhibitors with the objective that a drug could be generated to treat dynein dysfunctions. This research work also proposes a potential candidate involved in the 'glutamate switch' mechanism in dynein, which had not been observed yet in experimental crystal structures of cytoplasmic dynein 1.

The objectives of this thesis research were to explore the role of dynein and kinesin in the transport of viral particles in cells and to elucidate the binding site of inhibitors of cytoplasmic dynein 1 using *in silico* methods. Chapter 1 informs that while viruses exploit cellular delivery machinery to ensure their viability, the motor proteins kinesin and dynein are actors in generating the immunological response. Hence, therapies involving the target of the motor proteins through small-molecule inhibitors must consider the action of the proteins in promoting the immune response to avoid an impairment of the immunity system of host cells. The investigation on the binding profile of small-molecule inhibitors of dynein carried in Chapter 2 is a stepping-stone for future research on the refinement of the inhibitors against NDDs and viral infections to result in efficient inhibition of dynein and isoform selectivity.

Co-authorship Statement

Chapter 2 is an article co-authored with Dr. Alisaraie and published in the International Journal of Molecular Sciences.

CHAPTER 1

Introduction

1.1. Motor Proteins

Viruses are infectious agents that can be enveloped like the influenza virus, or non-enveloped like the Human Papillomavirus (HPV) [1]. The interior of the envelope of viruses displays a capsid, which refers to the protein shell protecting the nucleic acid of the viral genome [2]. Viruses contain either DNA or RNA as their genetic information, which they inject into host cells to hijack their cellular tools to replicate their viral genome [3]. The infectious agents are characterized by three stages, which are entry, genome replication, and exit or egress in their life cycle in cells. The entry step involves four steps: attachment, penetration, cytoplasmic trafficking, and uncoating. For successful viral infection, viruses completing genome replication at the nucleus of the host must cross the plasma membrane and the nuclear envelope, whereas the viruses replicating at the cytoplasm need only to cross the plasma membrane [3]. Viruses exploit the intracellular trafficking machinery of the host cell to ensure their proliferation.

Dynein and kinesin are motor proteins involved in cytoplasmic trafficking [4]. Dynein is responsible for retrograde transport [5] from the cell periphery towards the nucleus,

while kinesin ensures the anterograde transport [6] from the perinuclear region to the cell periphery. There are nine subfamilies of dynein: two cytoplasmic and seven axonemal dyneins [5]. Cytoplasmic dynein is a homodimer composed of two heavy chains (DYNC1H), two light intermediate chains (DYNC1LI), four intermediate chains (DYNC1I), and six light chains (DYNLT1 or TcTex-1, DYNLL1 or LC8, and DYNLRB) for an approximate weight of ~1.2 MDa [7]. Dynein employs its light intermediate chains (LICs) to carry cargoes to the perinuclear area, and these chains bind to the intermediate chains (ICs) [4]. This motor protein accomplishes its functions by forming a multifactor complex with its cofactor, dynactin [4].

The superfamily of motor proteins, called kinesins (KIFs), carry cargoes including organelles, mRNAs, and complexes of proteins through microtubules (MTs), and are characterized by the presence of a conserved domain in a globular shape called the head, containing approximately 360 residues, where hydrolysis of ATP occurs. The globular domain is followed by a stalk connected to a tail. The tail interacts with cargoes for accomplishing anterograde trafficking. A domain called the 'neck' displays features distinctive to each family of kinesins, is located between the head and the stalk, and is engaged in essential activities such as directing the movement of the motor protein on MTs [8]. Hence, the neck and the head compose the motor domain of KIFs. The motor domain is conserved in KIFs, but the stalk and tail domains differ from various families. Miki *et al.* categorized KIFs in 14 families using phylogenetic classification. Members of the kinesin-1 or kinesin heavy chain (KHC) family participate in the transport of organelles and trafficking at the nucleus. This family displays distinctive features such as

a β-sheet neck and a high amount of conserved residues in a coiled-coil stalk [8]. The three sub-families of animal KHCs, namely, KIF5A, KIF5B, and KIF5C, consist of a cargo-binding domain (CBD) located in the stalk and a light chain-binding domain (LCBD), which connects to a kinesin light chain (KLC) [8]. The kinesin-2 family or N-kinesins are composed of the following sub-families: KIF3A, KIF3B/C, and KIF17. Members of this family are involved in the transport of organelles, spermatogenesis, and intraflagellar transport (IFT). The kinesin-3 family is composed of the KIF1, KIF13, KIF14, KIF16, and KIF28 subfamilies and an indeterminate subfamily named NcKIF1C/Klp7. This family distinguishes itself with a forkhead-associated (FHA) domain following a β-sheet and an α-helix in the neck region specific to the family [8].

The viral infection stimulates an immunological response from the host, which results in the activation of cytotoxic T cells for the efficient neutralization of virally infected cells [9]. During the immune response, an immunological synapse is created between an antigen-presenting cell (APC) and the cytotoxic T cell accompanied by the translocation of the microtubule-organizing centre (MTOC) [10]. Studies have shown the involvement of dynein and kinesin in both the activation of T cells and in the formation of the immunological synapse as well as in the transport of critical players in an effective immune response from the host [9-11].

This chapter explores the involvement of the motor proteins at the three stages of the life cycle of viruses and the function of dynein and kinesin in the immunological response of the host cell to the viral infection.

1.2. Transport of viral genome from the cell membrane to the nucleus

1.2.1. Role of kinesin 1 and dynein 1 and the Polyomaviridae family

The polyomavirus simian virus 40 (SV40) from the *Polyomaviridae* family was first isolated from rhesus monkey kidney cells [12, 13]. The human equivalent viruses, namely BK (BKPyV) and JC (JCPyV) polyomavirus, have been shown to cause diseases such as hemorrhagic kidney and bladder infections as well as leukoencephalopathy and Merkel cell carcinoma in humans [14-16]. The virus displays a non-enveloped structure composed of seventy-two (72) pentamers of capsid protein VP1 in which DNA is enclosed, whereas each polymer displays a hydrophobic capsid protein VP2 or VP3 [14]. The penetration of SV40 in host cells for infection occurs with the binding of the virus to the ganglioside GM1 receptor [17] on the plasma membrane followed by endocytosis [18] and transport to endolysosomes [19] and penetration of the endoplasmic reticulum (ER) [20-23]. Ravindran *et al.* showed that kinesin 1 binds to J-protein B14, an ER membrane protein, and the motor protein causes the formation of foci, which are entry sites at the ER membrane, giving access to the cytosol. The research work revealed that the generation of foci at the ER membrane results from the distinctive ability of kinesin 1, unlike kinesin 2 and kinesin 3, in selecting acetylated MTs. Kinesin 1 typically carries cargoes from the cell centre to its periphery as the movement of the motor protein is directed towards the plus-end of the MT, a movement known as the anterograde transport [24]. However, the finding that kinesin facilitates the transportation of SV40 from the ER membrane to the cytosol is explained by the curved shapes of the acetylated MTs, located at the perinucleus, which allows for the transport of viral cargoes to the cytosol while moving

towards the plus-end [14]. Hence, kinesin 1 was shown to play a critical role in delivering SV40 to the cytosol.

Another research study from Ravindran *et al.* revealed that dynein 1 binds to SV40 particles to promote viral infection through disassembling the virus to release viral genetic information necessary for transcription and translation [25]. A cell-based semipermeabilized-membrane assay assessing the ER-to-cytosol transport showed that dynein is not involved in the delivery of SV40 from the plasma membrane to the ER nor to the cytosol but instead is an actor in post-cytosol transport of SV40 [25]. Treatment of infected cells 5 hpi (hour post-infection) with ciliobrevin D, a small-molecule inhibitor of dynein, revealed the motor protein not to be involved in the emergence of ER-to-cytosol penetration sites, as no inhibitory activity was observed at that stage [25]. Furthermore, mass spectrometry and precipitation analysis showed SV40 to bind to dynein 1 in the cytosol [25]. Mass spectrometry also showed dynactin, a sub-unit activator of dynein 1, to attach to SV40 located in the cytosol. The overexpression of dynactin subunit 4, which inhibits dynein activity, disrupted SV40 viral activity. Hence, dynactin also promotes SV40 activity [25]. Both Sucrose Density Sedimentation (SDS) and limited proteolysis experiments on SV40-infected cells (control) and infected cells treated with ciliobrevin D revealed that the inhibitor reduced the fraction of disassembled SV40, which demonstrated that disruption of dynein 1 hindered SV40 disassembly [25]. Thus, this study showed that dynein 1 plays a role in transporting SV40 at a post-cytosolic stage and engages in disassembling the viral genome to release the genetic information during the cytosol-to-nucleus phase for promotion of viral infection [25].

Mouse polyomavirus (MPyV), from the *Polyomaviridae* family, is characterized by an entry in host cells through endocytosis, which is facilitated by the interaction between the major capsid protein VP1 and the ganglioside receptors, GD1a or GT1b, on the plasma membrane [26]. Zila *et al.* showed that dynein 1 plays a critical role in transporting MPyV virions from the periphery of cells to the ER, as inhibition of dynein caused a 40 to 50 % reduction in the colocalization of viral particles and BiP, an ER protein essential for infection [26]. A seventy percent (70%) reduction in MPyV infected cells was observed following the overexpression of dynamitin, which results in dynein inhibition through the disassembly of dynein and dynactin, a co-factor of the motor protein. Furthermore, confocal microscopy analyses of the overexpressed-dynamitin cells showed that virions significantly remained at the periphery of the cells at 5 hpi, while in mock-transfected cells, the virions accumulated near the nucleus at that moment [26]. Inhibition of kinesin 1 and 2 did not result in perturbation of MPyV infection, which suggested that these motor proteins do not play a critical role in transporting MPyV viral cargoes [26]. Hence, dynein 1 is the motor protein that the MPyV exploits to ensure efficient viral proliferation.

1.2.2. Dynein light chain LC8 and the Filoviridae and Rhabdoviridae families

Dynein light chain LC8 (8 kDa) is a subunit of cytoplasmic dynein 1, which binds to several viral proteins such as the Ebola virus VP35 from the *Filoviridae* family [27], the rabies virus (RAV) from the *Rhabdoviridae* family [28], and the human immunodeficiency virus integrase [29]; thus, promoting their viral activity [27]. LC8 was shown to interact with the multifunctional viral protein of the Ebola virus [27], namely

the VP 35, involved in evasion from the host cell immune reaction and synthesis of viral RNA [30, 31]. Luthra *et al.* showed that the interaction between LC8 and VP35 is specific as mutation of the binding motif (71-SQTQT-75) resulted in the disturbance of the interaction [27]. Furthermore, LC8 was shown to improve the activity of VP35 in RNA synthesis without improving the ability of the viral protein to evade the immune response [27]. The improved activity partially stems from the property of LC8 to stabilize the oligomerization domain of VP35 [27].

Rabies lyssavirus (RAV) is a negative single-stranded RNA, which is fatal following the emergence of symptoms. The structure of the virus encompasses an RNA-dependent RNA polymerase (RavL), a nucleoprotein that encloses the viral RNA (RavN), and a noncatalytic phosphoprotein (RavP). Dynein light chain LC8 plays a critical role in promoting viral infection of RAV through binding to RavP [28]. The complex, formed by LC8 and RavP, has a dissociation constant (K_d) of 82 ± 8 nM, making RavP the ligand that naturally binds the strongest to LC8 among other natural ligands [28].

1.2.3. Dynein light chain LL1 and the Hepadnaviridae and Circoviridae families

The Hepatitis B virus (HBV) from the *Hepadnaviridae* family is an enveloped pararetrovirus, which causes acute to chronic liver diseases [32]. HBV consists of the capsid containing 240 copies of core proteins (Cps), the relaxed circular viral DNA information (rcDNA), the viral polymerase (pol), and heat shock proteins [32]. The virus is endocytosed in host cells where the release of its capsid occurs, followed by retrograde transport from the cytosol to the nucleus [33]. Repair of rcDNA results in the formation

of covalently closed circular DNA (cccDNA), which is used for viral mRNAs transcription [34-36]. Through the binding to the pregenome, the pol interacts with the Cp and causes the assembly of RNA-containing capsids (rnaCs) [32]. Reverse transcription and incomplete second-strand DNA synthesis contribute to the maturation of the genome [37]. Liver cells infected with HBV carry the rnaCs, capsids with intermediate products from maturation, few capsids containing rcDNA (matC), and empty capsids (empCs) due to an overexpression of Cps [38]. The research work of Osseman *et al.* revealed that empCs and matCs are actively transported through the cytosol to the nucleus via their binding to the LL1 of dynein 1, which is simultaneously bound to DynIC [32]. Thus, dynein 1 facilitates the transport of viral capsids, promoting HBV viral infection.

Porcine circovirus (PCV) is affiliated to the family *Circoviridae* with two identified genotypes: PCV type 1 and PCV type 2 [39]. Porcine circovirus type 2 (PCV2) is an adenovirus pathogen and is the type responsible for diseases such as post-weaning multi systemic wasting syndrome (PMWS), porcine dermatitis, and nephropathy syndrome (PDNS) [40]. DYNLL1 was found to form a complex with PCV2 particles to carry the viral genome from the cell periphery to the nucleus resulting in the proliferation of the viral infection [40]. Molecular docking revealed that the C terminus of the PCV2 capsid (Cap) directly binds to the common site of cargo binding of DYNLL1 and the first proposed binding area consisted of Leu187, Gln188, Thr189 and Ser190 [40]. Thus, DYNLL1 was shown to facilitate viral infection by PCV2 by transporting its viral capsids to the perinuclear region.

1.2.4. Dynein intermediate chain IC1 and the Circoviridae and Nimaviridae families

There are eleven possible open reading frames (ORFs) in the genetic information of PCV [39, 41-44]. The ORF2 encodes the capsid protein (Cap), which encloses the PCV genome [39]. Dynamic images of PCV2 infection revealed that at 6 hpi, virions were located within Rab5-positive endosomes suggesting that viral infection involved endocytosis of PCV2 viral particles [39]. Treatment of PCV2-infected cells with Na_3VO_4, an inhibitor of dynein, showed the viral particles to be located at the periphery of the cells, indicating that the entry of the virus in cells is not prevented when dynein is inhibited [39]. Further experiments showed dynein intermediate chain 1 (IC1) location to overlap that of the PCV2 Cap protein and a reduction in expression of Cap. Cao *et al.* showed that IC1 is recruited at the cytoplasm and translocated to the nucleus by the nuclear localization signal (NLS) of the PCV2 Cap using confocal microscopy. Co-immunoprecipitation assays revealed that the D2 domain of PCV2 Cap, which is the N-terminal composed of residues 42-100, directly interacts with IC1. The knock-down of IC1 resulted in the inhibition of PCV2 viral replication, underlying the crucial action of the dynein subunit in promoting the infection. Cao *et al.* suggested that determining a peptide to compete with the fragment of the IC1 of dynein interacting with the N-terminus of Cap of PCV2 represents an avenue to inhibit PCV2 infection. Hence, dynein IC1 was shown to engage in the transport of PCV2 contained in endosomes from the cell periphery to the nucleus through direct binding to Cap.

Dynein IC1 is involved in PCV2 viral transcription and exporting PCV2 particles from the nucleus, as silencing dynein IC1 caused a reduction in nuclear export of PCV2 viral particles and downregulated genes responsible for PCV2 capsid proteins [39]. Noteworthy that dynein IC1 was located at the nuclei of PCV2 infected cells, although the motor protein was found in the cytoplasm of non-infected cells. Cao *et al.* suggested that IC1 is carried to the nucleus for the efficient viral proliferation of PCV2 through an unknown mechanism. Furthermore, the presence of the complex IC1/Cap in the cytoplasm at the latest stages of the infection implied the involvement of IC1 in exporting viral particles from the nucleus. Therefore, IC1 is not only involved in the transport of the PCV2 genome from the cell periphery to the nucleus but might also be involved in the nuclear entry of the viral genome and the export of viral particles to the cell periphery.

White spot syndrome virus (WSSV) from the *Nimaviridae* family is among the predominant significantly deadly viruses attacking Penaeid shrimps [45]. Confocal microscopy revealed that WSSV virions and cytoplasmic dynein colocalized in hemocytes of shrimps [46]. The knockdown of FcDYNCI, the intermediate chain of cytoplasmic dynein of *Fenneropenaeus Chinensis* or Chinese white shrimp, inhibited WSSV viral infection, supporting the involvement of dynein in the transport of the virions from the cell periphery to the nucleus [46]. The mechanism through which the intermediate chain of dynein facilitates WSSV viral infection was not determined yet, and further work on the topic is needed.

1.2.5. Dynein 1 and viruses from the Flaviviridae family

Hepatitis C virus is a positive-strand RNA virus and is classified under the Hepacivirus genus in the family of *Flaviviridae* [47]. Eyre *et al.* showed that ciliobrevin D, an inhibitor of cytoplasmic dynein [48], reduces the replication of viral RNA of HPC by about 40% [47]. The knockdown of the heavy chain of cytoplasmic dynein 1 significantly reduced the motility of the non-structural protein NS5A, which engages in crucial steps of HCV viral infection such as the regulation of viral RNA replication and the assembly of virions [47]. Thus, dynein was shown to promote viral infection through the transport of viral proteins. However, further research on the mechanism and the binding site between dynein 1 and NS5A is needed for designing antiviral drugs targeting this interaction.

Dengue virus (DENV) is an enveloped virus from the family of *Flaviviridae*, with a positive sense RNA [49]. Its entry into the host cell is facilitated by endocytosis [49]. A dynamic analysis showed that 30 mins were required for endosomes containing the envelope (E) proteins to move from the cell periphery to the perinuclear region, supporting that endosomes carry the viral genome to the nucleus for efficient replication following endocytosis [49]. Confocal microscopy showed dynein 1 to interact with the E protein [46] progressively. At 4 hpi, dynein 1 colocalized with the E protein, although the protein was at a low concentration [49]. As time elapsed, the concentration of the E protein increased, and the maximum concentration of the dynein-E complex detected in the perinuclear region was reached between 24 and 48 hpi, with the complex splitting at 72 hpi [49]. The E protein and dynein 1 co-immunoprecipitated in an assay, further

indicating the formation of this complex during DENV viral infection [49]. Computational docking of DENV-E protein (PDB: 1TG8) and dynein (PDB: 2P2T), which is dynein light chain LC8 interacting with residues 123-138 of intermediate chain IC74, revealed putative residues where interaction occurs, but further studies are required to elucidate the exact residues involved in the dynein-E complex interaction [49]. The inhibition of dynein through overexpression of dynamin resulted in a low cytosolic concentration of E protein, suggesting that dynein is involved in the high concentration of E protein in the cytosol [49]. The inhibition of dynein also resulted in the restriction of DENV core (C) proteins to the cytosol [49], while it was previously shown that the C proteins are carried to the nucleus [50]. Hence, dynein plays a critical role in DENV viral infection through transporting E and C proteins towards the perinuclear region [49].

1.2.6. Dynein 1 and the Alphaherpesvirinae family

Pseudorabies virus (PRV) is highly virulent and characterized by its ability to invade the neurological system of mammalians [51]. PRV belongs to the *Alphaherpesvirinae* family along with human herpes simplex virus types 1 and 2 (HSV-1 and HSV-2) and the varicella-zoster virus (VZV) [52]. A membrane vesicle in which an enveloped virion composed of the PRV nucleocapsid and teguments contains the viral and host transmembrane proteins such as Us9p [52]. Viral protein VP1/2 complex is directly attached to the exterior of the capsid and is crucial to the transport of viral particles to nuclear pores and the delivery of DNA into the nucleus [51]. Co-immunoprecipitation assays showed VP1/2 interacting with the dynein/dynactin complex through interactions

with the proline-rich region of VP1/2 [51]. Thus, dynein 1 engages in transporting a key component of PRV viral infection.

1.2.7. DYNLT1 (former Tctex-1) and DYNLT3, and the Papillomaviridae family

Human papillomaviruses (HPV) from the *Papillomaviridae* family are non-enveloped adenoviruses with an icosahedral shape [53]. There are 360 copies of the major capsid (L1) and 72 proteins of the minor capsid (L2). The entry of the virus to deliver its circular double-stranded DNA genetic information is initiated by endocytosis. It was detected that DYNLT1 interacted directly with the L2 viral proteins using the two-yeast hybrid technique, verified with co-immunoprecipitation and western blotting [53].

Co-precipitation of DYNLT3 and the L2 proteins showed that the other family member of DYNLT1 interacts with the minor capsid proteins. An accumulation of the L2 proteins in the nuclear domain 10 (ND10) of infected cells followed by the localization of DYNLT1 and DYNLT3 from the cytoplasm to the ND10 implied that the increased expression of the capsid protein triggered translocation of the light chains of dynein. Immunofluorescence deconvolution microscopy showed DYNLT1 and DYNLT3 interacting with the L2 proteins in the cytosol and the nucleus during HPV16, a subset of HPV infection. Treatment with siRNA and antibodies against DYNLT1 and DYNLT3 showed a reduction in the infectivity of HPV in HeLa (reduced to 26% for anti-DYNLT1 and 65% for anti-DYNLT3) and HaCaT (reduced to 34% for anti-DYNLT1 and 81% for anti-DYNLT3) cells, indicating the critical action of these light chains of dynein in promoting viral infection [53]. Colocalization of the L2 and the ND10 was reduced to

19% for DYNLT1 and 26% for DYNLT1 when treated with siRNAs, indicating that the two light chains are involved in the transport of the L2 to the nucleus. Therefore, the two light chains of dynein DYNLT1 and DYNLT3 were shown to play an essential role in HPV16 viral infection.

1.2.8. DYNLRB2 and the Retroviridae family

Murine Leukemia Virus (MLV) is from the *Retroviridae* family [54]. It relies on cellular division to enter the nucleus, similar to members of the *Gammaretrovirus* genus, due to a lack of the ability to traverse the nuclear membrane of cells that are not experiencing cell division [54]. The knockdown of light chains DYNLL1, DYNLL2, DYNLT1, and DYNLT3 did not significantly inhibit MLV viral infection, indicating that the two light chains do not play a crucial role in promoting the viral infection. However, the knockdown of DYNLRB1 resulted in overexpression of DYNLRB2, which significantly contributed to a 2.5-fold increase in the level of infection. Furthermore, the knockdown of DYNLRB2 caused a reduction in the rate of MLV infection. The detection of physical interaction between DYNLRB2 and MLV proteins was not revealed. Opazo *et al.* suggested that the light chain might not directly interact with viral proteins but indirectly through a protein interacting with DYNLRB2 [54]. They also suggested that the function of DYNLRB2 might lie in bringing the preintegration complex (PIC) and the nucleus at a proximal distance, as the disruption of the nuclear envelope is required for MLV to access the nucleus. Thus, the light chain of dynein DYNLRB2 was shown to be essential in the MLV viral infection.

The light intermediate chain of dynein, DYNCLI2, promotes MLV infection, as its knockdown caused a partial inhibition of MLV infection [55]. However, dynein regulators, p50 a critical component of the dynactin complex and NudEL, play a crucial role in MLV infection before nuclear entry, as their knockdowns caused nearly complete inhibition of viral infection [55]. Hence, the regulators of dynein play a critical role in MLV infection.

1.3. Role of the motor proteins in nuclear entry

Once delivered to the perinuclear region, the entry of viral capsids in the nucleus allows the replication of viral genetic information.

1.3.1. Disruption of Nuclear Pore Complex (NPC) by kinesin 1 in the Adenoviridae family

The Nuclear Pore Complex (NPC) consists of more than 30 various proteins, and transmembrane nucleoporins (Nups) attach the complex to the nuclear envelope [56]. Nup358 is a peripheral PheGly-repeats-containing nucleoporins. The size restriction for transport through the nucleus is 39 nm for transport carried through receptors and 40 kDa for solutes. Despite the size restriction, some viruses succeed in crossing the NPC and accessing the nuclear envelope [56]. Strunze *et al.* showed that kinesin light chains 1 and 2 (KLC1/2) bind to the virion protein pIX to execute uncoating of adenoviruses [56]. Knockdown experiments revealed that Nup214 and Nup358 are necessary for the uncoating step; however, the attachment between NPC and the virus is achieved only by Nup214 [56]. The binding of kinesin 1 to viral capsids triggers the NPC to release the

Nups from the nuclear envelope, which causes an increase in the permeability of the envelope. Mutational studies involving pIX, which binds to the kinesin light chain, revealed that this virion protein is also involved in increasing the permeability of the nuclear envelope. Thus, kinesin 1 is involved in disassembling the capsids of adenoviruses and the NPC of host cells to facilitate the entry of the viral genome into the nucleus [56].

1.3.2. Dynein Light Chain 1 (DLC1) as a transcription factor for viral synthesis in the Rhabdoviridae family

Dynein light chain (DLC1) acts as a transcription factor to encourage viral transcription of Rabies Virus (RABV) [57]. The viral RNA of RABV encodes L, an enzymatic subunit, and P, a cofactor [57]. A PL complex is formed and ensures RNA replication and transcription. Dynein Light Chain 1 (DLC1) binds to the PL complex. RABV-L complex was found to localize at acetylated MTs. The putative RMTQ motif in DLC1 binding to the RABV-L motif is responsible for MTs reorganization, as the L mutant did not show any rearrangement of the MTs. The binding of DLC1 to P and L through conserved motifs in both proteins is essential to the reorganization (i.e., stabilization) of the MTs [57]. Viral protein complexes trap DLC1, which triggers activation of transcription factor of DLC1, thus producing free DLC1. Noteworthy that DLC1 negatively regulates its transcription by binding to the transcription activator ASCIZ, and DLC1 binds to the P and the L, acting as a transcription factor for replication of RABV1 [57].

1.4. Role of the motor proteins in egress of viral particles at the plasma membrane

After the entry and replication of the viral genome into the nucleus, the viral genome is packaged, and the capsids are assembled in preparation for extracellular release. The motor proteins are involved in delivering viral particles to the plasma membrane for egress.

1.4.1. KIF13A and KIF18A and the Orthomyxoviridae family

The influenza A virus (IAV) of the *Orthomyxoviridae* family [6] belongs to the group of negative-strand RNA viruses, and its virions possess eight ribonucleoproteins (vRNPs) in the inner core [58]. The GTPase Rab11 protein, whose traffic is modified during IAV infection, interacts with KIF13A, which belongs to the kinesin 3 family. Ramos-Nascimento *et al.* showed KIF13A is involved in the delivery of vRNPs to the cell periphery, as overexpression of this motor protein caused vRNPs to agglomerate near the plasma membrane along with Rab11 vesicles and KIF13A. The inhibition of KIF13A did not affect the synthesis of viral proteins, indicating that the motor protein is not involved in the retrograde delivery of the viral genome to the nucleus nor in its nuclear entry. Thus, KIF13A was shown to engage in the anterograde delivery of vRNPs to the cell surface through forming a complex with Rab11 and vRNPs [58].

Following IAV infection, an increase in the expression of KIF18A, a member of kinesin 8, occurs [59]. Inhibition of the motor protein by BTB-1, a specific small-molecule inhibitor, reduced the cytopathic effect (CPE) in infected cells [6]. Treatment with BTB-1 and cytometric experiments showed a decrease in the rate of IAV replication,

the expression of viral proteins, and the manufacturing of infectious viral particles [6]. Furthermore, knockdown experiments of KIF18A using siRNA revealed that inhibition of the motor protein significantly decreases viral proteins expression, whereas the viral activity is restored when the function of KIF18A is recovered in infected cells [6]. However, an augmentation in viral proteins expression was obtained following overexpression of KIF18A [6]. Immunofluorescence experiments showed that treatment of infected cells with BTB-1 caused viral NP to remain in the nucleus [6]. Viral NP is carried from the nucleus to the plasma membrane as a vRNP complex. The retention of these particles at the nucleus when KIF18A is inhibited by BTB-1 indicates the critical action of the motor protein in promoting viral infection [6]. The inhibitor BTB-1 prevents the nuclear export of vRNPs by hindering the activation of AKT, p38, SAPK, and RanBP3 pathways required to export proteins via Chromosomal Maintenance 1 (CRM1)-mediation [6]. Noteworthy, BTB-1 significantly decreased both the symptoms and the death rate in infected mice [6]. Hence, KIF18A contributes to viral infection and represents a target for drugs aiming to treat IAV infection. The small-molecule inhibitor BTB-1 displayed efficient inhibitory activity towards IAV infection [6].

Lassa virus is of the *Arenaviridae* family and is composed of two groups: the Old World arenaviruses and the New World arenaviruses. The Old World arenaviruses (LCMV, LASV, and Lujo virus) are characterized by acute hemorrhagic fever in humans. The New World arenaviruses encompass the MACV, JUNV Guanarito, Chapare, and Sabiá viruses, causing epidemic hemorrhagic fever in South America [60]. Fehling *et al.* revealed that KIF13A is involved in the transport of the viral protein matrix Z, which is

engaged in essential stages of the viral infection such as synthesis of viral RNA, assembly and delivery of the virus, and replication of the virus [60]. Overexpression of KIF13A caused Z proteins to relocalize to the plasma membrane along with mannose-6-phosphate receptor (M6PR), indicating that the M6PR trafficking pathway is used for the delivery of the viral protein Z to the cell periphery through the motor activity of KIF13A [60]. However, immunofluorescence revealed that the motor protein does not transport other viral proteins (i.e., LASV nucleoprotein NP or the glycoprotein GP) [60].

Co-immunoprecipitation experiments showed that KIF13A specifically binds to the matrix Z protein [60].

Furthermore, a double-negative mutation of KIF13A, resulting in inhibition of the motor activity of the protein, showed that the motor protein could bind to the Z protein of LASV with no relocation of the viral protein, as KIF13A co-precipitated with the protein but was not able to deliver the latter to the plasma membrane [60]. Knock-down of the motor protein using small interfering RNA (siRNA) revealed a decrease in the anterograde delivery of virus-like proteins (VLPs), which are released from the expression of the Z protein; showing that KIF13A plays an essential role in the transport of VLPs to the site of virus assembly [60]. The JUNV and MACV of the New World arenaviruses group also displayed an interaction with KIF13A, revealing a conserved mechanism of anterograde transport within the *Arenaviridae* family [60]. Hence, the motor protein KIF13A is engaged in promoting viral infection in *Arenaviridae* viruses.

1.4.2. KIF1A, KIF5A, KIF5B, and KIF5C and the Alphaherpesvirinae family

The delivery of viral proteins of HSV-1 and PRV from the nucleus to the axon involves the action of three membrane proteins encoded by the viruses, namely the Us9p and glycoproteins E and I. They ensure the anterograde transport following viral capsids' assembly and DNA packaging [61]. Kratchmarov *et al.* showed that phosphorylation of the membrane protein Us9p at Ser51 and Ser53 contributes to the efficient transport of viral proteins through the interaction between Us9p and KIF1A [62]. The interaction is critical for ensuring the anterograde transport of PRV particles [52]. However, the phosphorylation step is not essential to the delivery of viral particles, as its inhibition resulted in a decrease of ~4 fold in viral anterograde transport without complete inhibition [62]. Glycoproteins E and I form a heterodimer (gE/gI) and stimulate interaction between KIF1A, a kinesin 3 subunit, and Us9p [61].

Furthermore, KIF5C, a subunit of kinesin 1, has been shown to interact with HSV-1 bound to Us9p [63]. Inhibition of the gE/gI-Us9p complex caused a reduction in the efficiency of the recruitment of KIF1A and KIF5C in PRV particles [61]. Diwaker *et al.* showed that the complex does not interact with both subunits of the motor protein simultaneously, as immunostaining revealed the motor proteins to bind to different populations [61]. The authors suggested that the complex first binds to KIF1A to carry PRV particles to the axon initial segment (AIS). Next, the motor protein is replaced with KIF5C, as the loading of KIF5C onto PRV cells was conditioned by the differentiation of cells [61]. Therefore, KIF1A and KIF5C activity are usurped by the viruses to ensure efficient viral promotion.

Noteworthy that Duraine *et al.* showed kinesin 1 heavy chains (KIF5A, KIF5B, and KIF5C) to be involved in the anterograde transport of HCV particles, as their inhibition resulted in an 84% decrease in transportation and inhibition of kinesin light chains (KLC1 and KLC2) resulted in an 87% decrease [63]. However, only a 6% decrease in the rate of anterograde transport was observed when kinesin 3 motor, KIF1A, was silenced [63].

1.4.3. Recruitment of kinesin 1 to mitochondria in the Alphaherpesvirinae family

Alphaherpesviruses cause a reduction in the kinetics of mitochondria in axons to promote viral infection efficiently [61]. Following PRV infection, an increase in Ca^{2+} is observed, caused by a rise in action potential [64]. Miro, a cellular protein sensitive to Ca^{2+}, prevents the recruitment of kinesin 1 heavy chain (kin-1 HC) to the mitochondria, as the binding of Ca^{2+} to Miro induces the release of kin-1 HC from the organelle [64]. The PRV infection was characterized by a decrease in anterograde transport of mitochondria, with the retrograde transport being predominant [64]. Hence, alphaherpesviruses cause an alteration of mitochondria kinetics involving kin-1 HC to ensure successful viral infection.

1.4.4. Tctex-1 (also known as DYNLT1) and the Flaviviridae family

Flaviviruses encompass the dengue virus (DENV), the West Nile virus (WNV), the Japanese encephalitis (JEV), and the yellow fever virus (YFV). They belong to the *Flaviviridae* family and are characterized by a positive single-stranded RNA. It encodes a polyprotein responsible for the production of viral proteins such as seven nonstructural

proteins, three structural proteins, an envelope protein (E), and a membrane protein (M) [65]. To produce viral particles, the membrane protein M is generated from the synthesized precursor protein preM [65]. The M protein comprises an ectoderm (ectoM) domain and two transmembrane domains (TMDs). Brault *et al.* revealed the C-terminal of ectoM to be involved in the assembly and entry of the virus [65]. Tctex-1, also known as DYNLT1, is the light chain of dynein [53]. The ectoM domain of WNV directly interacts with DYNLT-1, and a mutation at the fifth residue replacing glutamine with proline prevented the interaction. Thus, the mutation revealed the critical role of Gln5.

Furthermore, immunofluorescence analysis revealed that precursor M proteins localized near the nucleus where DYNLT-1 expression is high [65]. In the experiment, the inhibition of DYNLT-1 caused a decrease of ~65% in viral titres in DENV and ~70% in WNV [65]. Brault *et al.* suggested that the role of DYNLT-1 occurs at later stages of viral infection, as the inhibition of the motor protein did not significantly alter the number of infected cells [65]. Hence, DYNLT-1, a member of the dynein light chains family, encourages viral proliferation by binding to ectoM protein, and its action might occur at the late stages of the infection. Further studies are necessary to establish the role of dynein and the stage at which it is involved in the infection.

1.5. The function of dynein and kinesin in stimulating an immune response

Dynein and kinesin are involved in ensuring viral proliferation. However, both motor proteins have also been shown to engage in the immune response of host cells following viral infection.

1.5.1. MTOC and immunological synapse

The immunological synapse (IS) refers to the junction between T cells and an antigen-presenting cell (APC) [66]. The APC exposes the antigen to the T cell, activating the latter and resulting in an immune response. It involved cytokines release and caused the reorganization of T cell receptor (TCR) signalling molecules and the microtubule-organizing centre (MTOC) [10]. Cytoplasmic dynein has been shown to play a critical role in the translocation of the MTOC to the IS, as imaging analysis revealed MTs to engage in the MTOC repositioning. However, inhibition of dynein causes the prevention of MTOC transport to the IS [67-69]. Dynein is also involved in the transport of vesicles towards the MTOC before and after its translocation at the IS [70-72]. The aggregation of dynein at the IS requires the nuclear distribution E homolog 1 (NDE1), which might act as an anchor to allow the association of dynein to membranes [10, 71]. It is noteworthy that inhibition of NDE1 causes abrogation of MTOC translocation, indicating its critical role in the process [10]. Furthermore, the knockdown of CLIP-170, a key player in targeting dynein to the plus end, the cell periphery, causes a perturbation in the repositioning of the MTOC and prevents efficient activation of T cells [10]. Additionally, phosphorylation of CLIP-170 at Ser312 allows the relocation of MTOC and the complete activation of T cells [10].

1.5.2. Recruitment of dynein to the immunological synapse

Retrograde transport allows the delivery of lytic granules, which are secretory lysosomes, to release their contents, including a lytic protein called perforin, to the target cell at the IS [9, 73]. Following recognition of target cells, cytotoxic T lymphocytes (CTL)

reorganize actin and microtubules to cause the centrosome to polarize towards the IS [9, 73]. Dynein was shown to be involved in the centrosome's polarization [9, 67, 68]. Danielle *et al.* showed that the association between CTL and the inactive form of Rab7, a GTPase protein, was more significant than the inactive form of the protein [9]. Inhibition of Rab7 using siRNAs resulted in a decrease to more than 25% of the killing activity of CTLs and murine cells [9]. Western blot analysis indicated that Rab7 interacts with Rab interacting lysosomal protein (RILP) [9]. Cantalupo *et al.* revealed that RILP recruits dynein to the late endosome [74]. Depletion of Rab7 reduced the killing activity of CTL by 30% in both cells with over-expression of RILP and without over-expression of RILP, underlying the importance of Rab7 and that over-expression of RILP does not compensate depletion of Rab7 [9]. Furthermore, Danielle *et al.* found that the interaction between active Rab7 and RILP causes dynein recruitment to secretory lysosomes by the latter [9]. Thus, dynein is a key actor in the immune response of the host cell.

1.5.3. Transport of activator and costimulatory receptors

CD70 is the protein-ligand of CD27, a member of the TNF (Tumor Necrosis Factor) family, and the dimer CD27-CD70 engages in the T cell immune response [75]. Keller *et al.* revealed that the complex dynein-dynactin protein is involved in the movement of CD70, as indicated through immune-EM analysis. The analysis showed that CD70 vesicles aggregated at the perinuclear region toward the IS [75], indicating that dynein is involved in transporting a critical component of the IS.

Guanylate kinase-associated kinesin (GAKIN), a member of the kinesin 3 family, known as KIF13B [11], acts as an inhibitor of Caspase Recruitment Domain Family

Member 11 (CARD11). It is a key adaptor in T cell receptor (TCR) signaling to NF-κB and a recruiter of critical signaling proteins to the IS [76]. NF-κB, which is a transcription factor, is crucial in T (Thymus) and B (Bone marrow) cells for causing proliferation, survival, and effector functions of lymphocytes [76]. Reduction of GAKIN activity using RNA interference resulted in an augmented NF-κB activity [76], suggesting that a member of the kinesin 3 family is involved in regulating the activity of NF-κB.

1.5.4. KIF5B and GTP-binding protein ADP-ribosylation factor-like 8b (Arl8b) and NK-mediated cytotoxicity

The small G protein ADP-ribosylation factor-like 8b (Arl8b) belongs to the Arf-like family and interacts with the heavy chain of kinesin 1, KIF5B, through a connecting protein called SifA and kinesin-interacting protein (SKIP) [77]. The small G protein localizes at secretory lysosomes of NK cells [78]. The complex composed of KIF5B, Arl8b, and SKIP delivers lysosomes towards the cell's periphery through the anterograde transport [77]. Natural killer T (NKT) cells work in conjunction with Major Histocompatibility Complex class I (MHCI) proteins to carry the innate immune response [79]. Tuli *et al.* showed that Arl8b is a key player in NK (i.e., natural killer) cell-mediated cytotoxicity and MTOC polarization [78]. Inhibition of KIF5B and Arl8 impaired polarization of MTOC, indicating the critical contribution of both proteins to this vital step of the IS formation [78]. Thus, a member of kinesin 1 engages in the immune response of the host against viral infection.

1.5.5. KIF3A phosphorylation and suppression of the immune response in the Herpesviridae family

The Herpes Simplex Virus 1 (HSV-1) belongs to the Herpesviridae family [80] and is the causative agent of oral-facial infections [79, 80]. This enveloped virus utilizes its US3 viral protein kinase for the downregulation of CD1d at the surface of APCs to evade NKT immune response [79, 81, 82]. The kinesin-2 subfamilies consist of KIF3A, KIF3B/C, and KIF17 [8]. Inhibition of KIF3A, a member of the kinesin superfamily, using siRNA and dominant-negative mutation knockdown resulted in the impairment of the delivery of viral genome from late endosome to the periphery of the cell [79]. Furthermore, the blockage of KIF3A using shKIF3A shRNA caused a reduction in the expression of CD1d, indicating the involvement of KIF3A in the expression of CD1d [79]. Immunofluorescence results and coprecipitation of US3K220A with KIF3A showed that US3 directly interacts with KIF3A [79]. Phosphorylation assays and mutational studies revealed that US3 directly phosphorylates the C-terminus of KIF3A at residue Ser687 [79]. This phosphorylation is critical to the downregulation of CD1d, as Ser687Ala mutation completely inhibited the downregulation of CD1d in infected cells [79]. Hence, HSV-1 evades immune response through downregulation of CD1d, a critical APC molecule, via phosphorylation of KIF3A [79].

1.6. Conclusion

Motor proteins, kinesin, and dynein are actively involved in the three stages of viral infection and in the host's immune response to suppress viral infection. The retrograde transport of viral genome during infection of viruses such as the polyomavirus simian virus 40 [14], the Hepatitis B [32], the porcine circovirus [39], engage different subunits of kinesin and dynein to ensure the efficient delivery of viral proteins from the plasma membrane to the perinuclear region of the host cells. Although dynein is the motor protein responsible for anterograde transport, kinesin is also involved in the transport of viral particles towards the perinuclear region [14].

Kinesin light chains 1 and 2 (KLC1/2) and dynein light chain 1 (DLC1) both play critical roles to favor the nuclear entry of viral particles [56, 57]. Through binding to the virion protein pIX, KLC1/2 engages in uncoating adenovirus and disrupts the Nuclear Pore Complex (NPC) [56]. DLC1 facilitates transcription of the rabies virus in acting as a transcription factor by binding to viral proteins, P and L, to ensure viral replication [57]. Several subfamilies of kinesin, such as KIF13A [58], KIF18A [60], KIF1A [61], and KIF5C [61], as well as DYNLT-1 [65], play critical roles in the anterograde transport of viral particles for the efficient proliferation of several viruses.

Kinesin and dynein are not only involved in promoting viral infection during retrograde and anterograde transport but also in the defensive response of the immune system. Dynein is recruited at the immunological synapse (IS), where T cells join APCs to execute an efficient immunological response to viral infection [66]. Dynein delivers CD70 vesicles to the IS, and GAKIN regulates the activity of NF-κB [75]. To ensure NK-

cytotoxicity, the heavy chain of kinesin 1 (KIF5B) forms a complex with Arl8 and SKIP to deliver lysosomes to the cell's periphery [78]. However, NKT immune response can be evaded through phosphorylation of KIF3A by downregulation of CD1d, a critical APC molecule by the HSV-1 [79].

The function of motor proteins kinesin and dynein in facilitating viral proliferation makes these proteins a target for drug discovery. However, the involvement of the motor proteins in stimulating the host's immune response indicates that inhibition of these proteins might also impact the defensive reaction of host cells. Thus, studies exploring the role of dynein and kinesin in infected cells and immune cells require further investigations to elucidate how to regulate either of their dual functions discussed in this chapter.

Bibliography

1. Robinson CM, Pfeiffer JK. Viruses and the Microbiota. Annual Review of Virology. **2014**;1(1):55-69. doi: 10.1146/annurev-virology-031413-085550.

2. Ryu W-S. Chapter 2 - Virus Structure. In: Ryu W-S, editor. Molecular Virology of Human Pathogenic Viruses. Boston: Academic Press; **2017**. p. 21-9.

3. Ryu W-S. Virus Life Cycle. Molecular Virology of Human Pathogenic Viruses. **2017**:31-45. Epub 2016/05/06. doi: 10.1016/B978-0-12-800838-6.00003-5. PubMed PMID: PMC7158286.

4. Merino-Gracia J, García-Mayoral MF, Rodríguez-Crespo I. The association of viral proteins with host cell dynein components during virus infection. Febs j. **2011**;278(17):2997-3011. Epub 2011/07/23. doi: 10.1111/j.1742-4658.2011.08252.x. PubMed PMID: 21777384; PubMed Central PMCID: PMCPMC7164101.

5. Steinman JB, Kapoor TM. 8 - Chemical probes for dynein. In: King SM, editor. Dyneins: Structure, Biology and Disease (Second Edition): Academic Press; **2018**. p. 172-91.

6. Cho YB, Hong S, Kang KW, Kang JH, Lee SM, Seo YJ. Selective and ATP-competitive kinesin KIF18A inhibitor suppresses the replication of influenza A virus. J Cell Mol Med. **2020**;24(10):5463-75. Epub 2020/04/08. doi: 10.1111/jcmm.15200. PubMed PMID: 32253833; PubMed Central PMCID: PMCPMC7214149.

7. Chen XJ, Xu H, Cooper HM, Liu Y. Cytoplasmic dynein: a key player in neurodegenerative and neurodevelopmental diseases. Sci China Life Sci. **2014**;57(4):372-7. Epub 2014/03/26. doi: 10.1007/s11427-014-4639-9. PubMed PMID: 24664850.

8. Miki H, Okada Y, Hirokawa N. Analysis of the kinesin superfamily: insights into structure and function. Trends Cell Biol. **2005**;15(9):467-76. Epub 2005/08/09. doi: 10.1016/j.tcb.2005.07.006. PubMed PMID: 16084724.

9. Daniele T, Hackmann Y, Ritter AT, Wenham M, Booth S, Bossi G, et al. A role for Rab7 in the movement of secretory granules in cytotoxic T lymphocytes. Traffic. **2011**;12(7):902-11. Epub 2011/03/29. doi: 10.1111/j.1600-0854.2011.01194.x. PubMed PMID: 21438969; PubMed Central PMCID: PMCPMC4116565.

10. Lim WM, Ito Y, Sakata-Sogawa K, Tokunaga M. CLIP-170 is essential for MTOC repositioning during T cell activation by regulating dynein localisation on the cell surface. Sci Rep. **2018**;8(1):17447. Epub 2018/11/30. doi: 10.1038/s41598-018-35593-z. PubMed PMID: 30487641; PubMed Central PMCID: PMCPMC6261991.

11. Mills J, Hanada T, Hase Y, Liscum L, Chishti AH. LDL receptor related protein 1 requires the I3 domain of discs-large homolog 1/DLG1 for interaction with the kinesin motor protein KIF13B. Biochimica et Biophysica Acta (BBA) - Molecular Cell Research. **2019**;1866(12):118552. doi: https://doi.org/10.1016/j.bbamcr.2019.118552.

12. Sweet BH, Hilleman MR. The vacuolating virus, S.V. 40. Proc Soc Exp Biol Med. **1960**;105:420-7. Epub 1960/11/01. doi: 10.3181/00379727-105-26128. PubMed PMID: 13774265.

13. Garcea RL, Imperiale MJ. Simian virus 40 infection of humans. Journal of virology. **2003**;77(9):5039-45. doi: 10.1128/jvi.77.9.5039-5045.2003. PubMed PMID: 12692206.

14. Ravindran MS, Engelke MF, Verhey KJ, Tsai B. Exploiting the kinesin-1 molecular motor to generate a virus membrane penetration site. Nat Commun. **2017**;8:15496. Epub 2017/05/26. doi: 10.1038/ncomms15496. PubMed PMID: 28537258; PubMed Central PMCID: PMCPMC5458101.

15. White MK, Gordon J, Khalili K. The rapidly expanding family of human polyomaviruses: recent developments in understanding their life cycle and role in human pathology. PLoS Pathog. **2013**;9(3):e1003206. Epub 2013/03/22. doi: 10.1371/journal.ppat.1003206. PubMed PMID: 23516356; PubMed Central PMCID: PMCPMC3597531.

16. White MK, Gordon J, Khalili K. The Rapidly Expanding Family of Human Polyomaviruses: Recent Developments in Understanding Their Life Cycle and Role in Human Pathology. PLOS Pathogens. **2013**;9(3):e1003206. doi: 10.1371/journal.ppat.1003206.

17. Tsai B, Gilbert JM, Stehle T, Lencer W, Benjamin TL, Rapoport TA. Gangliosides are receptors for murine polyoma virus and SV40. EMBO J. **2003**;22(17):4346-55. doi: 10.1093/emboj/cdg439. PubMed PMID: 12941687.

18. Engel S, Heger T, Mancini R, Herzog F, Kartenbeck J, Hayer A, et al. Role of Endosomes in Simian Virus 40 Entry and Infection. Journal of Virology. **2011**;85(9):4198. doi: 10.1128/JVI.02179-10.

19. Qian M, Cai D, Verhey KJ, Tsai B. A lipid receptor sorts polyomavirus from the endolysosome to the endoplasmic reticulum to cause infection. PLoS Pathog. **2009**;5(6):e1000465. Epub 2009/06/09. doi: 10.1371/journal.ppat.1000465. PubMed PMID: 19503604; PubMed Central PMCID: PMCPMC2685006.

20. Rainey-Barger EK, Magnuson B, Tsai B. A chaperone-activated nonenveloped virus perforates the physiologically relevant endoplasmic reticulum membrane. Journal of virology. **2007**;81(23):12996-3004. Epub 2007/09/19. doi: 10.1128/JVI.01037-07. PubMed PMID: 17881435.

21. Goodwin EC, Lipovsky A, Inoue T, Magaldi TG, Edwards APB, Van Goor KEY, et al. BiP and Multiple DNAJ Molecular Chaperones in the Endoplasmic Reticulum Are Required for Efficient Simian Virus 40 Infection. mBio. **2011**;2(3):e00101-11. doi: 10.1128/mBio.00101-11.

22. Schelhaas M, Malmström J, Pelkmans L, Haugstetter J, Ellgaard L, Grünewald K, et al. Simian Virus 40 depends on ER protein folding and quality control factors for entry into host cells. Cell. **2007**;131(3):516-29. Epub 2007/11/06. doi: 10.1016/j.cell.2007.09.038. PubMed PMID: 17981119.

23. Kartenbeck J, Stukenbrok H, Helenius A. Endocytosis of simian virus 40 into the endoplasmic reticulum. Journal of Cell Biology. **1989**;109(6):2721-9. doi: 10.1083/jcb.109.6.2721.

24. Carter AP. Crystal clear insights into how the dynein motor moves. J Cell Sci. **2013**;126(Pt 3):705-13. Epub 2013/03/26. doi: 10.1242/jcs.120725. PubMed PMID: 23525020.

25. Ravindran MS, Spriggs CC, Verhey KJ, Tsai B. Dynein Engages and Disassembles Cytosol-Localized Simian Virus 40 To Promote Infection. J Virol. **2018**;92(12). Epub 2018/03/30. doi: 10.1128/jvi.00353-18. PubMed PMID: 29593037; PubMed Central PMCID: PMCPMC5974495.

26. Zila V, Difato F, Klimova L, Huerfano S, Forstova J. Involvement of microtubular network and its motors in productive endocytic trafficking of mouse polyomavirus. PLoS One. **2014**;9(5):e96922. Epub 2014/05/09. doi: 10.1371/journal.pone.0096922. PubMed PMID: 24810588; PubMed Central PMCID: PMCPMC4014599.

27. Luthra P, Jordan DS, Leung DW, Amarasinghe GK, Basler CF. Ebola virus VP35 interaction with dynein LC8 regulates viral RNA synthesis. J Virol. **2015**;89(9):5148-53. Epub 2015/03/06. doi: 10.1128/jvi.03652-14. PubMed PMID: 25741013; PubMed Central PMCID: PMCPMC4403485.

28. Jespersen NE, Leyrat C, Gérard FC, Bourhis JM, Blondel D, Jamin M, et al. The LC8-RavP ensemble Structure Evinces A Role for LC8 in Regulating Lyssavirus Polymerase Functionality. J Mol Biol. **2019**;431(24):4959-77. Epub 2019/10/22. doi: 10.1016/j.jmb.2019.10.011. PubMed PMID: 31634467; PubMed Central PMCID: PMCPMC7060403.

29. Jayappa KD, Ao Z, Wang X, Mouland AJ, Shekhar S, Yang X, et al. Human immunodeficiency virus type 1 employs the cellular dynein light chain 1 protein for reverse transcription through interaction with its integrase protein. J Virol. **2015**;89(7):3497-511. Epub 2015/01/09. doi: 10.1128/jvi.03347-14. PubMed PMID: 25568209; PubMed Central PMCID: PMCPMC4403391.

30. Basler CF, Wang X, Mühlberger E, Volchkov V, Paragas J, Klenk H-D, et al. The Ebola virus VP35 protein functions as a type I IFN antagonist. Proceedings of the National Academy of Sciences. **2000**;97(22):12289. doi: 10.1073/pnas.220398297.

31. Leung DW, Prins KC, Basler CF, Amarasinghe GK. Ebolavirus VP35 is a multifunctional virulence factor. Virulence. **2010**;1(6):526-31. doi: 10.4161/viru.1.6.12984.

32. Osseman Q, Gallucci L, Au S, Cazenave C, Berdance E, Blondot ML, et al. The chaperone dynein LL1 mediates cytoplasmic transport of empty and mature hepatitis B virus capsids. J Hepatol. **2018**;68(3):441-8. Epub 2017/11/09. doi: 10.1016/j.jhep.2017.10.032. PubMed PMID: 29113909.

33. Rabe B, Glebe D, Kann M. Lipid-Mediated Introduction of Hepatitis B Virus Capsids into Nonsusceptible Cells Allows Highly Efficient Replication and Facilitates the Study of Early Infection Events. Journal of Virology. **2006**;80(11):5465. doi: 10.1128/JVI.02303-05.

34. Königer C, Wingert I, Marsmann M, Rösler C, Beck J, Nassal M. Involvement of the host DNA-repair enzyme TDP2 in formation of the covalently closed circular DNA persistence reservoir of hepatitis B viruses. Proceedings of the National Academy of Sciences. **2014**;111(40):E4244. doi: 10.1073/pnas.1409986111.

35. Qi Y, Gao Z, Xu G, Peng B, Liu C, Yan H, et al. DNA Polymerase κ Is a Key Cellular Factor for the Formation of Covalently Closed Circular DNA of Hepatitis B Virus. PLOS Pathogens. **2016**;12(10):e1005893. doi: 10.1371/journal.ppat.1005893.

36. Quasdorff M, Protzer U. Control of hepatitis B virus at the level of transcription. Journal of Viral Hepatitis. **2010**;17(8):527-36. doi: https://doi.org/10.1111/j.1365-2893.2010.01315.x.

37. Seeger C, Mason WS. Hepatitis B virus biology. Microbiol Mol Biol Rev. **2000**;64(1):51-68. Epub 2000/03/08. doi: 10.1128/mmbr.64.1.51-68.2000. PubMed PMID: 10704474; PubMed Central PMCID: PMCPMC98986.

38. Ning X, Nguyen D, Mentzer L, Adams C, Lee H, Ashley R, et al. Secretion of Genome-Free Hepatitis B Virus – Single Strand Blocking Model for Virion Morphogenesis of Para-retrovirus. PLOS Pathogens. **2011**;7(9):e1002255. doi: 10.1371/journal.ppat.1002255.

39. Cao J, Lin C, Wang H, Wang L, Zhou N, Jin Y, et al. Circovirus transport proceeds via direct interaction of the cytoplasmic dynein IC1 subunit with the viral capsid protein. J Virol. **2015**;89(5):2777-91. Epub 2014/12/30. doi: 10.1128/jvi.03117-14. PubMed PMID: 25540360; PubMed Central PMCID: PMCPMC4325748.

40. Theerawatanasirikul S, Phecharat N, Prawettongsopon C, Chaicumpa W, Lekcharoensuk P. Dynein light chain DYNLL1 subunit facilitates porcine circovirus type 2 intracellular transports along microtubules. Arch Virol. **2017**;162(3):677-86. Epub 2016/11/20. doi: 10.1007/s00705-016-3140-0. PubMed PMID: 27858289.

41. Hamel AL, Lin LL, Nayar GP. Nucleotide sequence of porcine circovirus associated with postweaning multisystemic wasting syndrome in pigs. J Virol. **1998**;72(6):5262-7. Epub 1998/05/30. doi: 10.1128/jvi.72.6.5262-5267.1998. PubMed PMID: 9573301; PubMed Central PMCID: PMCPMC110114.

42. Zhou JY, Chen QX, Ye JX, Shen HG, Chen TF, Shang SB. Serological Investigation and Genomic Characterization of PCV2 Isolates from Different Geographic Regions of Zhejiang Province in China. Veterinary Research Communications. **2006**;30(2):205-20. doi: 10.1007/s11259-006-3203-x.

43. Liu J, Chen I, Kwang J. Characterization of a Previously Unidentified Viral Protein in Porcine Circovirus Type 2-Infected Cells and Its Role in Virus-Induced Apoptosis. Journal of Virology. **2005**;79(13):8262. doi: 10.1128/JVI.79.13.8262-8274.2005.

44. He J, Cao J, Zhou N, Jin Y, Wu J, Zhou J. Identification and Functional Analysis of the Novel ORF4 Protein Encoded by Porcine Circovirus Type 2. Journal of Virology. **2013**;87(3):1420. doi: 10.1128/JVI.01443-12.

45. Sánchez-Paz A. White spot syndrome virus: an overview on an emergent concern. Vet Res. **2010**;41(6):43-. Epub 2010/02/26. doi: 10.1051/vetres/2010015. PubMed PMID: 20181325.

46. Feng J, Tang X, Zhan W. Cloning and characterization of cytoplasmic dynein intermediate chain in Fenneropenaeus chinensis and its essential role in white spot syndrome virus infection. Fish Shellfish Immunol. **2014**;39(2):407-14. Epub 2014/06/14. doi: 10.1016/j.fsi.2014.05.034. PubMed PMID: 24925758.

47. Eyre NS, Fiches GN, Aloia AL, Helbig KJ, McCartney EM, McErlean CS, et al. Dynamic imaging of the hepatitis C virus NS5A protein during a productive infection. J Virol. **2014**;88(7):3636-52. Epub 2014/01/17. doi: 10.1128/jvi.02490-13. PubMed PMID: 24429364; PubMed Central PMCID: PMCPMC3993538.

48. Firestone AJ, Weinger JS, Maldonado M, Barlan K, Langston LD, O'Donnell M, et al. Small-molecule inhibitors of the AAA+ ATPase motor cytoplasmic dynein. Nature. **2012**;484(7392):125-9. doi: 10.1038/nature10936. PubMed PMID: 22425997.

49. Shrivastava N, Sripada S, Kaur J, Shah PS, Cecilia D. Insights into the internalization and retrograde trafficking of Dengue 2 virus in BHK-21 cells. PLoS One. **2011**;6(10):e25229. Epub 2011/10/13. doi: 10.1371/journal.pone.0025229. PubMed PMID: 21991304; PubMed Central PMCID: PMCPMC3186794.

50. Wang SH, Syu WJ, Huang KJ, Lei HY, Yao CW, King CC, et al. Intracellular localization and determination of a nuclear localization signal of the core protein of dengue virus. J Gen Virol. **2002**;83(Pt 12):3093-102. Epub 2002/12/06. doi: 10.1099/0022-1317-83-12-3093. PubMed PMID: 12466486.

51. Zaichick SV, Bohannon KP, Hughes A, Sollars PJ, Pickard GE, Smith GA. The herpesvirus VP1/2 protein is an effector of dynein-mediated capsid transport and neuroinvasion. Cell Host Microbe. **2013**;13(2):193-203. Epub 2013/02/19. doi: 10.1016/j.chom.2013.01.009. PubMed PMID: 23414759; PubMed Central PMCID: PMCPMC3808164.

52. Kramer T, Greco TM, Taylor MP, Ambrosini AE, Cristea IM, Enquist LW. Kinesin-3 mediates axonal sorting and directional transport of alphaherpesvirus particles in neurons. Cell Host Microbe. **2012**;12(6):806-14. Epub 2012/12/19. doi: 10.1016/j.chom.2012.10.013. PubMed PMID: 23245325; PubMed Central PMCID: PMCPMC3527838.

53. Schneider MA, Spoden GA, Florin L, Lambert C. Identification of the dynein light chains required for human papillomavirus infection. Cell Microbiol. **2011**;13(1):32-

46. Epub 2010/12/21. doi: 10.1111/j.1462-5822.2010.01515.x. PubMed PMID: 21166973.

54. Opazo T, Garcés A, Tapia D, Barraza F, Bravo A, Schwenke T, et al. Functional Evidence of the Involvement of the Dynein Light Chain DYNLRB2 in Murine Leukemia Virus Infection. J Virol. **2017**;91(10). Epub 2017/03/03. doi: 10.1128/jvi.00129-17. PubMed PMID: 28250122; PubMed Central PMCID: PMCPMC5411577.

55. Valle-Tenney R, Opazo T, Cancino J, Goff SP, Arriagada G. Dynein Regulators Are Important for Ecotropic Murine Leukemia Virus Infection. Journal of Virology. **2016**;90(15):6896. doi: 10.1128/JVI.00863-16.

56. Strunze S, Engelke MF, Wang IH, Puntener D, Boucke K, Schleich S, et al. Kinesin-1-mediated capsid disassembly and disruption of the nuclear pore complex promote virus infection. Cell Host Microbe. **2011**;10(3):210-23. Epub 2011/09/20. doi: 10.1016/j.chom.2011.08.010. PubMed PMID: 21925109.

57. Bauer A, Nolden T, Nemitz S, Perlson E, Finke S. A Dynein Light Chain 1 Binding Motif in Rabies Virus Polymerase L Protein Plays a Role in Microtubule Reorganization and Viral Primary Transcription. Journal of Virology. **2015**;89(18):9591. doi: 10.1128/JVI.01298-15.

58. Ramos-Nascimento A, Kellen B, Ferreira F, Alenquer M, Vale-Costa S, Raposo G, et al. KIF13A mediates trafficking of influenza A virus ribonucleoproteins. J Cell Sci. **2017**;130(23):4038-50. Epub 2017/10/25. doi: 10.1242/jcs.210807. PubMed PMID: 29061883.

59. Soppina V, Norris SR, Dizaji AS, Kortus M, Veatch S, Peckham M, et al. Dimerization of mammalian kinesin-3 motors results in superprocessive motion.

Proceedings of the National Academy of Sciences. **2014**;111(15):5562. doi: 10.1073/pnas.1400759111.

60. Fehling SK, Noda T, Maisner A, Lamp B, Conzelmann KK, Kawaoka Y, et al. The microtubule motor protein KIF13A is involved in intracellular trafficking of the Lassa virus matrix protein Z. Cell Microbiol. **2013**;15(2):315-34. Epub 2013/01/03. doi: 10.1111/cmi.12095. PubMed PMID: 23279019.

61. Diwaker D, Murray JW, Barnes J, Wolkoff AW, Wilson DW. Deletion of the Pseudorabies Virus gE/gI-US9p complex disrupts kinesin KIF1A and KIF5C recruitment during egress, and alters the properties of microtubule-dependent transport in vitro. PLoS Pathog. **2020**;16(6):e1008597. Epub 2020/06/09. doi: 10.1371/journal.ppat.1008597. PubMed PMID: 32511265; PubMed Central PMCID: PMCPMC7302734.

62. Kratchmarov R, Taylor MP, Enquist LW. Role of Us9 phosphorylation in axonal sorting and anterograde transport of pseudorabies virus. PLoS One. **2013**;8(3):e58776. Epub 2013/03/26. doi: 10.1371/journal.pone.0058776. PubMed PMID: 23527020; PubMed Central PMCID: PMCPMC3602541.

63. DuRaine G, Wisner TW, Howard P, Johnson DC. Kinesin-1 Proteins KIF5A, -5B, and -5C Promote Anterograde Transport of Herpes Simplex Virus Enveloped Virions in Axons. J Virol. **2018**;92(20). Epub 2018/08/03. doi: 10.1128/jvi.01269-18. PubMed PMID: 30068641; PubMed Central PMCID: PMCPMC6158419.

64. Kramer T, Enquist LW. Alphaherpesvirus infection disrupts mitochondrial transport in neurons. Cell host & microbe. **2012**;11(5):504-14. doi: 10.1016/j.chom.2012.03.005. PubMed PMID: 22607803.

65. Brault JB, Kudelko M, Vidalain PO, Tangy F, Desprès P, Pardigon N. The interaction of flavivirus M protein with light chain Tctex-1 of human dynein plays a role in late stages of virus replication. Virology. **2011**;417(2):369-78. Epub 2011/07/20. doi: 10.1016/j.virol.2011.06.022. PubMed PMID: 21767858.

66. Onnis A, Baldari CT. Orchestration of Immunological Synapse Assembly by Vesicular Trafficking. Frontiers in Cell and Developmental Biology. **2019**;7(110). doi: 10.3389/fcell.2019.00110.

67. Combs J, Kim SJ, Tan S, Ligon LA, Holzbaur EL, Kuhn J, et al. Recruitment of dynein to the Jurkat immunological synapse. Proc Natl Acad Sci U S A. **2006**;103(40):14883-8. Epub 2006/09/23. doi: 10.1073/pnas.0600914103. PubMed PMID: 16990435; PubMed Central PMCID: PMCPMC1595445.

68. Martín-Cófreces NB, Robles-Valero J, Cabrero JR, Mittelbrunn M, Gordón-Alonso M, Sung C-H, et al. MTOC translocation modulates IS formation and controls sustained T cell signaling. J Cell Biol. **2008**;182(5):951-62. doi: 10.1083/jcb.200801014. PubMed PMID: 18779373.

69. Yi J, Wu X, Chung AH, Chen JK, Kapoor TM, Hammer JA. Centrosome repositioning in T cells is biphasic and driven by microtubule end-on capture-shrinkage. J Cell Biol. **2013**;202(5):779-92. Epub 2013/08/28. doi: 10.1083/jcb.201301004. PubMed PMID: 23979719; PubMed Central PMCID: PMCPMC3760611.

70. Mentlik AN, Sanborn KB, Holzbaur EL, Orange JS. Rapid lytic granule convergence to the MTOC in natural killer cells is dependent on dynein but not cytolytic commitment. Mol Biol Cell. **2010**;21(13):2241-56. Epub 2010/05/07. doi:

10.1091/mbc.e09-11-0930. PubMed PMID: 20444980; PubMed Central PMCID: PMCPMC2893988.

71. Nath S, Christian L, Tan SY, Ki S, Ehrlich LI, Poenie M. Dynein Separately Partners with NDE1 and Dynactin To Orchestrate T Cell Focused Secretion. J Immunol. **2016**;197(6):2090-101. Epub 2016/08/19. doi: 10.4049/jimmunol.1600180. PubMed PMID: 27534551; PubMed Central PMCID: PMCPMC5010990.

72. Poenie M, Kuhn J, Combs J. Real-time visualization of the cytoskeleton and effector functions in T cells. Curr Opin Immunol. **2004**;16(4):428-38. doi: 10.1016/j.coi.2004.05.016. PubMed PMID: 15245735.

73. Stinchcombe JC, Griffiths GM. Secretory mechanisms in cell-mediated cytotoxicity. Annu Rev Cell Dev Biol. **2007**;23:495-517. Epub 2007/05/18. doi: 10.1146/annurev.cellbio.23.090506.123521. PubMed PMID: 17506701.

74. Cantalupo G, Alifano P, Roberti V, Bruni CB, Bucci C. Rab-interacting lysosomal protein (RILP): the Rab7 effector required for transport to lysosomes. EMBO J. **2001**;20(4):683-93. Epub 2001/02/17. doi: 10.1093/emboj/20.4.683. PubMed PMID: 11179213; PubMed Central PMCID: PMCPMC145419.

75. Keller AM, Groothuis TA, Veraar EA, Marsman M, Maillette de Buy Wenniger L, Janssen H, et al. Costimulatory ligand CD70 is delivered to the immunological synapse by shared intracellular trafficking with MHC class II molecules. Proc Natl Acad Sci U S A. **2007**;104(14):5989-94. Epub 2007/03/29. doi: 10.1073/pnas.0700946104. PubMed PMID: 17389361; PubMed Central PMCID: PMCPMC1851604.

76. Lamason RL, Kupfer A, Pomerantz JL. The dynamic distribution of CARD11 at the immunological synapse is regulated by the inhibitory kinesin GAKIN. Mol Cell.

2010;40(5):798-809. Epub 2010/12/15. doi: 10.1016/j.molcel.2010.11.007. PubMed PMID: 21145487; PubMed Central PMCID: PMCPMC3032410.

77. Rosa-Ferreira C, Munro S. Arl8 and SKIP act together to link lysosomes to kinesin-1. Dev Cell. **2011**;21(6):1171-8. Epub 2011/12/17. doi: 10.1016/j.devcel.2011.10.007. PubMed PMID: 22172677; PubMed Central PMCID: PMCPMC3240744.

78. Tuli A, Thiery J, James AM, Michelet X, Sharma M, Garg S, et al. Arf-like GTPase Arl8b regulates lytic granule polarization and natural killer cell-mediated cytotoxicity. Mol Biol Cell. **2013**;24(23):3721-35. Epub 2013/10/04. doi: 10.1091/mbc.E13-05-0259. PubMed PMID: 24088571; PubMed Central PMCID: PMCPMC3842998.

79. Xiong R, Rao P, Kim S, Li M, Wen X, Yuan W. Herpes Simplex Virus 1 US3 Phosphorylates Cellular KIF3A To Downregulate CD1d Expression. J Virol. **2015**;89(13):6646-55. Epub 2015/04/17. doi: 10.1128/jvi.00214-15. PubMed PMID: 25878107; PubMed Central PMCID: PMCPMC4468489.

80. Arduino PG, Porter SR. Herpes Simplex Virus Type 1 infection: overview on relevant clinico-pathological features*. Journal of Oral Pathology & Medicine. **2008**;37(2):107-21. doi: https://doi.org/10.1111/j.1600-0714.2007.00586.x.

81. Yuan W, Dasgupta A, Cresswell P. Herpes simplex virus evades natural killer T cell recognition by suppressing CD1d recycling. Nature Immunology. **2006**;7(8):835-42. doi: 10.1038/ni1364.

82. Rao P, Pham Hong T, Kulkarni A, Yang Y, Liu X, Knipe David M, et al. Herpes Simplex Virus 1 Glycoprotein B and US3 Collaborate To Inhibit CD1d Antigen

Presentation and NKT Cell Function. Journal of Virology. **2011**;85(16):8093-104. doi: 10.1128/JVI.02689-10.

CHAPTER 2

Analysis of the Structural Mechanism of ATP Inhibition at the AAA1 Subunit of Cytoplasmic Dynein-1 Using a Chemical "Toolkit"

2.1. Introduction

Motor proteins, dynein, kinesin, and myosin, in eukaryotic cells are responsible for transporting cargoes within cells [1]. Dynein and kinesin perform their function in conjunction with the cytoskeletal protein microtubule (MT) [1]. MTs comprise 11–16 protofilament biopolymers [2] consisting of αβ-heterodimer proteins [1,3]. Nine subfamilies compose the dynein family, namely, seven axonemal and two cytoplasmic, dynein 1 and dynein 2 [4]. Cytoplasmic dynein 1 drives retrograde axonal transport [5] and also plays a role in the mitosis process of cell division [1].

Cytoplasmic dynein 2 guarantees transportation of cargoes through MTs in flagella, as well as motile and primary cilia [6,7]. This isoform is also referred to as intraflagellar transport (IFT) dynein [6,7]. IFT is critical to the Hedgehog pathway (Hh pathway), which is an essential mediator during the development of the embryo and oncogenesis [8]. It facilitates anterograde and retrograde trafficking of transcription factors such as Gli1 and Gli2 during the Hh pathway [9,10]. Impairment of dynein 2 could disturb the Hh pathway since it is involved in IFT [6,7]. Inhibitors of dynein such as ciliobrevin analogues cause the inhibition of the Hh pathway [10]. Dynein malfunction can promote cancer cell proliferation [7], as dynein 2 is involved in the Hh pathway and oncogenesis process [6].

Defects in the heavy chain of dynein are associated with neurodegenerative diseases (NDDs) [11], characterized by the degradation of neurons. NDDs refer to an array of neurological disorders, including Parkinson's disease (PD), Huntington's disease (HD), Alzheimer's disease (AD), and motor neuron diseases [5]. Three common features observed in the NDDs are the presence of protein aggregates, the involvement of nonautonomous factors, and the dysfunction in axonal transport [5]. PD is characterized by the death of dopaminergic cell groups producing dopamine in the substantia nigra, which results in symptoms such as resting tremors, bradykinesia, and rigidity of limbs [5]. HD is a condition associated with disturbance in muscle coordination and cognitive impairment caused by a polyglutamate fragment on the huntingtin protein resulting from the repetition of the CAG codon in exon 1 of the gene responsible for the mentioned protein [5,11]. Both PD and HD affect basal ganglia in the brain [5]. The occurrence of axonal dystrophy in the brain of patients with PD indicates abnormalities in axonal

transport. Dysfunction of the axonal transport, observed in animal and cellular models, represents indirect evidence of dynein involvement in PD and HD pathologies. Dysfunction of dynein causes the Golgi apparatus to fragmentize, a phenomenon observed in the brain of patients with PD, as well as cellular and animal models of PD and HD [5]. AD, affecting 25 million individuals globally, is characterized by progressive deterioration of memory that results in this pathology and the loss of cognitive abilities, poor judgment, and speech impairment [11]. AD is marked by the presence of clusters of misfolded proteins, i.e., amyloid plaques consisting primarily of amyloid β peptides (Aβ) in the brain of patients with AD [5]. Indirect evidence obtained through the knockdown of dynein, causing an increase in Aβ peptides, suggested the involvement of dynein in AD; however, further experiments are needed to exhibit a direct correlation between dynein activity and AD [5]. Eyre *et al.* revealed that dynein plays an essential role in the transportation of NS5A, a hepatitis C viral protein, inside cells. Dynein ensures the efficient replication of the virus, as well as the assembly of virions [6]. Chapter 1 extensively explores the function of dynein in viral proliferation and immune response.

Dynein was discovered before kinesin [4]; however, the former has been more challenging than the latter to solve its three-dimensional structure and to understand the exact mechanism of action of its multidomain construction. Indeed, the complexities result from its massive size, its two heavy chains of each 530 kDa [7]. Despite the complexity of dynein structure, characterization of some of its substructures or domains utilizing X-ray crystallography, electron microscopy, and mutagenesis studies have provided insights into its function and role in the cell [7]. Dynein is a homodimer protein [1], composed of two heavy chains (HCs), each 530 kDa, two light intermediate chains

(LICs), each 74 kDa, four intermediate chains (IC) with weight varying between 53 kDa and 59 kDa each, and six light chains (LCs), each 10–14 kDa [11]. The heavy chain of dynein consists of the tail, the linker, the hexameric head, the buttress, the stalk domains, and the microtubule- binding domain (MTBD) [12,13]. The N-terminus of dynein, representing approximately one-third of the 530 kDa heavy chain, constitutes the tail and the linker [1,14] (Figure 2.1).

The tail of the heavy chain of dynein represents the site for cargo binding, where the dimerization of both monomers occurs [1]. The tail also binds to the LICs and ICs [1,5]. The linker domain follows the tail and is thought to be involved in a force-generating process as its position changes upon binding of ATP, resulting in the motility of dynein [1]. The stalk of ~10–15 nm in length is attached to the MTBD at the C-terminus [15]. It is linked to and supported by the buttress [1] (Figure 2.1A).

The head or motor domain of dynein is comprised of six AAA+ subunits, four of which (AAA1 to AAA4) possess a nucleotide-binding site at the interface between one subdomain and the subsequent subdomain; the AAA1 nucleotide-binding site is enclosed between the AAA1 and AAA2 subdomains [1,12]. Three of the four binding sites, AAA1, AAA3, and AAA4, present the ability to hydrolyze ATP [1,12]. Each of the six AAA+ subdomains encompasses a small and a large subunit linked by a flexible unfolded segment [1] (Figures 2.1B and 2.2B).

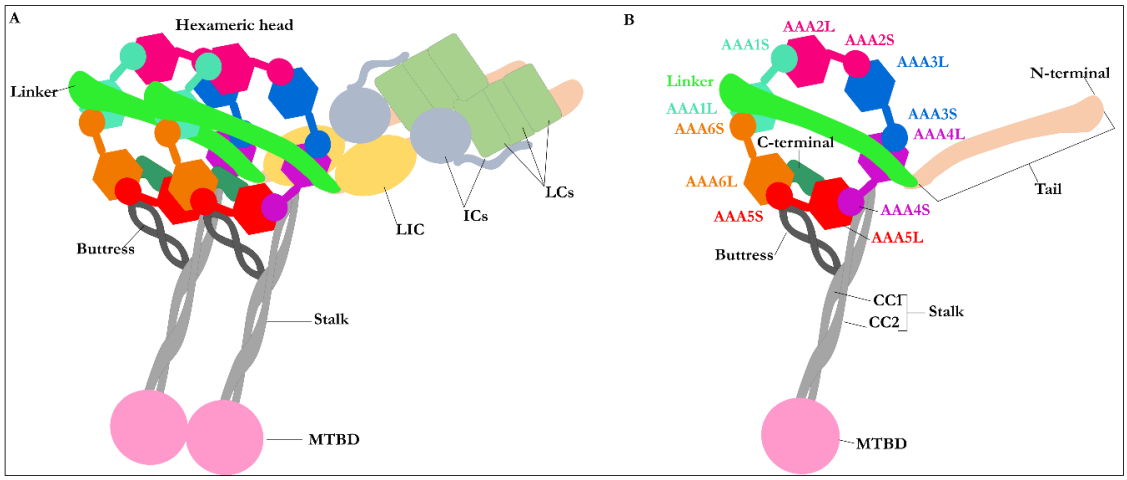

Figure 2.1: The multidomain structure of cytoplasmic dynein. (**A**) Schematic representation of the homodimer cytoplasmic dynein. For simplicity, only one monomer is labeled. The homodimer represents two heavy chains, two LICs, four ICs, and six LCs. Each set of the two heavy chains consists of a tail, a linker, a hexameric head, a buttress, a stalk, and an MTBD. The figures (e.g., the LCs, ICs, and LICs) are schematic. They do not represent their actual shape. (**B**) Schematic representation of the heavy chain of cytoplasmic dynein in its post-powerstroke conformation, with the linker straight and positioned on AAA4 near the stalk. The hexameric head represents the six AAA+ subunits with small (AAA + S) and large (AAA + L) subunits.

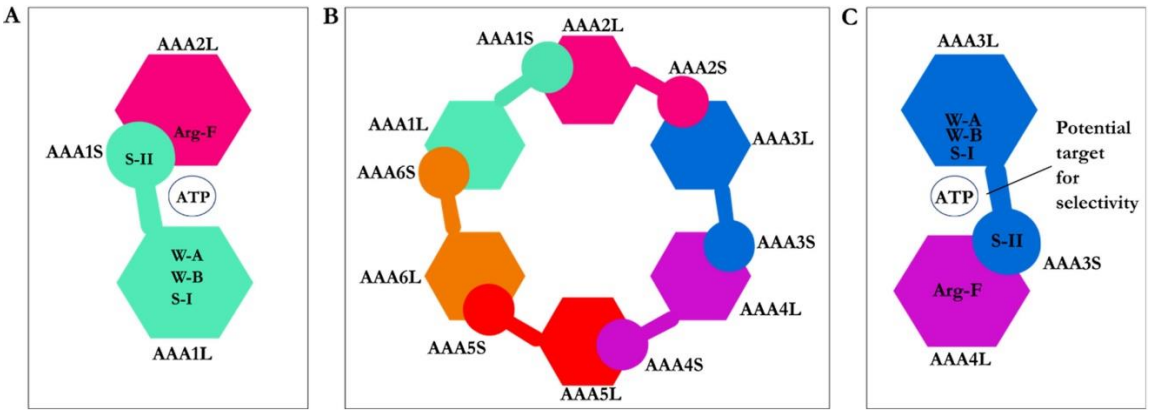

Figure 2.2: Composition of the AAA+ subdomains. (**A**) The AAA1 nucleotide-binding site composed of the small (AAA1S) and large (AAA1L) subunits of AAA1 and the prominent (AAA2L) subunit of AAA2. ATP motifs are represented: walker-A (W-A), walker-B (W-B), sensor I (the S-I), sensor II (the S-II) in AAA1, and arginine finger (Arg-F) in AAA2. (**B**) Hexameric head of cytoplasmic dynein. (**C**) The AAA3 nucleotide-binding site composed of its small (AAA3S) and large (AAA3L) subunits and the large subunit of AAA4. ATP motifs are represented as the walker-A (W-A), the walker-B (W-B), the sensor I (the S-I), the sensor II (the S-II) in AAA3, and the arginine finger (Arg-F) in AAA4.

AAA1 is the primary site of ATP hydrolysis in cytoplasmic dynein [1] since hydrolysis of ATP at this site is critical for dynein motility [16] and conserved in the dynein family [1]. AAA3 is the second major site of ATP hydrolysis [1], as mutation of K2675T in the *D. discoideum* species reduced ATPase activity of dynein by approximately 20-fold [16]. The nucleotide-binding sites of cytoplasmic dynein, similar to other AAA+ family members, display the following ATP motifs: the walker-A (GXXXGK) or P-loop, the

walker-B (catalytic Asp and Glu), the S-I (Asn), the S-II (Arg), an arginine finger (Arg), and directly interacting amino acids with the nucleotide base [1,7] (Figures 2.2 and 2.3).

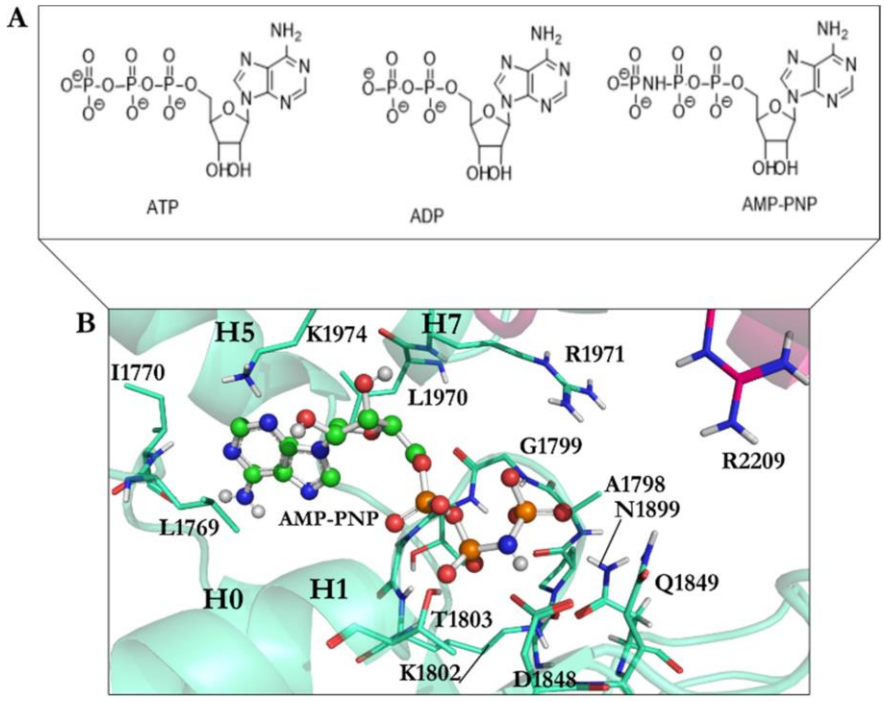

Figure 2.3: **(A)** The chemical structures of ATP, ADP, and AMPPNP, **(B)** AMPPNP in the ball-and-stick representation (green) interacts with amino acids in the AAA1 binding site of cytoplasmic dynein 1. Color code: AAA1 in cyan blue and AAA2 in sharp pink.

Considering the vital role of the heavy chain defects in causing some of the significant NDDs [11] and the gigantic size of dynein (~1.2 MDa), small-molecule inhibitors are suitable means to examine how the function of the dynein motor domain could be regulated or inhibited. Therefore, this structure–activity relationship (SAR) study attempted to

elucidate the structural effect of ciliobrevin A and D, as well as their analogues, on their potential regulatory or inhibitory [6] mechanisms concerning the function of the motor domain in cytoplasmic dynein 1. As the size and the complexity of the various structural domains of dynein lead to considerable challenges in solving their atomistic holo or apo structure *in vitro*, *in silico* methods in the presented work were utilized to address some of the current shortcomings.

2.2. Materials and Methods

2.2.1. Structure of Dynein Motor Subdomains

Three crystal structures of the motor domain of cytoplasmic dynein 1, including the linker, are available in the Protein Data Bank (PDB) [17]. The three crystal structures studied here are motor domains of *Dictyostelium* motor ADP (3VKG) [18] from *Dictyostelium discoideum*, as well as yeast motor apo, no ATP-bound (4AKG) [19] and yeast motor AMPPNP (4W8F) [20], both from *Saccharomyces cerevisiae*. The crystal structures were selected on the basis of their resolution, the conformation of the AAA1 binding site, and the nucleotide substrate in the binding site. Due to the complexity of the cytoplasmic dynein structure, the resolution of the crystal structures is low, as it ranges from 2.41 Å (*Dictyostelium* motor ADP (3VKG) [18]) to 3.54 Å (yeast motor AMPPNP (4W8F) [20]); however, they are the highest-quality structures of the domain currently available from the Protein Data Bank (Table 2.1).

Table 2.1: Summary of the features of the crystallographically solved structures of dynein used in this study.

PDB code	Uniprot code	Species	Resolution (Å)	Exp. pH	Nucleotide Binding Domain	Missing residues	Released date
4AKG	P36022	*Saccharomyces cerevisiae*	3.30	5.6	AAA1 (apo), AAA2 (ATP), AAA3 (ADP)	2944-2959 (AAA4) and 3658-3669 (AAA5-AAA6)	2012-03-14
4W8F	P36022	*Saccharomyces cerevisiae*	3.54	8.0	AMP-PNP in AAA1, AAA2, AAA3 and AAA4	2025-2029 (AAA1-AAA2), 2950-2953(AAA4), 3659-3668 (AAA5-AAA6)	2014-11-12
3VKG	P34036	*Dictyostelium discoideum*	2.81	7.0	ADP in AAA1, AAA2, AAA3 and AAA4	2061-2063 (AAA1), 2454-2488 (AAA2), 3212-3215 (AAA4), 3699-3703 (AAA5), 3725-3758 (AAA5), 4114-4115 (AAA6)	2012-03-14

The hexameric head from the *Dictyostelium* motor ADP [18] crystal structure accommodates one ADP molecule in the AAA1, AAA2, AAA3, and AAA4 subunits (3VKG) [18]. The hexameric head from the yeast motor AMPPNP crystal structure (4W8F) [20] possesses an AMPPNP molecule in each of the subunits. The yeast motor apo crystal structure (4AKG) [19] presents the AAA1 binding site in its unliganded state, whereas an ATP is found in the AAA2 and an ADP in the AAA3 binding site (4AKG) [19]. The three crystal structures have their linker in the post-powerstroke conformation. The linker is straight in the *Dictyostelium* motor ADP [18] crystal structure (3VKG) [18], spanning the AAA1 to AAA5 subunits. In comparison, the linker stretches from AAA1 to AAA4 in the yeast motor AMPPNP (4W8F) [20] and the yeast motor apo (4AKG) [19] crystal structures. The AAA1 binding sites of yeast motor AMPPNP [20] and *Dictyostelium* motor ADP [18] are in holo states in their crystal structures, with AMPPNP and ADP bound in each, respectively (Table 2.1).

2.2.2. Protein Structure Preparation

The accession codes of the three-dimensional structure of the motor domain of dynein collected from the PDB platform are 4AKG [19] from *S. cerevisiae* (Uniprot P36022 [21]), 4W8F [20] from *S. cerevisiae* (Uniprot P36022 [21]), and 3VKG [18] (Uniprot P34036 [21]) from *Dictyostelium Discoideum* (Uniprot P34036 [21]) (Table 2.1).

The amino-acid sequences of the two species, *S. cerevisiae* (P36022) and *D. discoideum* (P34036), were aligned according to the ClustalW algorithm [22,23]. There is

a sequence identity of ~25% between the cytoplasmic dynein of *S. cerevisiae* (P36022) containing 4092 residues and *D. Discoideum* (P34036) containing 4730 residues. According to the sequence alignment (Tyr1758–Val2273: *S. cerevisiae* and Tyr1936–Leu2531: *D. discoideum*), there are 35% conserved residues within the AAA1 and AAA2 subdomains of both species (Figure A1 and Table 2.2).

Table 2.1: Amino-acid sequence identity and similarity of the different parts of dynein, between *S. cerevisiae* and *D. discoideum*.

Dynein (*S. cerevisiae* and *D. Discoideum*)	**Sequence identity (%)**	**Sequence similarity (residues)**
Entire amino acids sequence of cytoplasmic dynein	24.83% (1193)	1668
AAA1	52.02% (116)	63
AAA2	28.14% (83)	95
AAA1 and AAA2	34.67% (207)	185

The yeast motor AMPPNP crystal structure (4W8F) [20] was subjected to E1849Q mutation to prevent ATP hydrolysis at the AAA1 nucleotide-binding site [20]. The yeast motor AMPPNP crystal structure was considered suitable for docking ATP competitive inhibitors in the AAA1 nucleotide-binding site and corresponded to the conformation of dynein before ATP hydrolysis [20]. The *Dictyostelium* motor ADP (3VKG) possesses a

molecule of ADP in the AAA1 nucleotide-binding site corresponding to the configuration succeeding ATP hydrolysis [18]. In contrast, the yeast motor apo (4AKG) pertains to motor domain conformation with low-affinity nucleotides binding [19]. Thus, the yeast motor AMPPNP conformation (4W8F) [20] was chosen over the *Dictyostelium* motor ADP (3VKG) [18] or the yeast motor apo (4AKG) [19] for the ligand docking experiment.

The missing residues (i.e., crystallographically unsolved) from the motor chain A in 4W8F [20] (i.e., Ala2025–Leu2029, Lys2950–Val2953, and Lys3659–Arg3668) were modeled and completed on the basis of the primary structure of the cytoplasmic dynein heavy chain of *S. cerevisiae* (P36022) (Table 2.1).

Fourteen residues from AAA1 and AAA2 subunits were located in the nucleotide-binding site. They consisted of the W-A or the P-loop region GPAGTGKT [4,7,18] (Gly1796– Thr1803 in *S. cerevisiae* and Gly1974–Thr1980 in *D. discoideum*), the W-B region [4,7,18] (Asp1848 and Glu1849 in *S. cerevisiae* compared to Asp2026 and Glu2027 in *D. discoideum)*, the S-I [4,7,18] (Asn1899 in *S. cerevisiae* and Asn2078 in *D. discoideum*), the S-II (Arg1971 in *S. cerevisiae* and Arg2150 in *D. discoideum)*, the Arg finger (Arg2209 in *S. cerevisiae* and Arg2410 in *D. discoideum)* [4,7,18], and the N-loop [4,7,18] (Leu1769 and Ile1770 in *S. cerevisiae* compared to Leu1947 and Val1948 in *D. discoideum*) (Table 2.3).

Table 2.2: The ATP motifs in *S. cerevisiae* and *D. discoideum*.

ATP Motifs	*S. cerevisiae*	*D. discoideum*
Walker-A	Gly1796-Thr1803	Gly1974-Thr1980
Walker-B	Asp1848-Glu1849	Asp2026-Glu2027
Sensor I	Asn1899	Asn2078
Sensor II	Arg1971	Arg2150
Arg finger	Arg2209	Arg2410
N-loop	Leu1769-Ile1770	Leu1947-Val1948

The retrieved X-ray crystal structure (4W8F) [20] was truncated to keep the required domains potentially affecting the nucleotide-binding sites to reduce the necessary CPU time for the motor subdomain conformational search. That reduced the number of atoms for calculating bonding and nonbonding interactions among ligand and protein atoms. The resulting truncated structure included the dynein hexameric head (AAA1–AAA4: Tyr1758–Val2984 and AAA5–AAA6: Leu3370–Asn3970), the linker subunit (within the tail: Gly1363–Gln1757), and a part of the stalk (Ile2993–Ser3125) interacting with the hexameric head. GROMACS [24] package (v. 2016.5, University of Groningen Royal Institute of Technology, Groningen, The Netherlands & Uppsala, Sweden) with the Gromos 96 force field 54A7 [25], was utilized for generating topology of protein atoms and energy minimization *in vacuo* to optimize bond lengths, angles, and orientation of the residues in the protein structure before docking any ligands.

2.2.3. Ligands 3D Structure Preparation

The AMPPNP's atomic coordination at the AAA1 site (4W8F) [20] was used as the reference. The binding site region was specified at a 15.0 Å radius spherical region around the reference structure as the center, covering an extra 2.0 Å broader region than that occupied by the AMPPNP interacting amino acids in the binding site of the AAA1 domain of cytoplasmic dynein 1 (Figure 2.3).

A library of 63 ligands (i.e., a chemical toolkit in this study) was created using SYBYL- X 2.1.1 (Certara Corporation©, St. Louis, MO, USA). Three-dimensional structures of the ligands were built up individually and minimized stepwise using the steepest descent algorithm according to the Tripos force field, with 0.0001 kJ/mol energy gradient and 10,000,000 iterations. The library contained previously synthesized and *in vitro* studied 46 analogues of ciliobrevin [10] and dynapyrazole A and B [26], as well as the protonated forms of the lead compounds ciliobrevin A and D and dynapyrazole A and B modeled *in silico*. It also included the nucleotides ATP, ADP, and AMPPNP, a nonhydrolyzable analogue of ATP (Figures 2.3–2.5).

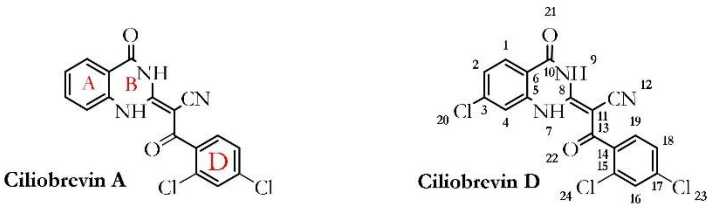

Protonation of ciliobrevin A and D

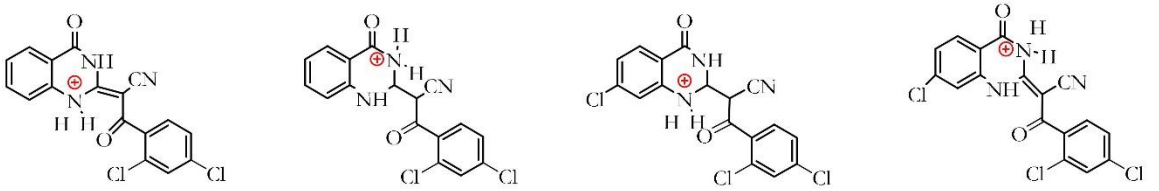

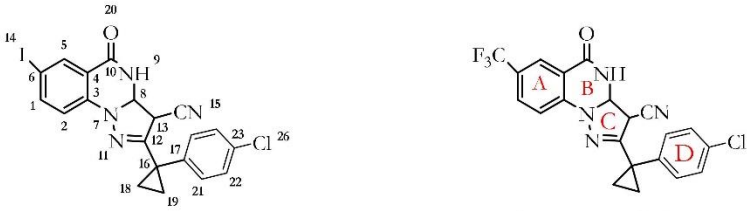

Protonation of dynapyrazole A and B

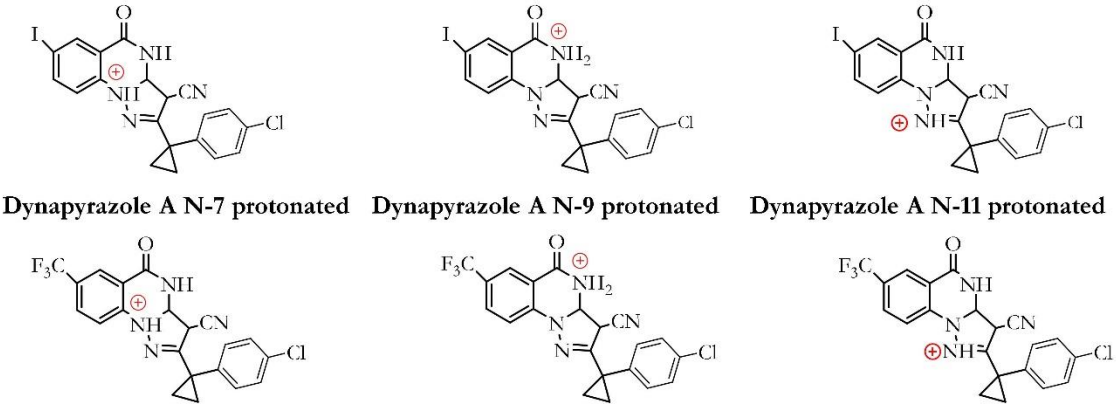

Figure 2.4: Chemical structures of ciliobrevin A and D, dynapyrazole A and B, and their protonated structures in the ligand library. Ciliobrevin A and D are analogues 1 and 2, respectively. Chemical structures and atom numbering were obtained utilizing Chemdraw software (v.19.1).

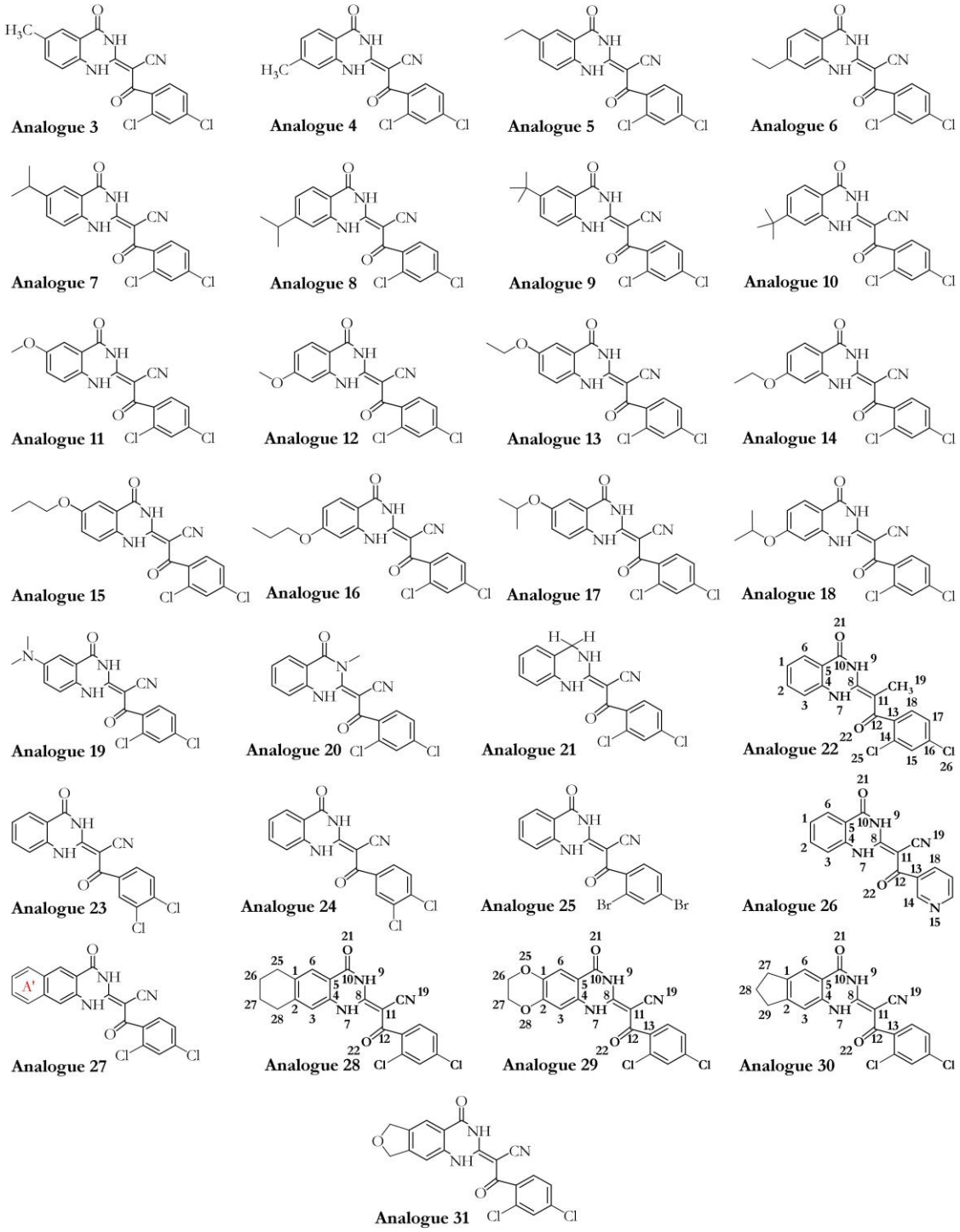

Figure 2.5. *Cont.*

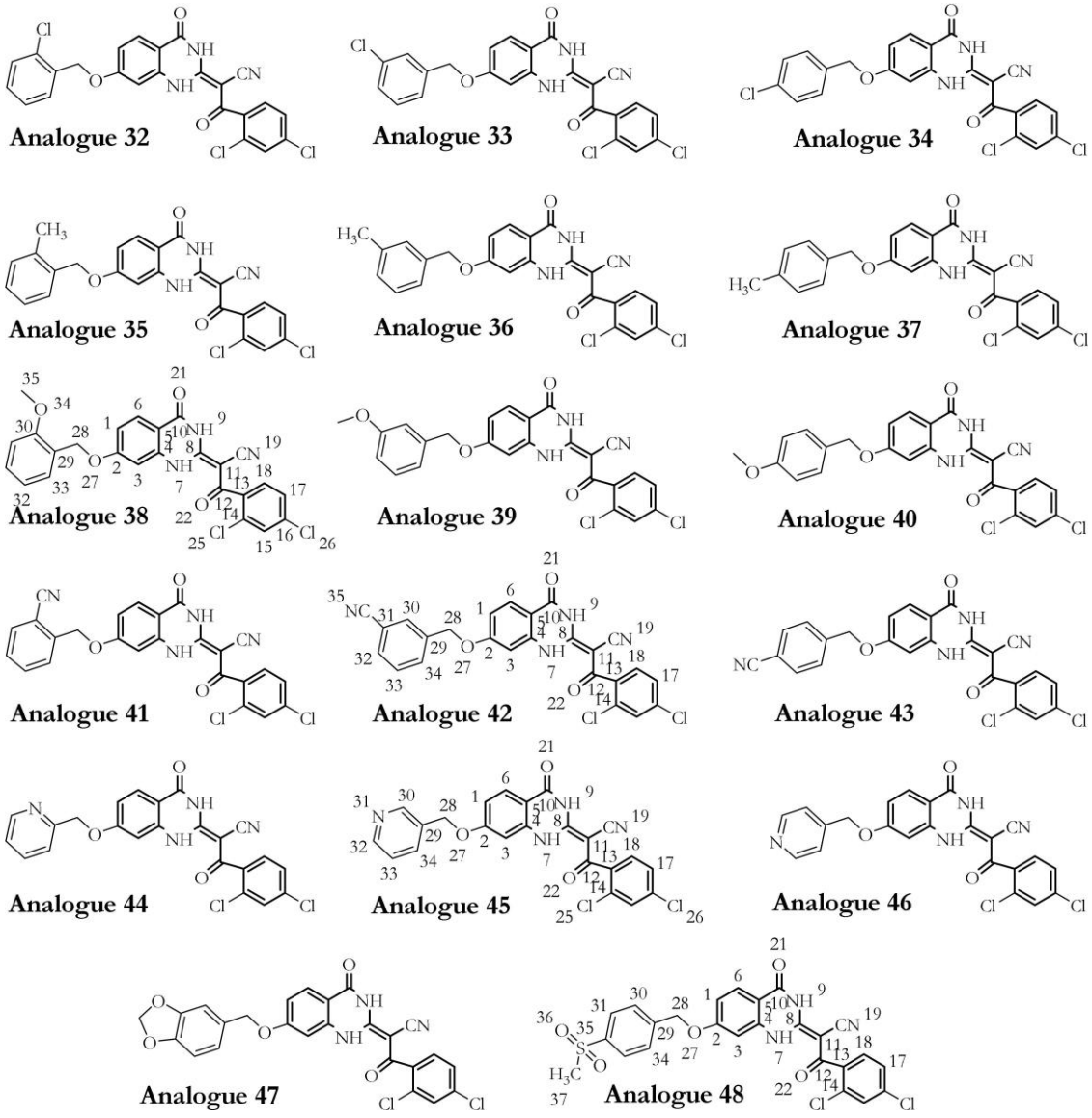

Figure 2.5: Forty-six analogues (from analogues 3–48) of ciliobrevin in the ligand library. Chemical structures and atom numbering were obtained utilizing Chemdraw software (v.19.1).

ATP and ADP are the endogenous substrates of dynein 1 [1]. Since the crystal structure of yeast motor AMPPNP did not possess ATP or ADP in any of the four nucleotide-binding sites (AAA1–AAA4), the endogenous substrates were docked into the AAA1 binding site to study their binding mode and quantify the magnitude of their binding affinity versus that of each ligand in the library. The deprotonated forms of ATP, ADP and AMPPNP, were based on the ATP pKa values [27]. The pH was 8.0 during the crystallization of the yeast motor AMPPNP(4W8F) [20], and the pKa of γ-phosphate is approximately 6.49 [27]. In comparison, the pKa of the α- and β-phosphates of ATP is estimated at ~1.6 [27]. Therefore, ATP, ADP, and AMPPNP molecules were also built and assessed in their fully deprotonated state and subjected to energy minimization. The protonated ciliobrevin A and D and dynapyrazole A and B structures were built up and energetically minimized. The pKa of the inhibitors has not yet been experimentally defined. A study on the different components of the ligands' chemical structures helped to study the effect of the most probable protonation states on their binding affinity. The pKa of arylamine groups, existing in the structures of the ligands, varies between 9–10 [28], meaning that, at the physiological pH, an arylamine (i.e., consisting of the N9 atom of dynapyrazole A and B, ciliobrevin A and D, and their analogues) could be protonated. It is noteworthy that the lone-pair electrons of the N7, N9, and N11 in dynapyrazole A and B could be involved in delocalized electronic systems of A, B, and C fragments, reducing the availability of the lone-pair electrons for protonation. Furthermore, the pKa of the quinazoline-4(3*H*)-one moiety of dynapyrazole (i.e., ring A and B) is expected to be more acidic than the estimated 3.51 of quinazoline [29], due to the electron withdrawal effect of the oxygen. Thus, the moiety is more likely to be deprotonated at the physiological pH (Figure 2.4).

FlexX [30,31] docking software, embedded in the LeadIT software package (v.2.1.8, BioSolveIT, Sankt. Augustin, Germany), was utilized for ligand–protein binding mode predictions, energy estimation, and ranking the solutions. It predicts the ligand–protein interactions on the basis of the incremental construction algorithm [32]. There are three fundamental stages to the FlexX docking algorithm: selecting a base fragment, placing the base fragments into the binding site, and incrementally constructing the complex, followed by calculating the interaction energies according to the Böhm scoring function for ranking the docking solutions [33,34].

2.3. Results and Discussion

2.3.1. Dynapyrazole, Ciliobrevin, and Their Analogues

In vitro and *in vivo* studies of ciliobrevin A and D, the two ATP-competitive ligands, have shown that they nonselectively bind to the ATP-binding sites of the hexameric head of both cytoplasmic dynein 1 and dynein 2 [7,10]. Dynapyrazole A and B resulted from a chemical structure modification to produce ciliobrevin analogues with higher potency [26] to overcome geometric isomerization complexity caused by the C8–C11 double bond in ciliobrevin (Figure 2.4).

Unlike the ciliobrevin analogues, which abrogate both MT-stimulated and basal ATPase activity, dynapyrazole analogues inhibit MT-stimulated ATPase activity with high potency without affecting basal ATPase activity [26]. This feature resembles She1, a microtubule-associated protein (MAP) that effectively reduces MT-stimulated ATPase activity without significantly decreasing its basal activity [35]. Experiments have shown that ciliobrevin A and D, which bind to AAA1, might bind to the AAA3 site [10]. In contrast, analogues of dynapyrazole, especially compound 20, abolished basal dynein activity by binding to AAA3 and AAA4 [36]. Forty-six analogues of ciliobrevin A and D were proposed to have potentially higher selectivity and potency than ciliobrevin A against dynein 2 [7]. However, only the IC50 values of four analogues (i.e., 18, 37, 43, and 47) against dynein 1 and 2 were reported [7] (Figure 2.5 and Table 2.4).

Table 2.3: IC50 values of ciliobrevin A and D, their analogues 18, 37, 43, and 47, and dynapyrazole A and B for dynein 1 and dynein 2.

Compounds	**IC_{50} (µM)** **Dynein 1**	**IC_{50} (µM)** **Dynein 2**
Ciliobrevin A	52.0	55.0
Ciliobrevin D	15.0	15.5
Dynapyrazole A	2.3	2.6
Dynapyrazole B*	_	2.9
Analogue 18	130.0	21.0
Analogue 37	280.0	11.0
Analogue 43	158.0	16.0
Analogue 47	130.0	11.0

* The IC50 of dynapyrazole B against dynein 1 is not available.

2.3.2. Binding Studies of Dynapyrazole, Ciliobrevin, and Their Analogues

Docking of the AMPPNP, obtained from the crystal structure, into the binding site of the yeast motor AMPPNP [20] of dynein resulted in a conformation with the lowest RMSD (1.67 Å) and binding energy (−22.06 kJ/mol). The ligand interacted with the N-loop (Pro1766–Leu1774) via residues Leu1769 and Ile1770, the W-A region (Gly1799–Thr1803), the β6 strand including the S-I motif (Ala1893–Asn1899) via Asn1899, Ile1929 from H5 (Ser1926–Ile1936), and Leu1970 and Lys1974 from the H7 (Leu1970–Pro1982) (Figure 2.6C–D, Figure A1, and Table 2.5).

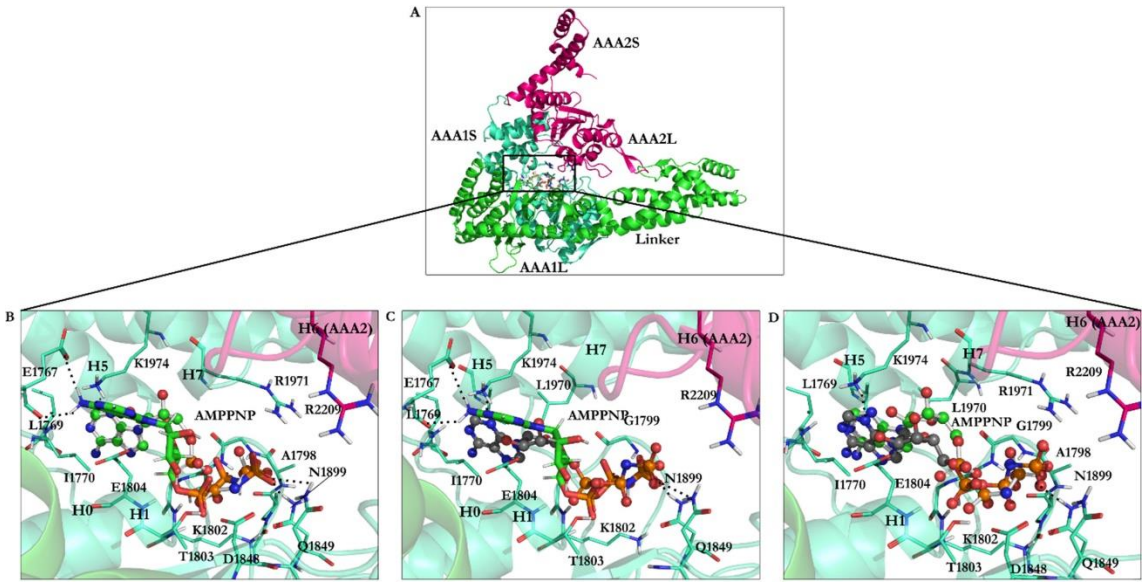

Figure 2.6: AMPPNP in the AAA1 binding site of dynein. (**A**) The linker and the AAA1 and AAA2 subunits of dynein and illustration of their inter-subunit binding site. (**B**) Docking solution of the minimized AMPPNP in the AAA1 binding site of the minimized conformation from the yeast motor AMPPNP crystal structure (4W8F). The docking solution is in stick representation, while the crystal structure of AMPPNP is in ball-and-stick representation. (**C**) The energy-minimized AMPPNP in the AAA1 binding site of the energy-minimized structure of yeast motor AMPPNP (4W8F) superimposed with the docking solution of the reference ligand, AMPPNP, from the crystal structure. (**D**) Crystal structure of AMPPNP docked in the AAA1 binding site of the crystal structure of yeast motor AMPPNP (4W8F). The calculated conformation (black-gray) in ball-and-stick representations and the crystal structure of AMPPNP (reference, green ball-and-stick representation). Nonessential hydrogen atoms are not shown for simplicity.

Table 2.4: Binding properties of the nucleotides' conformation obtained from the in silico experiments.

Ligand	RMSD *vs.* X-ray structure	Binding energy (kJ/mol)	Residues interacting with the compound
AMP-PNP	1.67	-22.06	Leu1769, Ile1770, Gly1799, Gly1801, Lys1802, Thr1803, Glu1804, Asn1899, Ile1929, Leu1970, Lys1974
AMP-PNP minimized structure	4.75	-40.18	Glu1767, Gly1799, Gly1801, Lys1802, Thr1803, Glu1804, Gln1849, Asn1899, Lys1974
Minimized ATP	—	-42.33	Ala1798, Gly1799, Thr1800, Gln1849, Asn1851, Arg1852, Asn1899, Arg1971
Minimized ADP	—	-31.89	Ala1798, Gly1799, Thr1800, Asp1848, Gln1849, Arg1852, Asn1899, Arg1971

Superposition of the domain crystal structures showed that the W-A region (Gly1796–Thr1803) in the yeast motor apo (4AKG) [19] is ~7.0 Å away from the W-A in the yeast motor AMPPNP (4W8F) [20]. The W-A region (Gly1974–Thr1980 in *D. discoideum* and

Gly1796– Thr1803 in *S. cerevisiae*) shifts by ~1.4 Å (*Dictyostelium* motor ADP) compared to that in yeast motor AMPPNP (4W8F) [20]. The H5 (Ser1926–Ile1936) of AAA1 in the yeast motor apo (4AKG) [19] crystal structure shifts by ~3.8 Å from the position of the equivalent helix in the yeast motor AMPPNP (4W8F) [20]. The H5 helices (Arg2105–Tyr2114 in *D. discoideum* and Ser1926–Ile1936 in *S. cerevisiae*) in the *Dictyostelium* motor ADP (3VKG) [18] and in the yeast motor AMPPNP (4W8F) [20] are ~1.3 Å apart, similar to the H7 (Leu1970–Pro1982) of AAA1 in the yeast motor AMPPNP (4W8F) [20] and yeast motor apo (4AKG) [19] at a ~3.9 Å distance. There is a ~2.0 Å distance between the H7 helices (Gly2148–Lys2165 in *D. discoideum* and Leu1970–Pro1982 in *S. cerevisiae*) of the *Dictyostelium* motor ADP (3VKG) [18] and yeast motor AMPPNP (4W8F) [20]. The displacements of the domain segments (i.e., yeast motor AMPPNP [20], yeast motor apo [19], and *Dictyostelium*-motor- ADP [18]) imply that AMPPNP binding caused an "induced fit"-driven conformational change in the binding site (Figures A2 and A3).

The docked AMPPNP conformation obtained from its energy minimization (−40.18 kJ/mol) had 4.75 Å RMSD due to the optimization of the bond lengths and angles according to the implemented force-field parameters. Similar to the reference ligand, the conformation of the docked, energy-minimized (i.e., the optimized) structure of AMPPNP interacted with ATP motifs [4,7]. However, the orientation of the aromatic nucleotide fragment of the energy minimized AMPPNP allowed the system to engage with positively charged Lys1974 of the H7 (Leu1970–Pro1982) via polar ionic interactions, which is not possible for the ligand with the conformation seen in the crystal structure. Unlike the latter, the amine group of the optimized conformation engaged in H-bond interactions with the

carboxylate group of Glu1767 (N-loop: Pro1766–Leu1774), and its γ-phosphate created an H-bond with Gln1849 (E1849Q) (Figure 2.6B–C, Tables 2.3 and 2.5).

The energy-minimized ATP's binding energy is lower than that of AMPPNP, which suggests ATP binds more strongly to cytoplasmic dynein 1 than AMPPNP (−42.33 kJ/mol vs. −40.18 kJ/mol). The ATP's binding mode obtained after the conformational search displayed its interaction with Ala1798, Gly1799, and Thr1800 from the W-A region (Gly1796– Thr1803), Gln1849 from the W-B motif in β3 (Ala1843–Asp1848), Asn1851 and Arg1852, between β3 (Ala1843–Asp1848) and H3 (Glu1854–Val1874), with the S-I (Asn1899 in β6: Ala1893–Asn1899), and Arg1971 from H7 (Leu1970–Pro1982) (Figure 2.7B, Tables 2.3 and 2.5).

The ADP's binding energy was −31.89 kJ/mol, which was the highest among the nucleotides (ATP with −42.33 kJ/mol and AMPPNP with −40.18 kJ/mol), thus presenting the lowest affinity toward the AAA1 binding site (Figure 2.7C and Table 2.5).

2.3.3. Ciliobrevin A and D

The calculated conformation of ciliobrevin A (binding energy −26.23 kJ/mol) had a stronger affinity than ciliobrevin D (binding energy −23.92 kJ/mol). Ciliobrevin A (IC50 of 52.0 μM [26]) had a lower potency than the D analogue (IC50 of 15.0 μM [26]). Ciliobrevin A and D both displayed weaker binding affinity than ATP (−42.33 kJ/mol), AMPPNP (−40.18 kJ/mol), and ADP (−31.89 kJ/mol) (Figure 2.4 and Tables 2.5 and 2.6).

The O21 atom of ciliobrevin A was involved in a ~2.1 Å hydrogen bond (H-bond). In contrast, the O21 of ciliobrevin D formed a ~1.8 Å H-bond with Lys1802 (the W-A motif,

Gly1796–Thr1803); the positively charged ammonium fragment of Lys1802 usually contributes to the stabilization of the negatively charged ATP γ-phosphate [37]. The O22 of ciliobrevin A and D engaged in an H-bond with the side-chain of Asn1899 S-I motif of the β6 (Ala1893–Asn1899) at a ~1.3 Å–1.4 Å distance. The S-I is involved in placing a water molecule near the γ-phosphate of ATP and the negative charge of Glu1849 of the W-B motif, thereby facilitating a nucleophilic attack for hydrolyzation [37]. The O22 in ciliobrevin A and D also formed an H-bond (~1.8 Å and ~1.9 Å, respectively) with Gln1849 (in E1849Q mutant). In the wild-type dynein, Glu1849 is responsible for activating a water molecule placed by the S-I (Asn1899 in yeast dynein 1) to trigger the network mechanism of ATP hydrolysis [37]. Therefore, the E1849Q mutation in the yeast motor AMPPNP crystal structure represents a conformation incapable of ATP hydrolysis [20]. In the *in silico* conformational search that the mutant of dynein was studied, Gln1849 showed interactions with ciliobrevin A and D via H-bond formation. The N9 atom of the ligands interacted with the hydroxyl group of Thr1803 of the W-A motif (Gly1796–Thr1803) through a 2.8 Å H-bond in ciliobrevin A and a 2.9 Å H-bond in ciliobrevin D, while Thr1803 usually participates in the stabilization of the ATP γ-phosphate [37]. Thus, by interacting with Thr1803, ciliobrevin A and D could block the activity of the subsites, which otherwise would be involved in the hydrolytic reaction on the ATP (Figures 2.4 and 2.8).

The cyanide (CN) moiety of ciliobrevin A formed an H-bond (~2.5 Å) with Thr1897 of β6 (Ala1893–Asn1899). The CN was involved with the hydroxyl (OH) moiety of Thr1897 in ciliobrevin D (at ~2.8 Å distance). It is noteworthy that Thr1897 does not belong to the ATP motifs, nor did it show any interactions in the *in silico* docking solutions

of the nucleotides. However, the CN moiety seemed to act as an auxiliary anchor to promote placements and orientations of the significant substructures of ciliobrevin A and D in the proximity of the critical ATP motifs, namely, the W-A and the S-I. Aliphatic chains of the W-A (by Gly1799, Lys1802), the S-I (by Asn1899), and the W-B motifs (by Asp1848 and Gln1849) were involved in van der Waals (VdW) interactions with the hydrophobic fragments of ciliobrevin A and ciliobrevin D. This suggests how ciliobrevin A and D's effects as ATP antagonists, on the ATP motifs and Thr1897, could disturb the activity of the motor domain by blocking the catalytic residues' action (Figure 2.8 and Table 2.3).

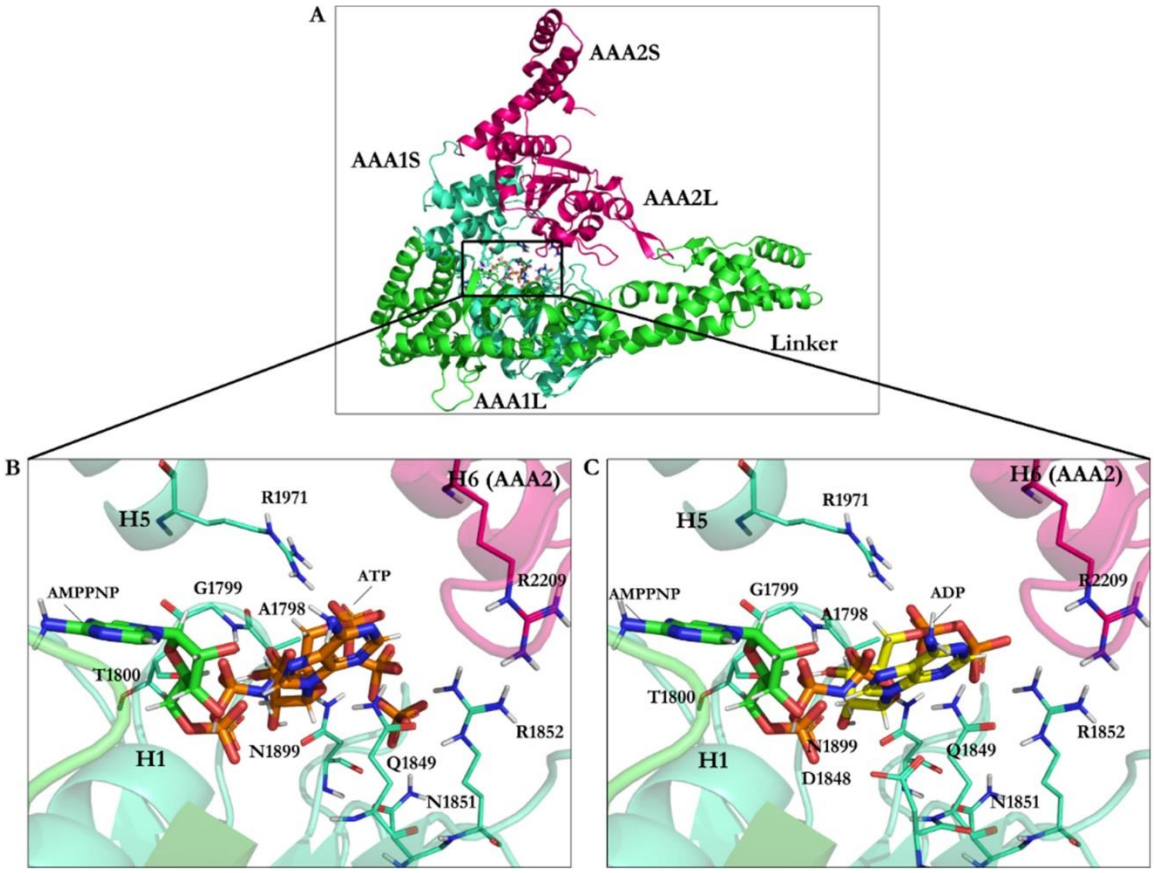

Figure 2.7: (**A**) The linker and the AAA1 and AAA2 subunits of dynein and illustration of their inter-subunit binding site. Binding interactions of docking solutions of (**B**) ATP (orange) and (**C**) ADP (yellow) compared to AMPPNP (green) at the AAA1 binding site.

Table 2.5: Amino acids affected by ciliobrevin A and D in their protonated and deprotonated states.

Compound	Binding energy (kJ/mol)	Residues interacting with the compound
Ciliobrevin A N9 protonated	-28.22	Ala1798, Lys1802, Thr1803, Glu1804, Asp1848, Gln1849, Thr1897, Asn1899, Arg1971
Ciliobrevin A	-26.23	Gly1801, Lys1802, Thr1803, Glu1804, Asp1848, Gln1849, Thr1897, Asn1899
Ciliobrevin D N9 protonated	-26.15	Lys1802, Thr1803, Glu1804, Asp1848, Gln1849, Thr1897, Asn1899
Ciliobrevin D	-23.92	Gly1801, Lys1802, Thr1803, Glu1804, Asp1848, Gln1849, Thr1897, Asn1899
Ciliobrevin A N7 protonated	-23.84	Gly1799, Thr1800, Gly1801, Lys1802, Thr1803, Glu1804, Leu1970, Arg1971
Ciliobrevin D N7 protonated	-23.55	Gly1801, Lys1802, Thr1803, Glu1804, Asp1848, Gln1849, Thr1897, Asn1899

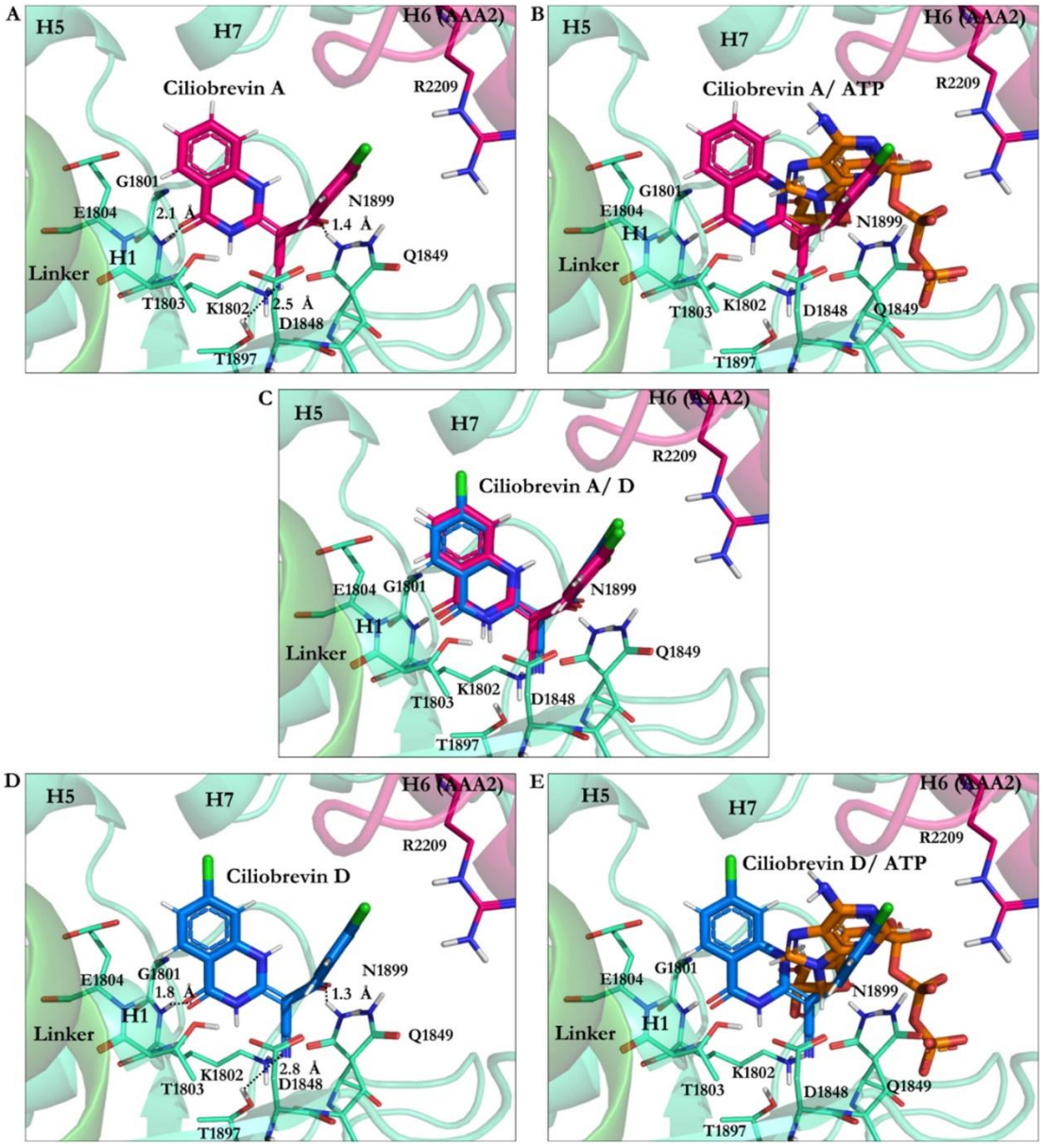

Figure 2.8: Ciliobrevin A and D conformation at the AAA1 binding site of motor domain of dynein 1. (**A**) Ciliobrevin A and (**B**) Ciliobrevin A superimposed on ATP. (**C**) Ciliobrevin A and ciliobrevin D superimposed. (**D**) Ciliobrevin D and (**E**) Ciliobrevin D superimposed on ATP.

2.3.4. The Analogues Binding Profile

Analogue 30 showed the best affinity, along with analogues 29 and 28 (the lowest energy −27.87 kJ/mol vs. respective −27.37 kJ/mol and −27.27 kJ/mol). The O21 in analogues 28, 29, and 30 was involved in an H-bond with the polar H of the amide bond moiety of Gly1801 in the ATP motif, the W-A (Gly1796–Thr1803). Furthermore, their N9 atom formed an H-bond with the OH moiety of Thr1803 of the W-A (Gly1796–Thr1803). In these analogues, the CN moiety played a similar role in ciliobrevin A and D. It was also involved in an H-bond formation with the OH of Thr1897 in the β6. The side-chains of Asn1899 in the S-I and Gln1849 of the W-B motif also created an H-bond with the O22 of the analogues. The hydrocarbon chains of Gly1799 and Lys1802 in the W-A motif, as well as Asp1848 and Gln1849 of the W-B motif, hydrophobically interacted with the C8 of quinazolinone ring B and the acrylonitrile moiety. Thus, analogues 28–30 engaged with ATP motifs and the β6, through which they could hinder the motor domain's natural function (Figures 2.5 and 2.9, Table A1).

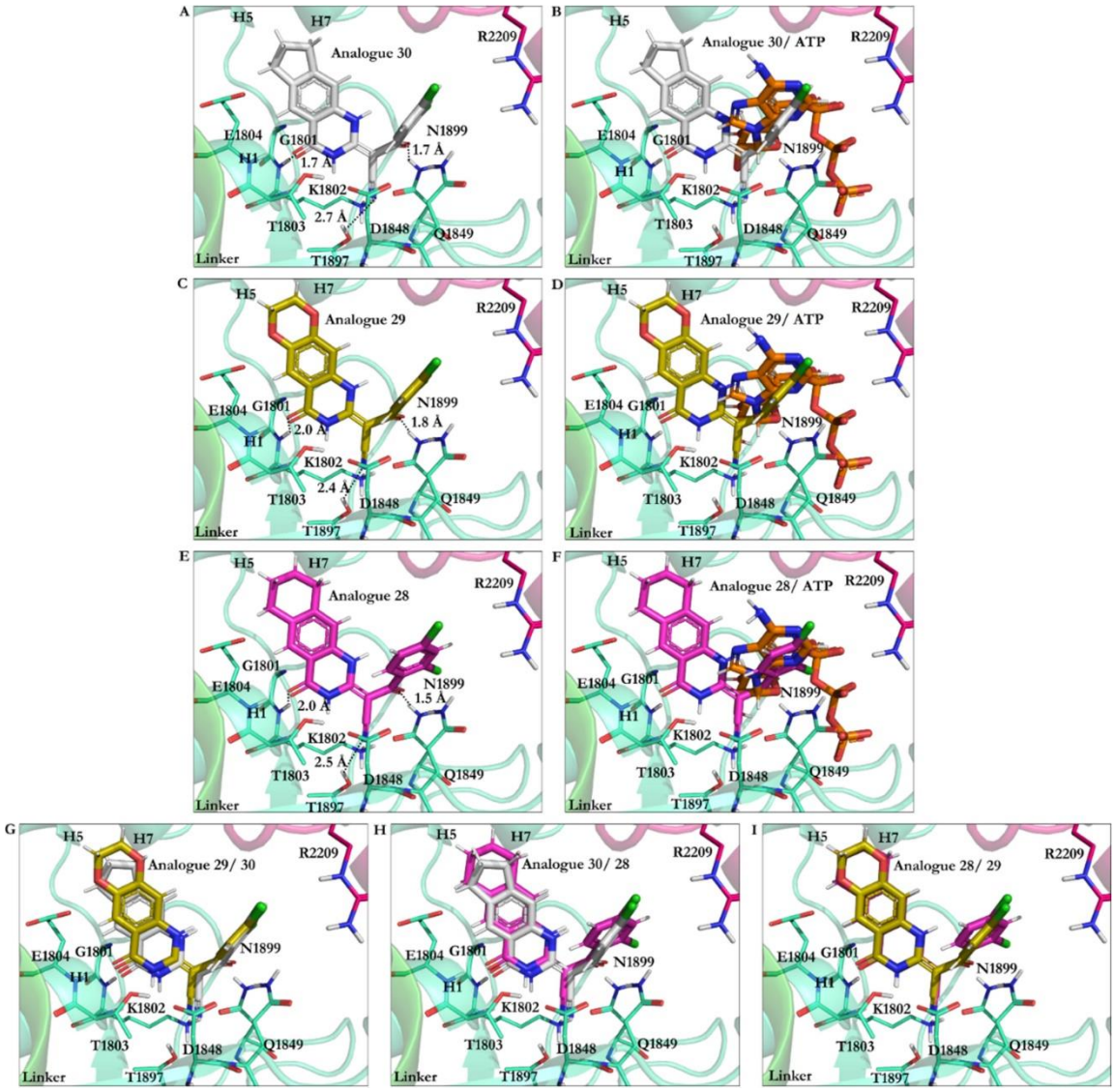

Figure 2.9: Analogues of ciliobrevin at the AAA1 binding site of dynein 1. (**A**) Analogue 30. (**B**) Analogue 30 superimposed on ATP. (**C**) Analogue 29. (**D**) Analogue 29 superimposed on ATP. (**E**) Analogue 28. (**F**) Analogue 28 superimposed on ATP. Superimposition of (**G**) analogues 29 and 30, (**H**) analogues 30 and 28, and (**I**) analogues 28 and 29.

Chemical modifications resulting in analogue 45 showed its improved binding affinity versus analogues 28–30, 38, and 42, as well as ciliobrevin A and D. However, the similarity in their binding profiles showed that they could comparably compete with ATP for binding to the functional motifs in the AAA1 nucleotide-binding site. The analogues' O21 atom formed an H-bond with the polar H of the Gly1801 in the W-A motif, and their N9 atom formed an H-bond with the OH of Thr1803 in the same ATP motif. There was also an H- bond between the O22 and Asn1899 of the S-I and Gln1849 of the W-B. Similar to analogues 28–30, the CN moiety of analogue 42 formed an H-bond with Thr1897 of the β6. Thr1897, which does not belong to the ATP motifs, also interacted with ciliobrevin A and D, as well as analogues 45, 30, 42, 29, 28, and 38. The OH of Thr1897 was involved with Gln1849 (in the W-B motif), known for its connection with water molecules to promote ATP hydrolysis. In analogue 38, the CN was replaced with a methoxy (–OMe) moiety. The O34 of the methoxy group interacted with Lys1974 via a 2.2 Å H-bond. The benzene ring was replaced with pyridine in analogue 45, whose N31 atom formed a 2.1 Å H-bond with Lys1974 in the H7 helix (Leu1970–Pro1982). The Lys1974 positive charge could potentially form a dipole-induced moment with the pyridine ring of analogue 45, although the positively charged amino acid is not perpendicular to the ring (Table A2, Table 2.3 and Figure A6).

The analogues of ciliobrevin (i.e., ciliobrevin A and D, as well as analogues 28, 29, 30, 38, 42, and 45) affect the ATP hydrolysis process also through binding to Asn1899 (in the S-I), which usually forms an H-bond with and positions water molecules for the nucleophilic substitution [37]. A conserved Asn residue (e.g., Asn64 in PspF, a member of the AAA+ proteins [38]) is involved in an H-bond formation with the conserved Glu

from the W-B motif (Glu108 in PspF of AAA+ proteins [38]) found at the AAA1 binding site of several dyneins [37]. Through the interactions of an ATP competitive inhibitor with the Glu or the Asn, the Asn (Asn64 in PspF [38]) cannot contribute to the ATP hydrolysis, as the glutamate residue of the W-B motif (Glu108 in PspF [38]) is unavailable to activate a water molecule through deprotonation [37]. The process is referred to as a "glutamate switch" and is thought to be an endogenous mechanism that regulates ATP hydrolysis in dynein to evade a nonproductive powerstroke [37]. H-bond formations of Asn1899 with ciliobrevin A and D, as well as its analogues, could disrupt the "switch" mechanism and, therefore, interfere with the regulation of the dynein powerstroke progression. The glutamate switch involving Glu108 in PspF [38] has not yet been detected in cytoplasmic dynein 1. The Asn residue involved in the "glutamate switch" is replaced with a cysteine (Cys1822 in *S. cerevisiae*) in the dynein 1 isoform [37]. However, an intramolecular H-bond of 2.1 Å between the side-chains of Gln1849 (E1849Q) and Arg1852 was visualized in the optimized (i.e., energy-minimized) structure of yeast motor AMPPNP dynein obtained through an *in silico* conformational search. In contrast, the crystal structure shows a relatively long distance (3.9 Å) between the residues. Thus, the energetically stabilized conformation demonstrated Arg1852 and Gln1849 in the positions and orientations capable of strong H-bond formation, where an arginine in place of the asparagine could interact with the glutamate to execute the "switch" mechanism in dynein 1 (Figure A7).

2.3.5. Geometrical Isomerization Effect on Ciliobrevin Binding to the AAA1

Ciliobrevin A and D exist in two geometric isomers of *E* or *Z* at the C8–C11 double bond

[10]. The potency of the ciliobrevin was thought to be affected by isomerization, where there is only a fraction of the isomer abrogating dynein [4]. The benzoylacrylonitrile group of the molecule favors the *E* isomer since the one-dimensional NMR spectrum and the result of a 2D nuclear Overhauser effect spectroscopy (NOESY) of ciliobrevin D showed an intramolecular H-bond between the hydrogen atom on the N7 and the O22 that stabilizes ciliobrevin D in solution [26]. The N7 is directly attached to the C8, and the O22 relates to the C11 via the double bond to the C13, which is covalently attached to the C11 (Figure 2.5 and Figure A8).

Ciliobrevin A: The effect of geometrical isomerization of ciliobrevin A was investigated, where its *Z* isomer showed binding with 6.82 kJ/mol higher energy than the *E* isomer (−26.23 kJ/mol). The O22 atom of the *Z* isomer engaged in a 1.9 Å H-bond with the side-chain of the S-I, through Asn1899 in β6 (Ala1893–Asn1899), and a 2.7 Å H-bond with β3 (Ala1843–Asp1848) of the W-B via Gln1849. The *Z* isomer did not interact with Thr1897 of the β6 (Ala1893–Asn1899), unlike the *E* isomer of ciliobrevin A. On the other hand, its CN moiety formed an H-bond with the S-II ATP motif through Arg1971 of the H7 helix (Leu1970–Pro1982). The N9 atom of the *Z* isomer was involved in a 2.2 Å H-bond with the carboxylate moiety of Asp1848 from β3 (Ala1843–Asp1848), and its O21 atom also formed a 2.2 Å H-bond with the amino group of Asn1821 in the β2 strand (Val1818–Asn1821). Ring A of the *Z* isomer oriented to form a π–π stacking with the guanidine moiety of Arg1852, a key element in the "glutamate switch" in dynein 1, as observed in the conformation obtained in this *in silico* conformational search. The binding energies of the *E* and *Z* isomers of ciliobrevin A indicated that the *E* is favorable over the *Z* isomer, as the former displayed a significantly higher binding affinity toward the AAA1 binding site

(Figure 2.10A–B and Table A3).

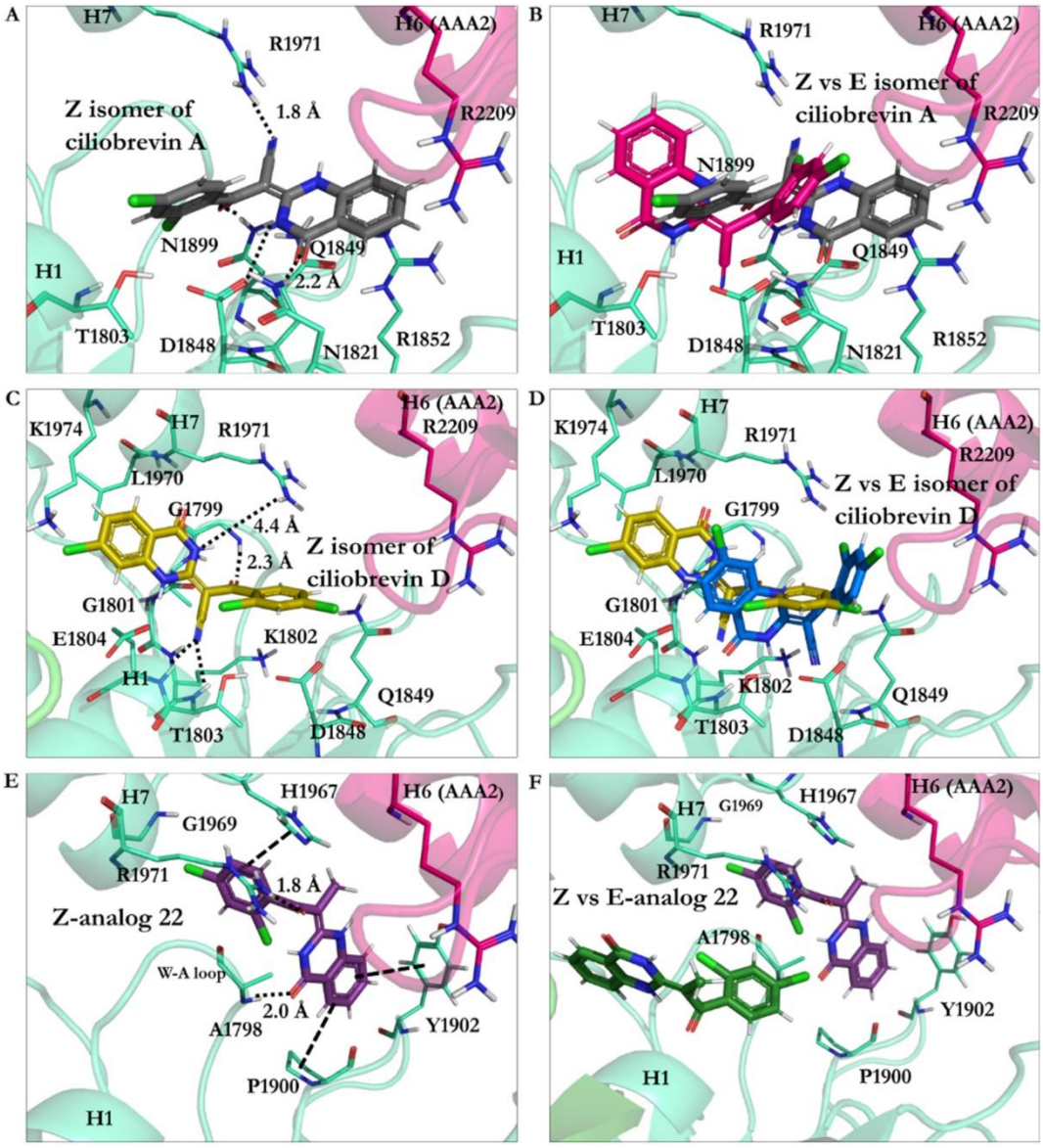

Figure 2.10: (**A**) Z isomer of ciliobrevin A at the AAA1 binding site of cytoplasmic dynein 1. (**B**) Superimposition of Z and E isomers of ciliobrevin A. (**C**) E isomer of ciliobrevin D at the AAA1 binding site of cytoplasmic dynein 1. (**D**) E isomer of ciliobrevin D superimposed on its Z isomer. (**E**) Z analogue 22 and the residues at the

AAA1 binding site of AAA1. (**F**) Z analogue 22 superimposed on its E isomer at the AAA1 binding site.

Ciliobrevin D: The binding energy of its *Z* isomer, similar to ciliobrevin A, was also higher than its *E* (−19.78 kJ/mol vs. −23.92 kJ/mol, respectively). The *Z* isomer utilized its O22 atom to engage in an H-bond with the polar hydrogen of the Gly1799 amide moiety in the W-A motif (Gly1796–Thr1803). The *Z* isomer's CN group was available to form H-bonds with Lys1802 (1.9 Å) of the W-A motif, as well as Thr1803 (2.5 Å) and Glu1804 (2.3 Å). The N9 of the *Z* isomer formed a weak H-bond with Arg 1971 in the H7 helix (Leu1970–Pro1982). It is noteworthy that the *Z* isomer of ciliobrevin D did not interact with the S-I motif via Asn1899 (Figure 2.10C–D and Table A3).

The effect of the CN elimination from ciliobrevin A and its replacement with a methyl group in analogue 22 [7] was examined through the study of its geometric isomers. The *E* isomer became weaker than *E*-ciliobrevin A and D; however, it was slightly stronger than its *Z* isomer (analogue 22 *E* isomer, −17.49 kJ/mol, versus −16.83 kJ/mol). The *E* was bound to the AAA1 site via H-bond with Lys1802. It also formed an H-bond via its N9 atom with the carboxylate group of Glu1804. The *Z* isomer of analogue 22 displayed a ~180° rotation in the binding site compared to its *E* isomer and ciliobrevin A and D. Its unique orientation resulted in H-bonds with Ala1798 and Arg1971 via its O22 atom. In addition, His1967 interacted with its ring D of the *Z* isomer through a T-shaped π–π stacking. Its ring A also showed a similar conformation against Tyr1902, while the Pro1900 orientation facilitated a proline–benzene VdW interaction via the ligand's ring D (Figure 2.10F and Table A3).

2.3.6. Dynapyrazole A and B

The O21 of dynapyrazole A and B formed H-bonds (~1.9 Å) with the W-A peptide backbones (Gly1796–Thr1803) via Lys1802 and the H1 helix (H1, Glu1804–Gly1810). The H atom on the N9 in dynapyrazole A and B was involved in a 1.6 Å H-bond with the W-A via Thr1803, whose OH moiety typically interacts with an Mg^{2+} resulting in stabilizing the charges on the ATP γ-phosphate [37]. Thus, the ligands, which have a slight binding difference (~0.32 kJ/mol), could similarly hinder the interaction between the cation and the Thr. In addition, the CN moiety of dynapyrazole A and B formed H-bonds with the β2 strand (Val1818–Asn1821) through Asn1821 (2.3 Å), which was ~4.0 Å away from Asp1848, a member of the W-B motif in the β3 (Ala1843–Asp1848). They could indirectly affect dynein's motility affecting the W-B's Asp1848, a segment that usually hosts ATP to undergo hydrolysis [4,37] (Figure 2.11 and Table A4).

2.3.7. Impact of Elimination of Carbon Double Bond on the Affinity of Dynapyrazole and Analogues

Ciliobrevin's derivatization led to the synthesis of dynapyrazole by eliminating the C8–C11 double bond and inserting the ring C in dynapyrazole and its analogues [26]. The process also consisted of replacing the O22 atom in ciliobrevin with the N11 in dynapyrazole to improve its potency. That resulted in the IC50 plummeting from 15 μM (ciliobrevin D) to 2.3 μM (dynapyrazole A) [26], whereas the binding strength of the former improved by ~−5 kJ/mol (Figure 2.4 and Table 2.4, Tables A3 and A4).

The double bond in ciliobrevin A and D positionally allowed the *E* isomer to form H-bonds both with Thr1897 of the β6 (Ala1893–Asn1899) via the nitrogen of its CN moiety

and with Asn1899 through its O22 atom. The energy contribution of this event could have been the cause of the difference in the total binding strength, considering that the N11 of the replaced ring C in dynapyrazole had no interaction with the AAA1 binding site, in contrast to the eliminated O22 in ciliobrevin. However, the CN nitrogen atom of dynapyrazole A and B formed an H-bond with Asn1821 (Figure 2.11F).

Among the analogues 37, 43, and 47 of ciliobrevin possessing the double bond, analogue 47 showed the lowest IC50 (130.0 µM [26]) and the strongest binding (−26.12 kJ/mol), whereas analogue 37 with the highest IC50 (280.0 µM [26]) had just 2.01 kJ/mol higher binding energy than analogue 47. Analogue 47 is suggested as the most suitable candidate for further *in vitro* and *in vivo* experimental evaluations for its effect on dynein motility and its selectivity profile (Figure 2.12).

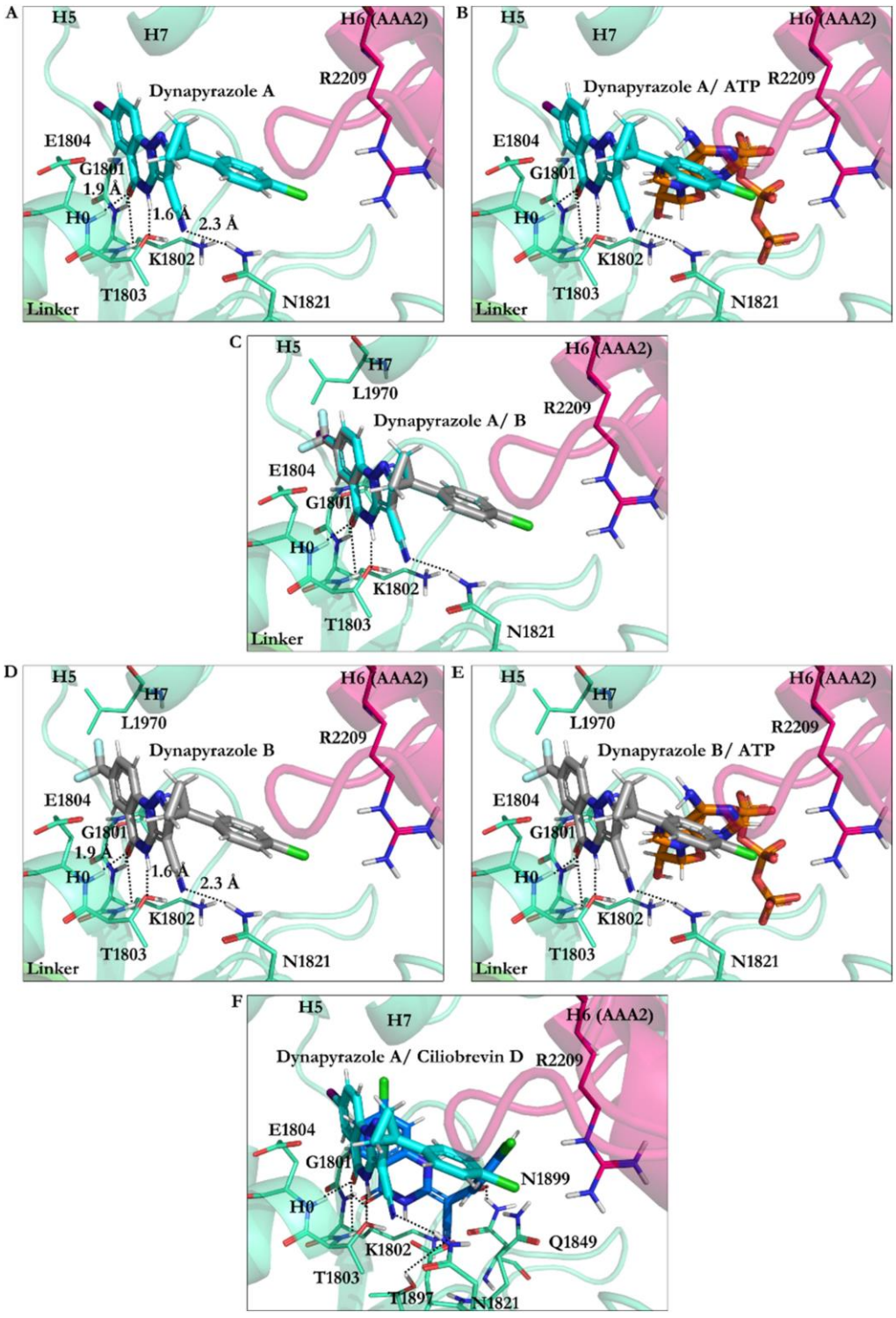

Figure 2.11: Dynapyrazole in the nucleotide-binding site of the AAA1. (**A**) dynapyrazole A. (**B**) Superimposition of dynapyrazole A and ATP. (**C**) Superimposition of dynapyrazole

A and B. (**D**) Binding modes of dynapyrazole B. (**E**) Superimposition of dynapyrazole B and ATP. (**F**) Superimposition of dynapyrazole A and ciliobrevin D.

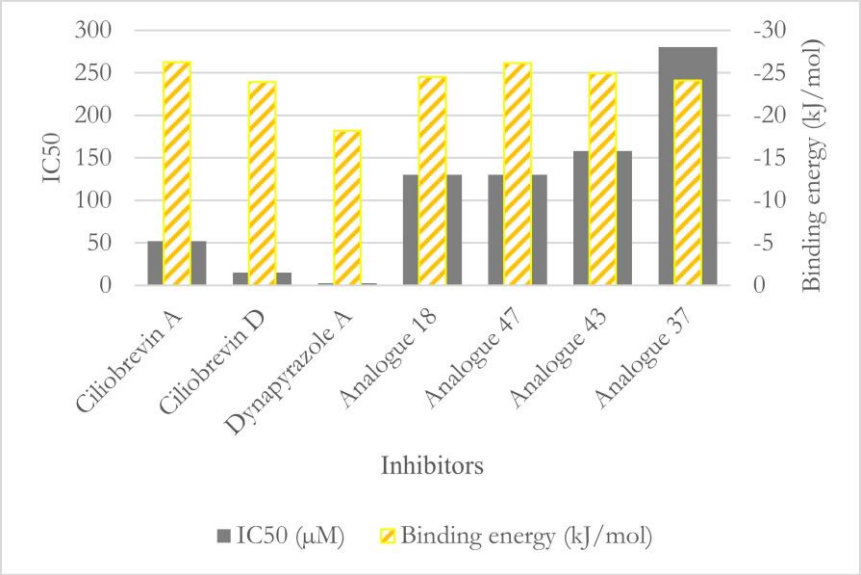

Figure 2.12: The ligands binding energy versus their IC50.

2.3.8. Protonation Effect on Ciliobrevin A and D Binding

Considering the pKa values of the chemical moieties of the inhibitors, as stated earlier, the N9 and N7 might be weak candidates for protonation at the tissues with alkaline pH (Figure 2.4, Figure A9, and Table 2.6).

Protonation of ciliobrevin A at the N9 position caused a ~−2.0 kJ/mol improvement in binding strength, suggesting that ciliobrevin A might be protonated at the N9 depending on the environmental pH, which would interfere with the motor function.

However, the possibility seems low concerning the juxtaposed carbonyl moiety at the C10. Unlike the neutral (unprotonated) ciliobrevin A, its protonated form interacted with Ala1798 of the W-A motif (Gly1796–Thr1803) through its benzylic ring D. The protonated N9 atom was 2.6 Å away from the carboxylate moiety of Asp1848 in the β3 (Ala1843–Asp1848), which could have also electrostatically affected the positively charged N9 atom and contribute to the strengthening of ciliobrevin A binding affinity.

The protonated N9 of ciliobrevin D projected a similar binding profile to that of the A analogue with enhanced binding compared to its neutral form (−23.92 kJ/mol vs. −26.15 kJ/mol). Therefore, ciliobrevin D, protonated under a proper pH, had a superior inhibitory effect on dynein 1 *in vitro*.

The protonated ciliobrevin A at the N7 was a weaker binder (~2.39 kJ/mol) compared to its neutral structure (with −26.23 kJ/mol), suggesting that the ligand is less likely to be protonated at the N7 position in solution, as the nitrogen atom's lone-pair electrons tend to participate in the delocalized electron cloud of the aromatic ring A.

Protonation of the N7 atom of ciliobrevin D had a minor effect on binding (0.37 kJ/mol), since protonated and unprotonated D analogues similarly treated the AAA1 nucleotide site through Gly1801, Lys1802, Thr1803, Glu1804, Asp1848, Gln1849, Thr1897, and Asn1899.

2.3.9. Effect of Protonation on Binding Mode of Dynapyrazole A and B

Protonation of dynapyrazole A at N9 resulted in a slight binding improvement (~−0.64 kJ/mol). This analogue was the only one in the library of 63 ligands to bind to the linker domain of dynein. An ionic interaction was formed between the protonated N9 and the

carboxylate group of Glu1586 in the T-turn 6 (Val1586–Glu1588 of the linker), while its O21 formed an H-bond with the amide moiety of Pro1766 in the N-loop (Pro1766–Leu1774). The aliphatic side-chains of Lys1696 and Glu1699 in the H13 of the linker domain (Asp1692–Asn1717) and Glu1767 in the N-loop (Pro1766–Leu1774) were hydrophobically affected by the hydrocarbon fragment of the ligand consisting of the C8, the C12, and the C13 atoms. The positively charged guanidine moiety of Arg1978 in the H7 (Leu1970–Pro1982) interacted with the monochloride benzylic ring D through polar interactions. These observations elucidated the improvement of the total binding strength of the N9-protonated dynapyrazole A.

Protonation of dynapyrazole A at N7 also benefited from protonation (~−8.72 kJ/mol). The considerable improvement indicated that the IC50 *in vitro* better correlated with the ligand's protonated at the N7 position. It electrostatically interacted with the negative charge of Glu1804 carboxylate in the H1 helix (Glu1804–Gly1810), while its N9 created an H-bond to the OH moiety of Thr1803 in the W-A (Gly1796–Thr1803). The data showed that protonation at the N7 site was beneficial to the ligand (Figures 2.4 and 2.13 and Table A4).

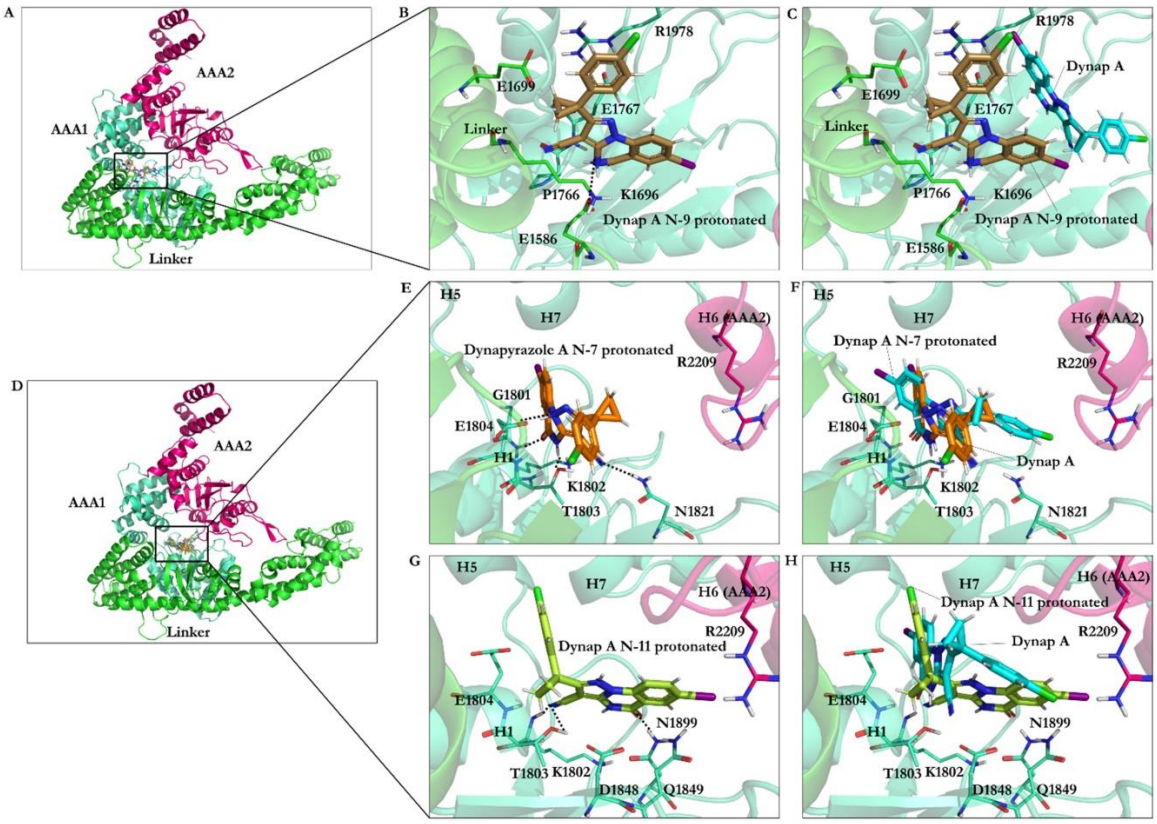

Figure 2.13: Binding of the protonated dynapyrazole A at the AAA1 binding site of dynein 1. (**A**) Overview of the AAA1 and AAA2 units, and linker domains. (**B**) Dynapyrazole A protonated at the N9 atom interacting with the linker residues. (**C**) Dynapyrazole A protonated at the N9 atom superimposed on dynapyrazole A. (**D**) Overview of the AAA1 and AAA2 units, and linker subdomains (as the panel A). (**E**) Dynapyrazole A protonated at the N7 atom. (**F**) Dynapyrazole A protonated at the N7 atom superimposed on dynapyrazole A. (**G**) Dynapyrazole A protonated at the N11 atom. (**H**) Dynapyrazole A protonated at the N11 atom superimposed on dynapyrazole A.

Protonation of N11 in dynapyrazole A caused slight weakness of the binding (0.27 kJ/mol) compared to its neutral form due to a minor difference of the interaction network set up by the N11-protonated ligand. The protonated N11 atom showed no ionic interactions. Dynapyrazole A in this configuration was the only analogue, among the protonated and neutral dynapyrazole A and B, to interact with the β6 (via Asn1899) and the β3 strand (via Asp1848 and Gln1849), resembling the binding mode of ciliobrevin and its analogues.

Protonation of dynapyrazole B at N11 also had an insignificant effect on its binding (~0.62 kJ/mol), similar to its protonated A analogue. It had the lowest predicted affinity toward the AAA1 subunit in the ligands library and involved Val1819 through VdW forces via its ring D. In summary, protonation at the N11 was disadvantageous to dynapyrazole A and B and weakened their binding affinities to the AAA1 site (Figure 2.4, Figure A10E–F, and Table A4).

2.4. Conclusions

The presented work provides structural data according to an SAR study to explain how ciliobrevin A and D, dynapyrazole A and B, and their protonated structures, as well as the 46 analogues, could inhibit ATP binding and its hydrolysis in the nucleotide-binding site of the AAA1 subunit of the motor domain in cytoplasmic dynein 1. The lowest binding energy of ATP among the 63 ligands of the library suggested its superior binding affinity over all the competitive inhibitors. However, ciliobrevin A and D, as well as most of the analogues could bind to the functionally key subsites, including the Sensor I and II, N-loop, and the W-A and B, also known as the ATP motifs; thus, optimizing the concentration of the competitive inhibitors *in vitro* could result in blocking the AAA1 nucleotide site in the absence of ATP or its lower concentration. In particular, analogue 47 is suggested as the most suitable candidate for further *in vitro* and *in vivo* experimental evaluations due to its strong binding affinity and low IC50. The ligands' structural mechanism of interference with the ATP binding and hydrolysis was shown to vary depending on their critical functional fragments. The presence of the carbonyl oxygen on ring B of the ligands, for instance, in ciliobrevin D, resulted in its O21 atom forming an H-bond with the Lys1802 amine moiety in the W-A motif. The positively charged ammonium group of the Lys usually acts as an anchor by applying electrostatic forces on the negatively charged γ-phosphate, thereby contributing to the catalytic network for ATP hydrolysis. At the same time, the O22 of the ligand formed an H-bond with Asn1899 of the S-I motif in the β6 strand. The S-I is involved in placing a water molecule near the γ-phosphate of ATP and the negative charge of Glu1849 of the W-B motif and enables a water molecule for a nucleophilic attack, required for the ATP hydrolyzation. The O22 also facilitated the ligand's hydrogen

bond formation with the Gln1849 in the Glu1849Gln protein mutant.

Eliminating the C8–C11 double from ciliobrevin, removing O22 and, replacing it with the N11 by insertion of the ring C in dynapyrazole, resulted in the alteration of the chemical structure, which lowered the IC50 in dynapyrazole. However, the N11 of the ring did not mimic the O22 effect and diminished dynapyrazole binding strength, despite being at a relatively similar position in the ligand structure. Protonation at the N11 atom did not enhance its contribution to the binding energy, as shown in a separate attempt. However, dynapyrazole A benefited from the N7 and N9 atoms' protonation according to the improvement gained in their binding energy. The N9-protonated dynapyrazole A was the only analogue in the ligand library to bind to the linker domain of dynein. The ligand conformational pose and the consequent binding to the linker domain were facilitated by the electrostatic interaction between the protonated N9 and the carboxylate group of Glu1586 in the T-turn 6 of the linker and an H-bond with the amide moiety of Pro1766 in the N-loop. The aliphatic side-chains of the H13 helix in the linker domain, as well as the N-loop, interacted with the ligand hydrophobic sites, namely, the C8, the C12, and the C13 atoms. The observation explained the improvement of the total binding strength of the N9-protonated dynapyrazole A against its unprotonated form.

There are two geometrical isomers *E* and *Z* of ciliobrevin, according to its C8–C11 double bond. The *E* isomer enabled H-bond formation of the ligand with the β6 via its Thr1897 through the nitrogen of the ligand CN moiety and with Asn1899 via its O22 atom. The *Z* isomer of the analogue D interacted with the W-A motif, showing no substantial effect on the S-I motif. In contrast, the *Z* isomer of ciliobrevin A interacted with the S-I motif through Asn1899 of the β6 and the β3 strand, as well as with the W-B via Gln1849.

Unlike its *E* isomer, the *Z* of ciliobrevin A showed no effect on Thr1897 of the β6. However, its CN moiety caused an H-bond with the S-II motif. Ring A, the benzene moiety of the *Z* isomer, had a polar interaction with Arg1852 in a position suitable for a π–π stacking with the guanidine moiety of the arginine. It also appeared to contribute to the "glutamate switch" mechanism in dynein 1. The binding energies of the geometric isomers of ciliobrevin A and D indicated that the *E* had a significantly higher affinity than the *Z* toward the AAA1 binding site. Assessing the effect of geometrical isomerization on analogue 22 resulted in the conformation of its isomers in two opposite orientations in the binding site. This was likely due to the replacement of the CN moiety with a methyl group in that particular analogue, causing a drastic change in the isomer binding modes.

The benzene ring replaced with a pyridine moiety in analogue 45 led to a polar interaction with Lys1974. Analogue 45, similar to other pyridine-possessing analogues of ciliobrevin (i.e., 28, 29, 30, 38, 42, and 45) could affect the ATP hydrolysis via binding to Asn1899, a conserved residue of the S-I motif that facilitates placing water molecules for nucleophilic substitution in ATP hydrolysis.

The glutamate switch (involving Glu108 in PspF [38]) has not yet been detected in cytoplasmic dynein 1; however, an intramolecular H-bond of 2.1 Å between the side-chains of Gln1849 (E1849Q) and Arg1852 was detected in the most energetically favorable conformation of the yeast motor domain through the *in silico* conformational search. It exhibited a conformation with Arg1852 and Gln1849 in orientations capable of a close and strong H-bond formation, suggesting that arginine could also interact with the glutamate in regulating the "switch" mechanism in dynein 1.

New analogues of dynapyrazole, recently introduced by Santarossa et al., [36] were

shown to be potent in inhibiting basal ATPase activity of dynein while binding to AAA3 and AAA4. The binding assessment of analogues 3–48 will be critical in evaluating their inhibitory mode of action at the AAA3 binding site, which is not conserved in axonemal dynein and cytoplasmic dynein 2. This makes the AAA3 subunit a suitable target in the future direction of this study. Utilizing the presented information can contribute to setting up experiments with a focus on the most promising analogues for their selectivity to dynein 1 versus its second isoform. This research suggests avenues to improve the potency and selectivity of the small-molecule inhibitors that could target cytoplasmic dynein's activity to treat neurodegenerative and cancer diseases.

2.5. Bibliography

1. Carter, A.P. Crystal clear insights into how the dynein motor moves. *J. Cell Sci.* **2013**, *126*, 705–713.
2. Bechstedt, S.; Brouhard, G.J. Fluorescence-based assays for microtubule architecture. *Methods Cell Biol.* **2013**, *115*, 343–354.
3. Li, Z.; Alisaraie, L. Microtubules dual chemo and thermo-responsive depolymerization. *Proteins Struct. Funct. Bioinform.* **2015**, *83*, 970–981.
4. Steinman, J.B.; Kapoor, T.M. 8-Chemical probes for dynein. In *Dyneins: Structure, Biology and Disease*, 2nd ed.; King, S.M., Ed.; Academic Press: Cambridge, MA, USA, 2018.
5. Eschbach, J.; Dupuis, L. Cytoplasmic dynein in neurodegeneration. *Pharmacol. Ther.* **2011**, *130*, 348–363.
6. Roossien, D.; Miller, K.; Gallo, G. Ciliobrevins as tools for studying dynein motor function. *Front. Cell. Neurosci.* **2015**, *9*, 252.
7. See, S.K.; Hoogendoorn, S.; Chung, A.H.; Ye, F.; Steinman, J.B.; Sakata-Kato, T.; Miller, R.M.; Cupido, T.; Zalyte, R.; Carter, A.P.; et al. Cytoplasmic Dynein Antagonists with Improved Potency and Isoform Selectivity. *ACS Chem. Biol.* **2016**, *11*, 53–60.
8. Höing, S.; Yeh, T.-Y.; Baumann, M.; Martinez, N.E.; Habenberger, P.; Kremer, L.; Drexler, H.C.A.; Küchler, P.; Reinhardt, P.; Choidas, A.; et al. Dynarrestin, a Novel Inhibitor of Cytoplasmic Dynein. *Cell Chem. Biol.* **2018**, *25*, 357–369.
9. Eguether, T.; Cordelieres, F.P.; Pazour, G.J. Intraflagellar transport is deeply integrated

in hedgehog signaling. *Mol. Biol. Cell* **2018**, *29*, 1178–1189.

10. Firestone, A.J.; Weinger, J.S.; Maldonado, M.; Barlan, K.; Langston, L.D.; O'Donnell, M.; Gelfand, V.I.; Kapoor, T.M.; Chen, J.K. Small-molecule inhibitors of the AAA+ ATPase motor cytoplasmic dynein. *Nature* **2012**, *484*, 125–129.
11. Chen, X.-J.; Xu, H.; Cooper, H.M.; Liu, Y. Cytoplasmic dynein: A key player in neurodegenerative and neurodevelopmental diseases. *Sci. China Life Sci.* **2014**, *57*, 372–377.
12. Kikkawa, M. Big steps toward understanding dynein. *J. Cell Biol.* **2013**, *202*, 15–23.
13. Redwine, W.B.; Hernandez-Lopez, R.; Zou, S.; Huang, J.; Reck-Peterson, S.L.; Leschziner, A.E. Structural basis for microtubule binding and release by dynein. *Science* **2012**, *337*, 1532–1536.
14. Carter, A.P.; Cho, C.; Jin, L.; Vale, R.D. Crystal structure of the dynein motor domain. *Science* **2011**, *331*, 1159–1165.
15. Heale, K.A.; Alisaraie, L. C-terminal Tail of β-Tubulin and its Role in the Alterations of Dynein Binding Mode. *Cell Biochem. Biophys.* **2020**, *78*, 331–345.
16. Kon, T.; Nishiura, M.; Ohkura, R.; Toyoshima, Y.Y.; Sutoh, K. Distinct functions of nucleotide-binding/hydrolysis sites in the four AAA modules of cytoplasmic dynein. *Biochemistry* **2004**, *43*, 11266–11274.
17. Berman, H.M.; Westbrook, J.; Feng, Z.; Gilliland, G.; Bhat, T.N.; Weissig, H.; Shindyalov, I.N.; Bourne, P.E. The Protein Data Bank. *Nucleic Acids Res.* **2000**, *28*, 235–242.
18. Kon, T.; Oyama, T.; Shimo-Kon, R.; Imamula, K.; Shima, T.; Sutoh, K.; Kurisu, G. The 2.8 Å crystal structure of the dynein motor domain. *Nature* **2012**, *484*, 345–350.

19. Schmidt, H.; Gleave, E.S.; Carter, A.P. Insights into dynein motor domain function from a 3.3-Å crystal structure. *Nat. Struct. Mol. Biol.* **2012**, *19*, 492–497.
20. Bhabha, G.; Cheng, H.C.; Zhang, N.; Moeller, A.; Liao, M.; Speir, J.A.; Cheng, Y.; Vale, R.D. Allosteric communication in the dynein motor domain. *Cell* **2014**, *159*, 857–868.
21. UniProt Consortium. UniProt: A worldwide hub of protein knowledge. *Nucleic Acids Res.* **2019**, *47*, D506–D515.
22. Raghava, G.P.S.; Searle, S.M.J.; Audley, P.C.; Barber, J.D.; Barton, G.J. OXBench: A benchmark for evaluation of protein multiple sequence alignment accuracy. *BMC Bioinform.* **2003**, *4*, 47.
23. Chenna, R.; Sugawara, H.; Koike, T.; Lopez, R.; Gibson, T.J.; Higgins, D.G.; Thompson, J.D. Multiple sequence alignment with the Clustal series of programs. *Nucleic Acids Res.* **2003**, *31*, 3497–3500.
24. Berendsen, H.J.C.; van der Spoel, D.; van Drunen, R. GROMACS: A message-passing parallel molecular dynamics implementation. *Comput. Phys. Commun.* **1995**, *91*, 43–56.
25. Schmid, N.; Eichenberger, A.P.; Choutko, A.; Riniker, S.; Winger, M.; Mark, A.E.; van Gunsteren, W.F. Definition and testing of the GROMOS force-field versions 54A7 and 54B7. *Eur. Biophys. J.* **2011**, *40*, 843.
26. Steinman, J.B.; Santarossa, C.C.; Miller, R.M.; Yu, L.S.; Serpinskaya, A.S.; Furukawa, H.; Morimoto, S.; Tanaka, Y.; Nishitani, M.; Asano, M.; et al. Chemical structure-guided design of dynapyrazoles, cell-permeable dynein inhibitors with a unique mode of action. *eLife* **2017**, *6*, e25174.

27. Tribolet, R.; Sigel, H. Influence of the protonation degree on the self-association properties of adenosine 5′-triphosphate (ATP). *Eur. J. Biochem.* **1988**, *170*, 617–626.
28. David, A.W. *Foye's Principles of Medicinal Chemistry*, 7th ed.; Wolters Kluwer: Alphen aan den Rijn, The Netherlands, 2012.
29. Baumgarten, H.E. Advances in heterocyclic chemistry. *J. Chem. Educ.* **1963**, *40*, 559.
30. Schellhammer, I.; Rarey, M. FlexX-Scan: Fast, structure-based virtual screening. *Proteins Struct. Funct. Bioinform.* **2004**, *57*, 504–517.
31. Rarey, M.; Kramer, B.; Lengauer, T. Docking of hydrophobic ligands with interaction-based matching algorithms. *Bioinformatics* **1999**, *15*, 243–250.
32. Rarey, M.; Kramer, B.; Lengauer, T. Multiple automatic base selection: Protein–ligand docking based on incremental construction without manual intervention. *J. Comput.-Aided Mol. Des.* **1997**, *11*, 369–384.
33. Böhm, H.J. The development of a simple empirical scoring function to estimate the binding constant for a protein-ligand complex of known three-dimensional structure. *J. Comput.-Aided Mol. Des.* **1994**, *8*, 243–256.
34. Böhm, H.J. Prediction of binding constants of protein ligands: A fast method for the prioritization of hits obtained from de novo design or 3D database search programs. *J. Comput.-Aided Mol. Des.* **1998**, *12*, 309–323.
35. Ecklund, K.H.; Morisaki, T.; Lammers, L.G.; Marzo, M.G.; Stasevich, T.J.; Markus, S.M. She1 affects dynein through direct interactions with the microtubule and the

dynein microtubule-binding domain. *Nat. Commun.* **2017**, *8*, 2151.

36. Santarossa, C.C.; Mickolajczyk, K.J.; Steinman, J.B.; Urnavicius, L.; Chen, N.; Hirata, Y.; Fukase, Y.; Coudray, N.; Ekiert, D.C.; Bhabha, G.; et al. Targeting Allostery in the Dynein Motor Domain with Small Molecule Inhibitors. *Cell Chem. Biol.* **2021**, in press.
37. Schmidt, H.; Carter, A.P. Review: Structure and mechanism of the dynein motor ATPase. *Biopolymers* **2016**, *105*, 557–567.
38. Mogni, M.E.; Costa, A.; Ioannou, C.; Bell, S.D. The glutamate switch is present in all seven clades of AAA+ protein. *Biochemistry* **2009**, *48*, 8774–8775.

Summary

The first chapter of this research work explored the dual function of dynein and kinesin in promoting viral proliferation and their essential contribution to the host cell's immune response. The literature review informed of the usurpation of dynein and kinesin by viruses to complete delivery of their genome from the cell periphery to the site of their replication and from this site back to the plasma membrane for the release of the replicated genome to facilitate viral spread. This study showed the involvement of kinesin and dynein at each phase of viral infection, namely, entry, genome replication, and exit or egress. However, the motor proteins are also involved in the immunological response of the host cell to inhibit viral infection. Small-molecule inhibitors of kinesin (BTB-1) and dynein (ciliobrevin) displayed the inhibitory activity of viral infection.

The second chapter of this thesis focused on studying the binding profile of small-molecule inhibitors of dynein, ciliobrevin and its analogues, and dynapyrazole A and B. The binding site of the chemical inhibitors was revealed through computational methods. The effect of protonation on the inhibitors was discussed, and that of the isomerization of ciliobrevin A. The careful analysis of data collected from this study helped to propose the identity of a residue that could engage in the 'glutamate switch' mechanism, which had not been observed in cytoplasmic dynein 1 yet through *in vivo* or *in vitro* experimental structures of the protein. Thus, this work represents an assortment of valuable knowledge that will contribute to a better understanding of the dynein mechanism and to the amelioration of the chemical inhibitors whose binding profiles have now been revealed.

Appendix A

Figure A1: Amino acids sequence alignment of the AAA1 and AAA2 subunits of dynein corresponding to *S. cerevisiae* (1758-2273) and *D. discoideum* (1936-2531) with the ClustalW program. The W-A motif is highlighted in blue. The grey highlights represent sequence similarity. A singular dot (.) indicates that residues belong to a different group of amino acids, while a colon (:) indicates that residues belong to the same group of amino acids, and an asterisk (*) indicates sequence identity.

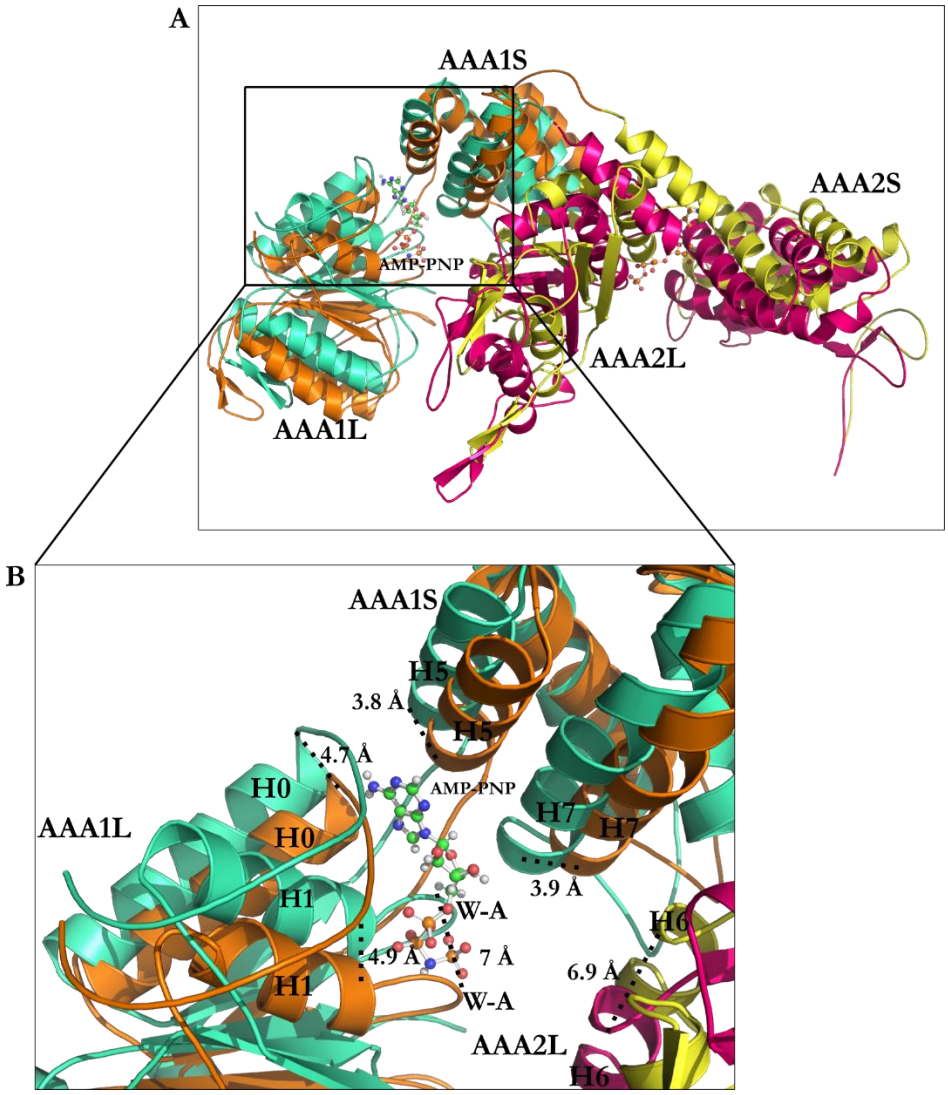

Figure A2: (A) Structural alignment of the AAA1 and AAA2 of yeast-AMPPNP (4W8F) and yeast-apo (4AKG). **(B)** A close-up of the AAA1 binding site. Helices (H0, H1, H5, and H7) of the AAA1 subdomain, the Walker-A (W-A) loops with the AMP-PNP in the ball and stick representation in green located at the AAA1 nucleotide-binding site and the H6 of the AAA2 subdomains of the yeast-AMPPNP (4W8F) and yeast-apo (4AKG). Color code: yeast-AMPPNP (AAA1 in green cyan and AAA2 in sharp pink) and yeast-apo (AAA1 in orange and AAA2 in yellow).

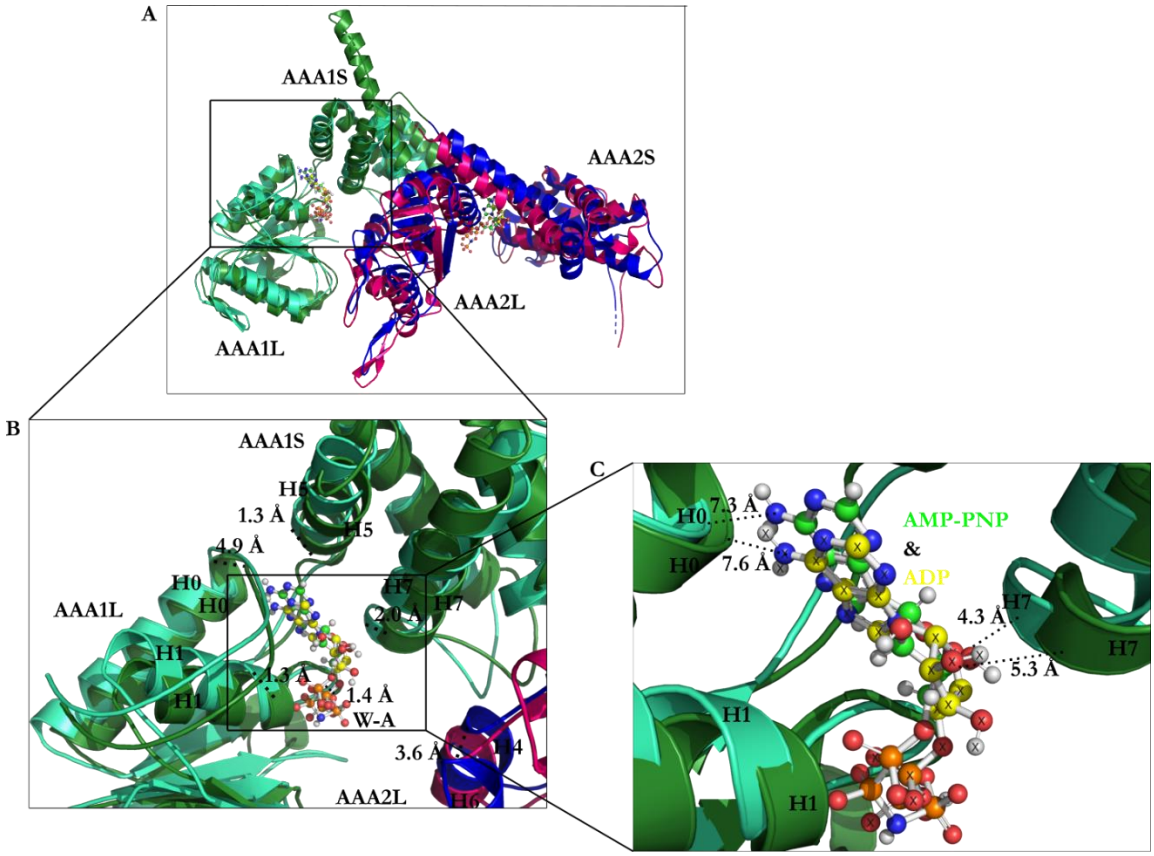

Figure A3: (A) Structural alignment of the AAA1 and AAA2 subunit of the *Dictyostelium-ADP* (3VKG) and yeast-AMPPNP (4W8F). **(B)** A close-up of the AAA1 binding site. Helices (H0, H1, H5, and H7) of the AAA1 subdomain, the Walker-A (W-A) loops with the AMP-PNP in the ball and stick representation in green and ADP in the ball and stick representation in yellow located at the AAA1 nucleotide-binding site and the H4 of the AAA2 subdomain of the *Dictyostelium-ADP* (3VKG) and the H6 of the AAA2 subdomain of the yeast-apo (4AKG). **(C)** Structural alignment of ligands at the AAA1 nucleotide-binding site of the *Dictyostelium-ADP* (3VKG) and yeast-AMPPNP (4W8F) with AMP-PNP in the ball and stick representation in green and ADP in the ball and stick representation in yellow with a cross (x) on its atoms to distinguish them from

the atoms of AMP-PNP. Color code: *Dictyostelium*-ADP (AAA1 in green and AAA2 in blue) and yeast-AMPPNP (AAA1 in green cyan and AAA2 in sharp pink).

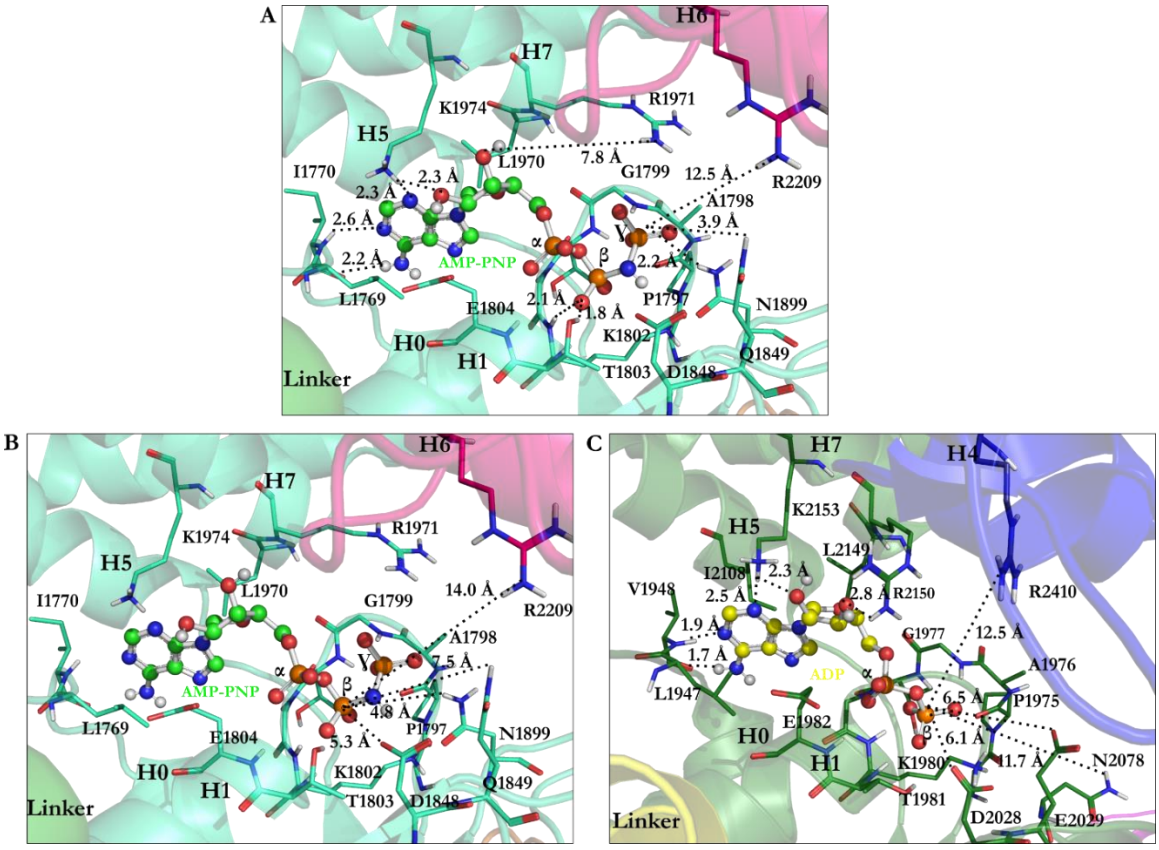

Figure A4: (A) AMP-PNP interacting and residues of the AAA1 nucleotide-binding site. Distances between catalytic residues of the AAA1 nucleotide-binding site of dynein and the β-phosphate of **(B)** AMP-PNP and **(C)** ADP.

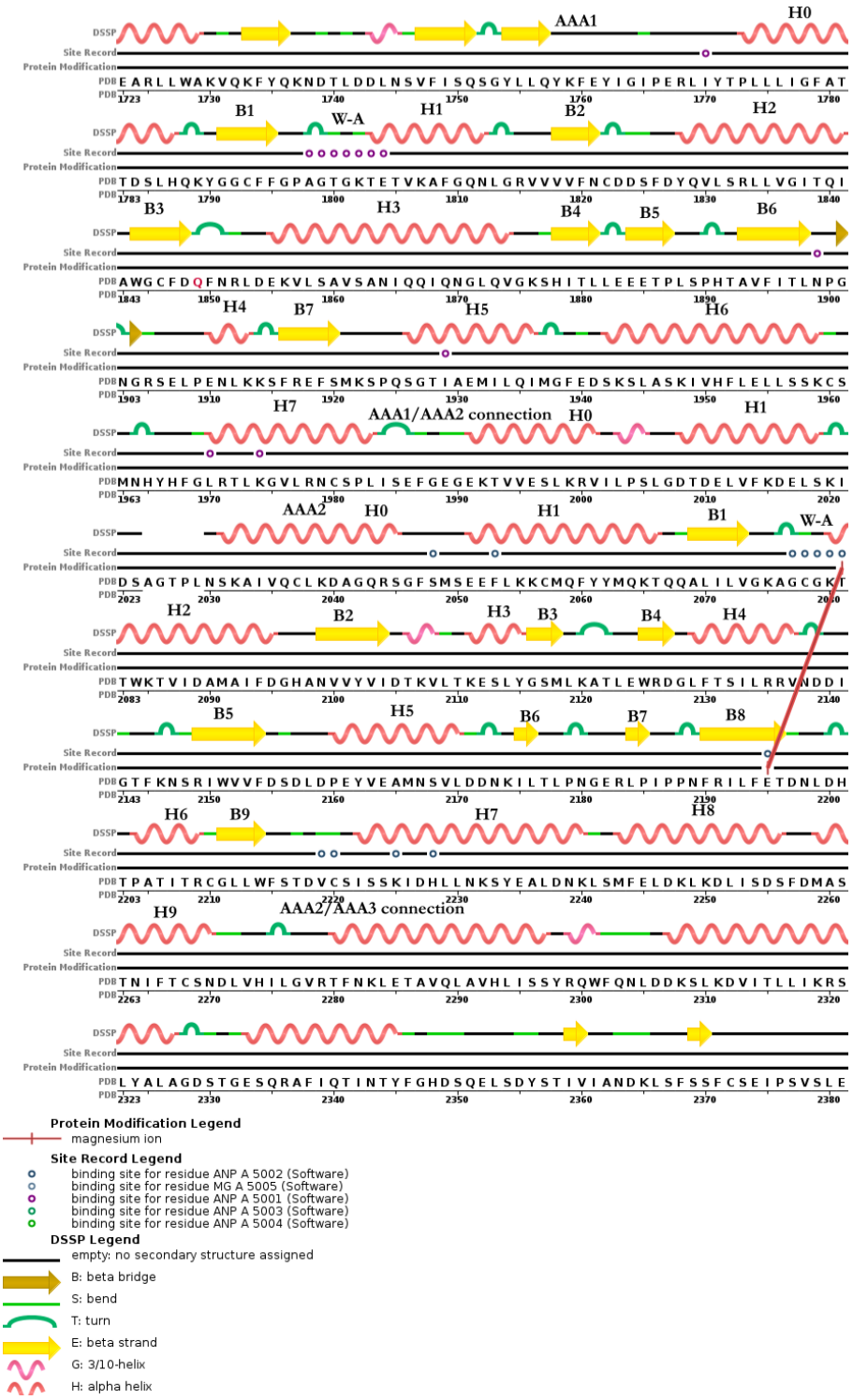

Figure A5: Annotation of the secondary structure of AAA1 and AAA2 domains of cytoplasmic dynein according to the 4W8F crystal structure retrieved from the PDB.

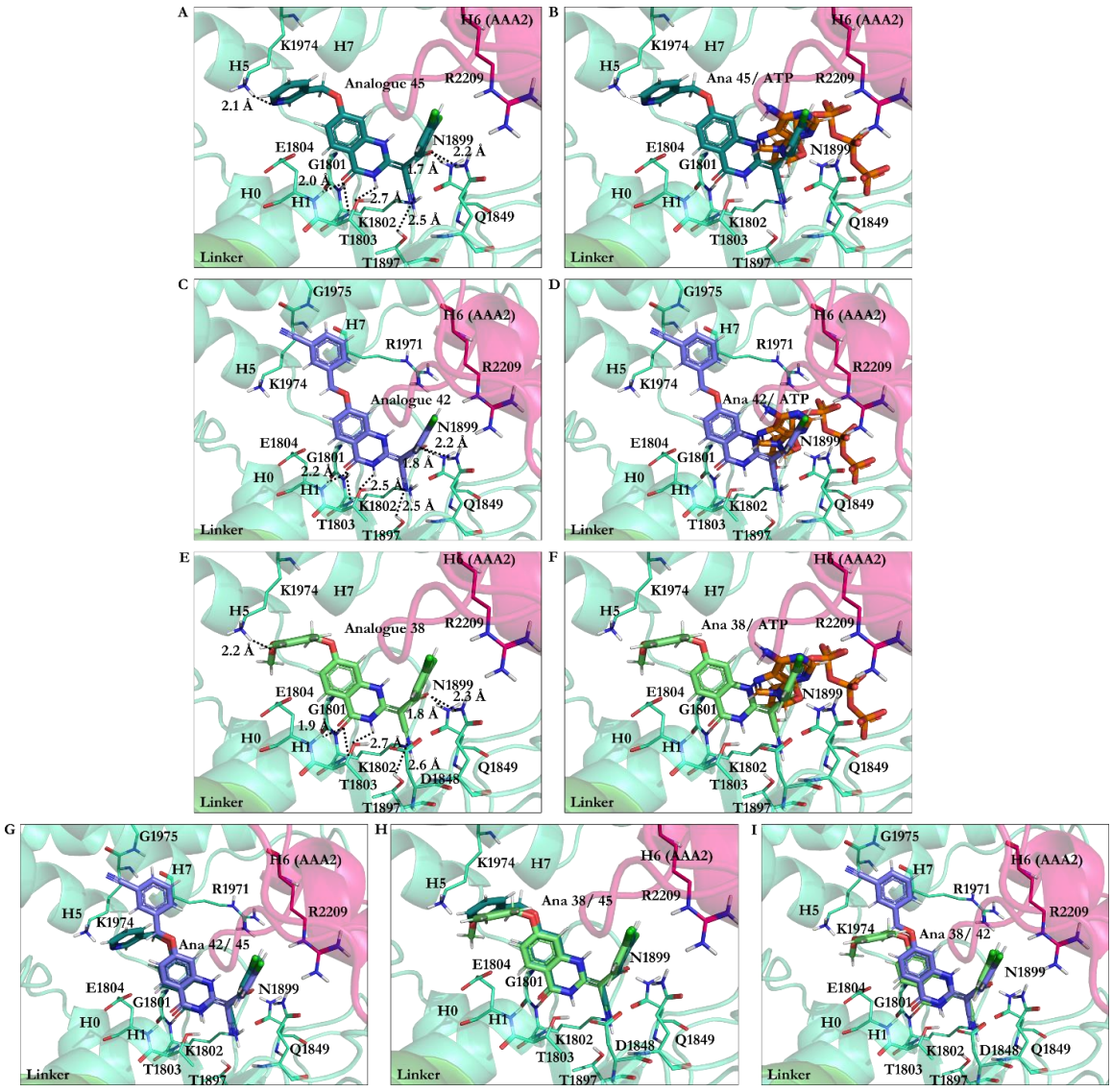

Figure A6: Binding modes of ciliobrevin analogues at the AAA1 binding site of dynein 1. **(A)** Analogue 45. **(B)** Analogue 45 superimposed on ATP. **(C)** Analogue 42, **(D)** Analogue 42 superimposed on ATP. **(E)** Analogue 38. **(F)** Analogue 38 superimposed on ATP. Superimposition of **(G)** Analogues 42 and 45, **(H)** Analogues 38 and 45, **(I)** Analogues 38 and 42.

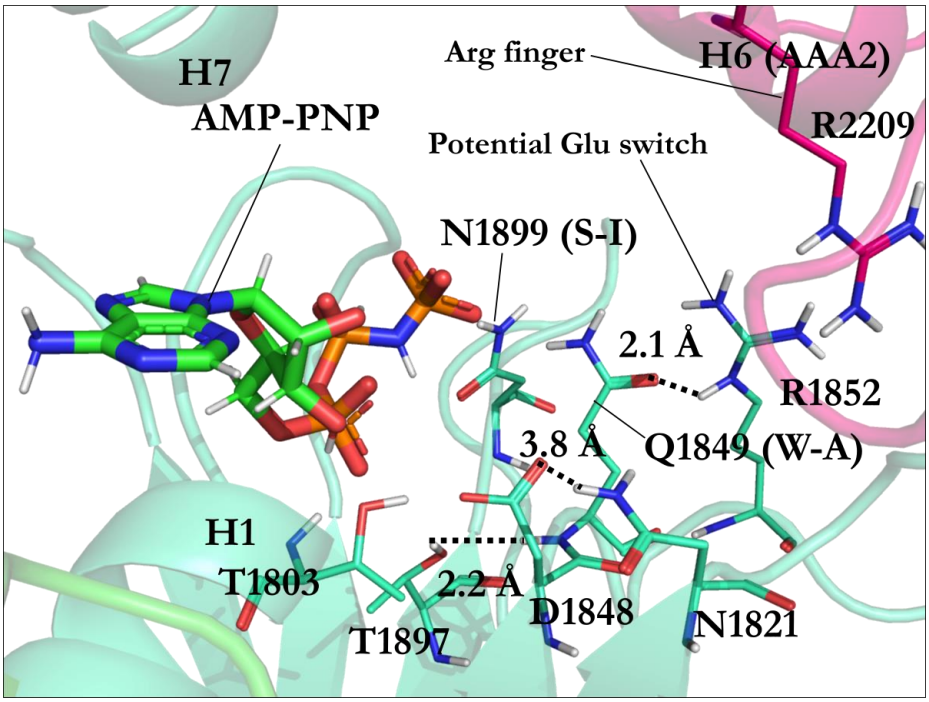

Figure A7: Intramolecular interactions between the catalytic residues at the AAA1 binding site and Arg1852 involving a potential glutamate switch. The docking solution of AMP-PNP is represented in green and stick. Thr1803 and Asp1848 accommodate Mg^{2+} during ATP hydrolysis. Sensor I (N1899), W-B (E1849Q), R-finger (R2209) play catalytic roles during ATP hydrolysis.

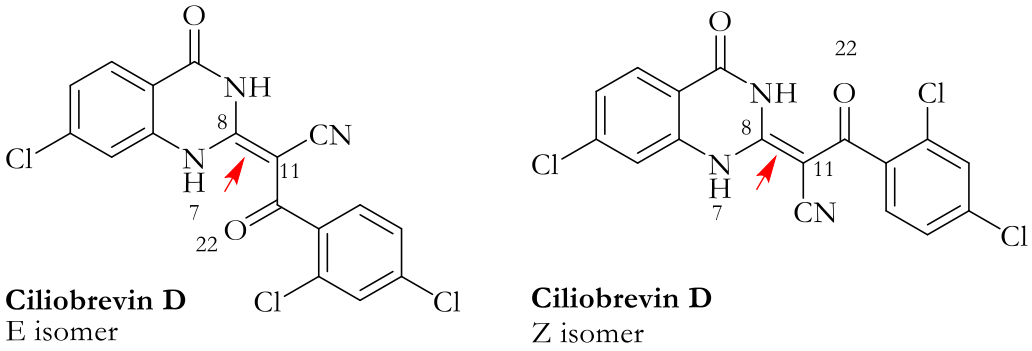

Figure A8: *E* and *Z* configurations of ciliobrevin D. Red arrows point to the double bond between the C8 and C11 atoms.

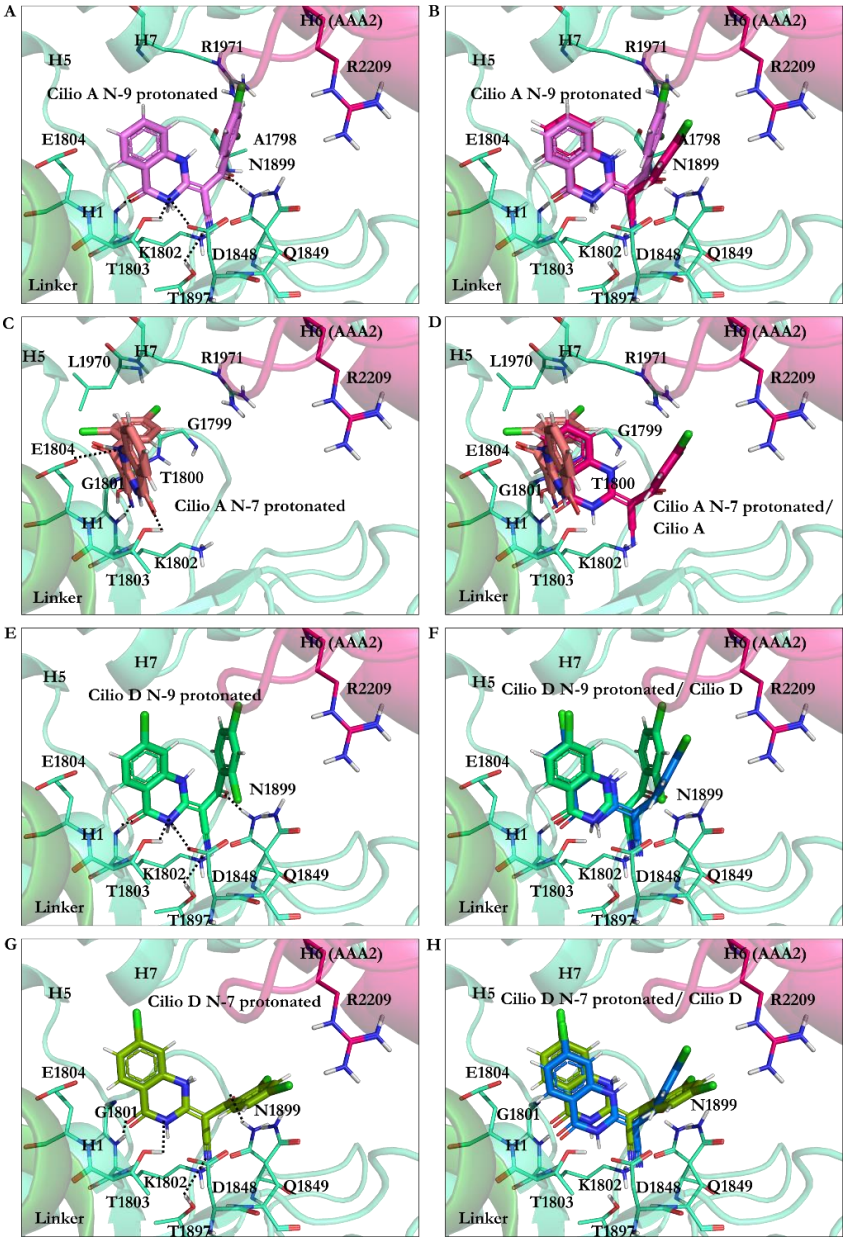

Figure A9: Binding modes of the protonated forms of ciliobrevin at the AAA1 binding site of dynein 1. **(A)** Ciliobrevin A protonated at the N9 atom. **(B)** Ciliobrevin A protonated at the N9 atom superimposed on ciliobrevin A. **(C)** Ciliobrevin A protonated at the N7 atom. **(D)** Ciliobrevin A protonated at the N7 atom superimposed on ciliobrevin A. **(E)** Ciliobrevin D protonated at the N9 atom. **(F)** Ciliobrevin D protonated at the N9

atom superimposed on ciliobrevin D. **(G)** Ciliobrevin D protonated at the N7 atom. **(H)** Ciliobrevin D protonated at the N7 atom superimposed on ciliobrevin D.

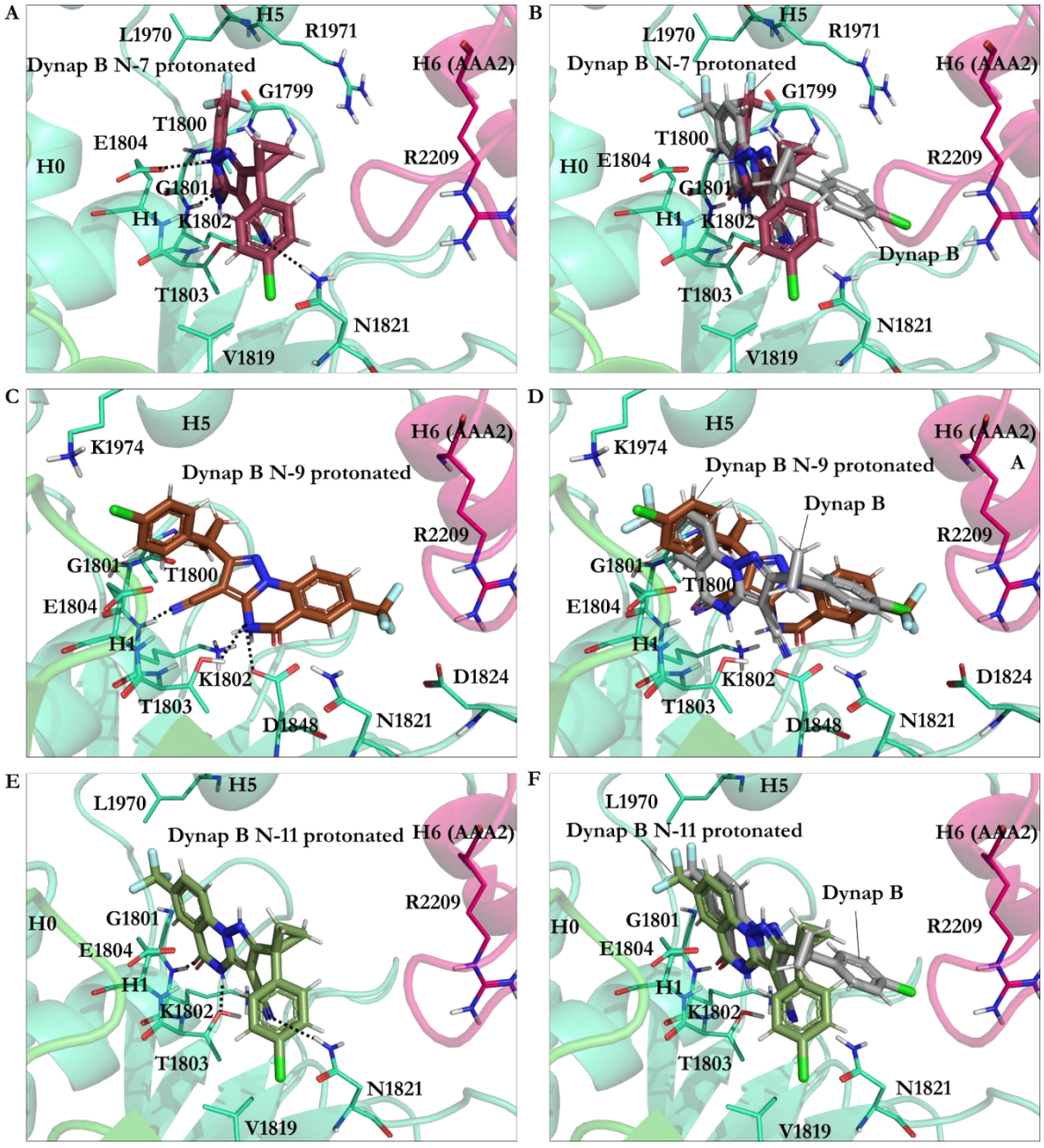

Figure A10: Main binding interactions of the protonated forms of dynapyrazole B at the AAA1 binding site of dynein 1. **(A)** Dynapyrazole B protonated at the N7 atom. **(B)** Dynapyrazole A protonated at the N7 atom superimposed on dynapyrazole B. **(C)** Dynapyrazole B protonated at the N9 atom. **(D)** Dynapyrazole B protonated at the N9

atom superimposed on dynapyrazole A. **(E)** Dynapyrazole B protonated at the N11 atom. **(F)** Dynapyrazole B protonated at the N11 atom superimposed on dynapyrazole B.

Table A1: Networking interactions of analogues 28, 29, and 30 with AAA1 of dynein 1.

Compound	Binding Energy (kJ/mol)	Residues interacting with the compound
Analogue 30	−27.87	Gly1801, Lys 1802, Thr1803, Glu1804, Asp1848, Gln1849, Thr1897, Asn1899
Analogue 29	−27.37	Gly1801, Lys1802, Thr1803, Glu1804, Asp1848, Gln1849, Thr1897, Asn1899
Analogue 28	−27.27	Gly1801, Lys1802, Thr1803, Glu1804, Asp1848, Gln1849, Thr1897, Asn1899

Table A2: Interacting amino acids with analogues 38, 42, and 45.

Compound	Binding energy (kJ/mol)	Residues interacting with the ligand
Analogue 45	−29.72	Gly1801, Lys1802, Thr1803, Glu1804, Gln1849, Thr1897, Asn1899, Lys1974
Analogue 42	−27.43	Gly1801, Lys1802, Thr1803, Glu1804, Gln1849, Thr1897, Asn1899, Lys1974, Gly1975, Arg1971
Analogue 38	−27.27	Gly1801, Lys1802, Thr1803, Glu1804, Asp1848, Gln1849, Thr1897, Asn1899, Lys1974

Table A3: The binding energy of *E* and *Z* isomers of ciliobrevin A and ciliobrevin D.

Compound	Binding energy (kJ/mol)	Residues interacting with the docked ligand
Ciliobrevin A *E*-isomer	−26.23	Gly1801, Lys1802, Thr1803, Glu1804, Asp1848, Gln1849, Thr1897, Asn1899
Ciliobrevin A *Z*-isomer	−19.41	Thr1803, Asn1821, Asp1848, Gln1849, Arg 1852, Asn1899, Arg1852, Arg1971
Ciliobrevin D *E*-isomer	−23.92	Gly1801, Lys1802, Thr1803, Glu1804, Asp1848, Gln1849, Thr1897, Asn1899
Ciliobrevin D *Z*-isomer	−19.78	Gly1799, Thr1800, Gly1801, Lys1802, Thr1803, Glu1804, Asp1848, Gln1849, Leu1970, Arg1971, Lys1974
***E*-Analogue 22**	−16.83	Ala1798, Gly1969, Tyr1902, Pro1900, Arg1971, His1967
***Z*-Analogue 22**	−17.49	Leu1769, Gly1801, Lys1802, Glu1804, Leu1970, Lys1974

Table A4: Interacting amino acids with dynapyrazole A and B in the protonated and deprotonated states.

Compounds	Binding energy (kJ/mol)	Residues interacting with the compound
Dynapyrazole B N-7 protonated	−26.95	Gly1799, Thr1800, Gly1801, Lys1802, Thr1803, Glu 1804, Val1819, Asn1821, Leu1970, Arg1971
Dynapyrazole A N-7protonated	−25.99	Gly1801, Lys1802, Thr1803, Glu1804, Asn1821
Dynapyrazole A N-9 protonated	−19.81	Glu1586, Lys1696, Glu1699, Pro1766, Glu1767, Arg1978
Dynapyrazole B	−18.49	Thr1800, Gly1801, Lys1802, Thr1803, Glu1804, Asn1821, Leu1970
Dynapyrazole B N-9 protonated	−18.47	Thr1800, Gly1801, Lys1802, Thr1803, Glu1804, Asn1821, Asp1824, Asp1848, Lys1974
Dynapyrazole A	−18.17	Gly1801, Lys1802, Thr1803, Glu1804, Asn1821
Dynapyrazole A N-11 protonated	−17.49	Lys 1802, Thr1803, Glu1804, Asp1848, Gln1849, Asn1899
Dynapyrazole B N-11 protonated	−17.13	Gly1801, Lys1802, Thr1803, Glu1804, Val1819, Asn1821, Leu1970